Aalborg Universitet

Innovative Design of a Darrieus Straight Bladed Vertical Axis Wind Turbine by using Multi Element Airfoil

Chougle, Prasad Devendra

Aalborg University
Department of Civil Engineering
Division of Water and Soil

DCE Thesis No. 52

Innovative Design of a Darrieus Straight Bladed Vertical Axis Wind Turbine by using Multi Element Airfoil
04.11.2015

by

Prasad Vijaymala Devendra Chougule

November 2015

Scientific Publications at the Department of Civil Engineering

Technical Reports are published for timely dissemination of research results and scientific work carried out at the Department of Civil Engineering (DCE) at Aalborg University. This medium allows publication of more detailed explanations and results than typically allowed in scientific journals.

Technical Memoranda are produced to enable the preliminary dissemination of scientific work by the personnel of the DCE where such release is deemed to be appropriate. Documents of this kind may be incomplete or temporary versions of papers or part of continuing work. This should be kept in mind when references are given to publications of this kind.

Contract Reports are produced to report scientific work carried out under contract. Publications of this kind contain confidential matter and are reserved for the sponsors and the DCE. Therefore, Contract Reports are generally not available for public circulation.

Lecture Notes contain material produced by the lecturers at the DCE for educational purposes. This may be scientific notes, lecture books, example problems or manuals for laboratory work, or computer programs developed at the DCE.

Theses are monograms or collections of papers published to report the scientific work carried out at the DCE to obtain a degree as either PhD or Doctor of Technology. The thesis is publicly available after the defence of the degree.

Latest News is published to enable rapid communication of information about scientific work carried out at the DCE. This includes the status of research projects, developments in the laboratories, information about collaborative work and recent research results.

Prasad V.D. Chougule

Preface

The present thesis, Innovative Design of a Darrieus straight bladed vertical axis wind turbine by using multi element airfoil is the outcome of the research of a PhD study within the period July 2010 to November 2015 at the department of Civil Engineering, Aalborg University, Aalborg, Denmark. The thesis is presented as a collection of peer-reviewed articles published within this period in a number of journals and conferences. I would like to thank my supervisor Prof.Dr.Techn. Søren R.K. Nielsen for his enthusiast and perseverance in this project. I would like to specially appreciate his belief in me and giving me consistence support. Special thanks should be directed to Prof.Biswajit Basu of Trinity College Dublin, Ireland who played important role in my research topic and hosted me couple of times during this period. I would like to also appreciate Prof. Lasse Rosendahl from Department of Energy Technology, Aalborg University, Denmark for providing me an educational wind tunnel to carry out the testing without charging. I would also like to thank Prof. Niels Sørensen from Wind Energy Department of Danish Technical University, Denmark for his precise technical comments on my research findings. I would like to thank to lab technicians who helped me to carry out experiments successfully and safely. The SYSWIND project (project no. 238325) funded by the Marie Curie Actions is acknowledged for the financial support under the grant Seventh Framework Programme for Research and Technological Development of the European Union. I would like to thank my friends and colleague for their support in technical discussions and motivating me during time of intense work.

I would like to thank my parents, my three sisters and their husbands, my three uncles, my five nephews for their everlasting support and morality. I would like to dedicate this work to my parents for their immense motivation and routine checks on my progress of PhD work time to time. Finally, I would highly appreciate my wife Neha Kiran Durugkar for correcting my writing and giving me time to focus on my Thesis.

Aalborg, November, 2015 Prasad V.D. Chougule

Summary in English

30% of electrical energy is being consumed by households, and the demand for energy is increasing rapidly causing a strain on existing electricity solutions. Electricity production plants have been seen on larger scales but they have failed to reach every single potential user of electricity. The demand for electricity is rapidly growing in urban areas as people are migrating towards the big cities. So governments around the world are focusing on the electricity needs in urban areas and on the industrialized special economic zones consuming all their resources and leaving behind rural electrification. However, electricity demand in developed countries is far more different than the developing countries. Developed countries need massive supply of electricity for its own cities for future exponential demand whereas developing countries needs to lift up their un-electrified population with supplying electricity for livelihood along side with urban demand. The price of electricity is increasing every day as well.

With this immense opportunity for off-grid electricity production in energy field new renewable energy and technological devices are getting lots of attention around the world. A wind energy convertor is seen as the most potential energy convertor to supply electricity and has gone through technological developments in last two decades. Wind energy convertors are growing bigger in size and going through new design procedures on a massive scale that the world has never seen before, as big as 10 MW wind energy convertors. Today wind turbines are the biggest structures on the earth. The knowledge and experiences from aviation and a construction industry has made quicker developments in the wind turbines. This research work is aimed at design and development of a small wind turbine.

Mainly, there is the horizontal axis wind turbine (HAWT) and vertical axis wind turbine (VAWT). HAWTs are more popular than VAWTs due to failure of VAWT commercialization during the late of 1980s on a large scale. However, in recent research work it has been documented that VAWTs are more economical and suitable for urban use due to their noise-free and aesthetic design. Still there is a room to improve the efficiency of the VAWTs since they are not completely understood. The reason for smaller development of VAWTs is the non-availability of an accurate aerodynamic model and very few experimental data for validation. In this PhD research, a development of wind turbine rotor is planned based on the multi-element airfoil technology used in aviation for aeroplanes.

A method of experimental and numerical analysis is combined together for successful research. A double-element airfoil design is carried out, and the wind tunnel testing of double-element airfoil is performed. It is found that the aerodynamic characteristics of the airfoil increased considerably by delaying the angle of stall. These two facts are very suitable for vertical axis wind turbine since they operate in a larger range of angle of attack, $\pm 40°$, compared to the horizontal axis wind turbines which operate in the range of attack, $\pm 15°$. A new design of vertical axis wind turbine is then proposed, and aerodynamic performance is evaluated based on double multiple stream tube methods. The performance parameters are almost doubled compared to the traditional straight-bladed vertical axis wind turbine. Theoretical study of blade pitch control methods for a vertical axis wind turbine has also been carried and compared with each other.

Summary in Danish

30% af elektrisk energi, som forbruges af husholdninger, og efterspørgslen efter energi er stigende hurtigt forårsage en stamme på eksisterende el-løsninger. El produktionsanlæg har blevet set på større skalaer, men de har undladt at nå hver eneste potentiel bruger af elektricitet. Efterspørgslen efter elektricitet er hastigt voksende i byområder, som folk er tiltrukket de store byer. Så regeringer verden fokuserer på el-behov i byerne områder og på de industrialiserede særlige økonomiske zoner indtager alle deres ressourcer og forlader bag elektrificering i landdistrikter. Men elektricitet efterspørgsel i de udviklede lande er langt mere anderledes end udviklingslandene. De udviklede lande har brug for massiv forsyning af elektricitet til sine egne byer for fremtidig eksponentiel efterspørgsel mens udviklingslandene har behov for at løfte deres un-elektrificeret befolkning med at levere elektricitet til levebrød langs siden med urban efterspørgsel. Prisen på elektricitet er stigende hver dag, så godt.

Med denne enorme mulighed for off-grid elproduktion på energiområdet nye vedvarende energi og teknologiske enheder bliver masser af opmærksomhed i hele verden. Et vindenergi konverter ses som themost potentielle energi konverter til at levere elektricitet og er gået igennem teknologiske udvikling i de sidste to årtier. Vindenergi omformere vokser større i størrelse og går gennem nye design procedurer på en massiv skala, som verden aldrig har set før, så stor som 10 MW vindenergi konvertere. I dag er vindmøller er de største strukturer på jorden. Den viden og erfaringer fra luftfart og en byggebranchen har gøres hurtigere udvikling i vindmøller. Denne forskning er rettet mod design og Udviklingen af lille en vindmølle.

Hovedsageligt er der den vandrette akse vindmølle (HAWT) og lodrette akse vindmølle (VAWT). HAWTs aremore populære end VAWTs grund af svigt af VAWT kommercialisering i slutningen af 1980'erne på en stor skala. Men i nyere forskning arbejde, det er dokumenteret, at VAWTs er mere økonomisk og egnet til brug i byområder på grund af deres støjfri og æstetiske design. Still der er plads til at forbedre effektiviteten af de VAWTs da de ikke er helt forstået. Årsagen til mindre udvikling af VAWTs er den manglende adgang til en præcis aerodynamisk model og meget få eksperimentelle data til validering. I denne Ph.d.-forskning, udvikling af vindmøllerotor planlægges baseret på multi-element airfoil teknologi, der anvendes inden for luftfarten til flyvemaskiner.

En metode til eksperimentel og numerisk analyse er kombineret sammen for vellykket forskning. En dobbelt-element airfoil design udføres, og afprøvning af dobbelt-element vindtunnelen airfoil udføres. Det konstateres, at de aerodynamiske egenskaber af bæreplanet forøges betydeligt ved at forsinke vinkel stall. Disse to kendsgerninger er meget velegnet til lodrette akse vindmølle da de opererer i et større sortiment af angrebsvinkel, $\pm 40°$, i forhold til den vandret akse vind turbineswhich opererer i området for angreb, $\pm 15°$. En ny konstruktion af vertikal akse vindmølle derefter foreslået, og aerodynamik er evalueret baseret på dobbelt flere stream rør metoder. De performance parametre er næsten fordoblet i forhold til traditionel straight-bladet lodrette akse vindmølle. Teoretisk undersøgelse af bladet pitch kontrol metoder til en lodret akse vindmølle er også blevet foretaget og sammenlignet med hinanden

Prasad V.D. Chougule

Contents

List of Figures

List of Tables

CHAPTER 1
Introduction

1.1   Wind energy convertors

Kinetic energy of a wind flow is converted into the mechanical energy by using different devices often called 'windmills' because it is used to grind the grain, and it is also used to pump the water. The automatic grain grinding and water pumping systems were invented 20 centuries ago, and operated on wind forces. The historical evidence of the earliest known design of the vertical axis system developed in Persia about 500-900 AD has been found, but the exact functioning of the water transport is not clear. The first known documented design is also of a Persian windmill; this one had vertical sails made up of bundles of reeds or wood attached to the central vertical shaft by a horizontal struts. In this Persian panemone design, the rotor can only harvest half of the wind striking the collection area. In modern days, the kinetic energy of the wind flow is converted into electrical energy by the wind turbines. The panemone windmill is one of the least efficient, but most commonly reinvented (and patented in modern days) wind turbine concepts, eventually called vertical axis wind turbines (VAWT). In Europe, between 1270 AD, and 1390 AD new configurations of windmills were developed in which rotor rotates about the horizontal axis, called horizontal axis wind turbines (HAWTs). This was the technological break through at that point of time, since a drag-operated horizontal axis windmill is almost twice as efficient as the drag-operated Persian vertical axis windmill. The lift-operated windmill based on sails was designed by the Dutch in late 18th century, which has almost all features of a modern wind turbine blade. These features constitute a camber along the leading edge, a blade twist along the length, a placement of the spar at the quarter chord position and the aerodynamic center at the same position. A historical development of the windmill is given in 'Wind Turbine Technology'(Spera 2009).

A Finnish engineer, Sigurd Savonius, invented a drag-operated VAWT in 1922 called the Savonius rotor (Savonious 1931). Later on, the French aeronautical engineer George Darrieus invented a new rotor of VAWT type which became well known within its type in 1931 (Darrieus 1931). During 1930 to 1940, many wind turbines were installed in the US to produce electricity. But the development of the wind turbines stopped due to the invention of the steam engine and its ability to convert heat energy into a mechanical power and thereby electrical energy. In

(a) Small horizontal axis wind turbine (HAWT)

(b) Darrieus vertical axis wind turbine (VAWT)

(c) Straight bladed vertical axis wind turbine (VAWT)
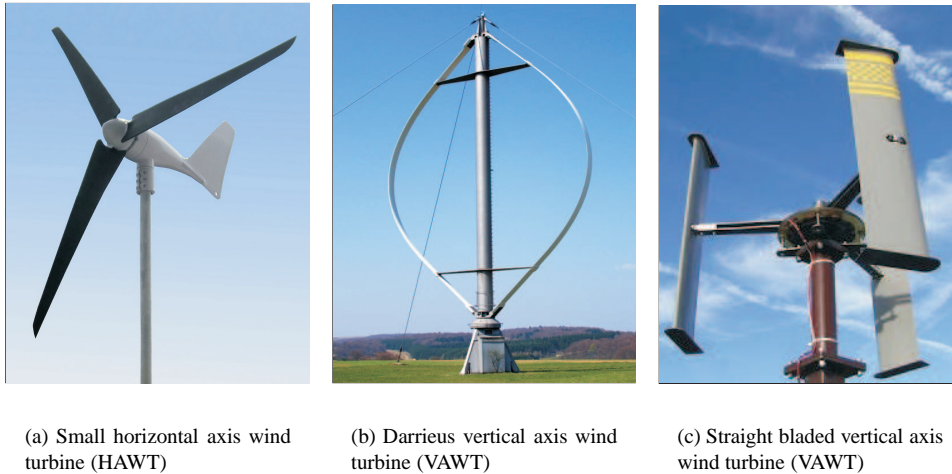
Figure 1.1 Wind turbine configurations

1970s, the oil crisis cause increase in the development of big sized VAWT and HAWT designs. Due to less efficiency and the mechanical periodic vibration of the column structure of a VAWT, they lost the interest of researchers and the companies. By late 1980s, researchers developed moderns wind turbines with sophisticated control mechanisms for a HAWT. HAWT's essentially have blades with an aerodynamic shape which operates on lift force.

Figure 1.1 (a) is a typical three-bladed horizontal axis wind turbine. Figure 1.1 (b) is a photo of the Darrieus egg beater shaped wind turbine which is not a small wind turbine type in this case. Figure 1.1 (c) shows the three-straight bladed vertical axis wind turbines. The photographs have been taken from an open source on the internet. The present PhD project is focused on small VAWTs and HAWTs in the range of 1kw to 100 kw. Therefore, assumptions and procedures discussed in this study are related to small wind energy convertors.

1.2   Political effect on development of wind turbines

Wind energy convertors are getting more notice in the energy crisis all over the world. The Directive $2009/28/EC$ on renewable energy, implemented by Member States by December 2010, has sets ambitious targets for all Member States in that the EU will reach a 20% share of energy from renewable sources by 2020 and a 10% share of renewable energy specifically in the transport sector (Energy 2012). In addition to that, the radiation leakage from the nuclear power plant in Japan in 2011 has meant that renewable energy has gotten tremendous attention in public and with politicians. Immediately after that, a public protest to close down the nuclear power plants took place in Germany, and the European Union kicked off a public debate on extending 2020 renewable energy targets to 2030. Denmark has been first country in the world to reach the 20% target of renewable energy dependency and has set new targets for 2020 (Denmark 2012). They

Prasad V.D. Chougule

are summarized here: i) more than 35% of renewable energy in final consumption, ii) approximately 50% of electricity consumption to be supplied by wind power, iii) 7.6% reduction in gross energy consumption in relation to 2010, and iv) 34% reduction in greenhouse gas emmisions in relation to 2010. All these policies bring a huge amount of money into the development of wind turbines, and today modern wind turbines are growing bigger and bigger with offshore installations. Today modern horizontal axis wind turbines have reached to their maximum practical efficiency between 42 to 45% (Hansen 2008). Due to the availability of funds and the demand of high energy, the development focus has shifted towards bigger sized and optimized designs to reduce the cost of energy produced. The size of a modern HAWT is getting bigger, making it very expensive for offshore transportation and maintenance. Also, there is a focus towards technological change, such as direct drive wind turbines eliminating gearboxes and rethinking of different configurations such as lift-operated vertical axis wind turbines. The technological shift in wind power has resulted in different wind turbine designs on a Mega watt scale. Design of a Aerogenerator 10MW vertical axis wind turbine (Aerogenerator 2010). The first deep wind (150 m) 5MW baseline design of a Darrieus floating type has been launched in Norway (Paulsen *et al.* 2012). A document was published on 'Tilting at Wind Mills' focusing on ultility scale VAWT towards 10MW and beyond (Eurowind 2005).

1.3   An overview of the problem

The VAWTs have advantages over the HAWTs such as: a simple construction, less maintenance, economical, noiseless operation, highly suitable for building integration and urban use (Eriksson *et al.* 2008),(Bhutta *et al.* 2012). But the fact that the VAWTs are less efficient than HAWTs has been ignored by the researchers in the development of more accurate analytical models, meaning a commercial failure of the VAWT products. Recently, it has been understood that the small VAWTs are more economical and suitable for household applications due to the rapid increase in electricity prices at the moment (Eriksson *et al.* 2008). There has been new inventions of the VAWT which overcomes the drawback of less efficiency and which are substitutes to a small HAWT. A review of such designs and techniques of VAWTs is summarized by Bhutta and coauthors (Bhutta *et al.* 2012), the performance of these designs are also compared. Due to new airfoil shapes and a more clear understanding of the flow physics around VAWTs has proven that the they are as efficient as HAWTs.

The earlier research carried out by the Sandia National Laboratory, Natural Resources Canada and several commercial companies using straight-bladed VAWT models used mainly symmetric airfoils. The airfoils used in all earlier research of VAWTs are usually designed for a low altitude flight conditions of the airplane by a National Advisory Committee of Aeronautics (NACA). A reason for this is that the physical condition of the air flow around an aeroplane resembles the physical condition around the VAWT (Islam *et al.* 2007). However, it is important to keep in mind that the other aspects such as the structural strength of the blade differs dramatically in both cases. A VAWT blade with thin airfoil gives highest maximum power coefficient; however, in case of a low altitude flying bi-plane the wings must be thick. So the thickness of the airfoil cross section will change the aerodynamic characteristics. Hence it is critical to decide the airfoil and the optimized dimensions in application to VAWTs. The self-start problem is associated with

symmetric airfoil shape, if it is solved by new airfoil design it will be a significant contribution in the VAWT field. Therefore, it is necessary to select a proper airfoil which fulfills the low Reynolds number condition as well as aerodynamic load conditions of the VAWT. Typically, a VAWT with a Reynolds number around 500,000 with which there is a high chance of flow separation, and it has been considered to be the most difficult part of the flow physics of an airfoil. However, few airfoils exist which work even for a Reynolds number < 200,000 (Selig *et al.* 1995). The flow under a Reynolds number of 200,000 is a combination of the laminar and turbulent flow, and there is a possibility of the bubble formation which soon separates the flow. One more critical parameter is the boundary layer which is very small as compared to that of the aeroplane wings. All these parameters need to be taken into consideration in the design of a VAWT blade. Apart from the mentioned physics problems associated with the low Reynolds number airfoil, other design problems of VAWT can be summarized as follows:

❶ Self starting issues due to low torque

❷ Low power efficiency

❸ Less adaptable for building integration

The aerodynamics of a VAWT is still not fully developed as the aerodynamics of the HAWT. However, it is possible to predict the performance of a VAWT with available aerodynamic models based on streamtube method (Paraschivoiu 2009).

1.4   An overview of the solution

In last decade, many new design configurations of the VAWT have been invented, and the efficiency has considerably improved as compared to the efficiency of the horizontal axis wind turbine. Significantly improved vertical axis wind turbine configurations and their advantageous are mentioned in Table 1.

The efficiency of a VAWT can be improved by the different methods: aerodynamic design of a VAWT blade, combination of different configurations of the VAWT, use of series of fixed blades infront of the rotor blade, and use of the diffuser to increase the wind speed at the inlet of the rotor. All these methods are well know, and the improvement in the efficiency is a few percents which is not sufficient enough to compare with the efficiency of a HAWT. There has been successful attempts to improve the VAWT efficiency which is comparable with the HAWT (Darrieus 1931), (Ponta *et al.* 2007), (Sharpe *et al.* 2010), (Gorelov *et al.* 2008). Vertical axis wind turbines mentioned in Table 1 use special blade geometry which is expensive, and most of them are complex designs. In a traditional Darrieus turbine, the blades rotate around a central vertical axis. In the variable-geometry oval-trajectory (VGOT) configuration, each blade instead of rotating around a central vertical axis, slides over rails mounted on a wagon formed by a reticulated structure supported by standard train boogies as shown in Figure 1.2 (a) (Ponta *et al.* 2011). Each wagon contains its own electrical generation system coupled to the power wheels, and the electricity is collected by a classical third rail system. The power efficiency is so high due

Table 1.1 Existing VAWT configurations

Sr.No.	Source	Name of Wind Turbine	Efficiency	Advantageous
1.	(Darrieus 1931)	Darrieus rotor egg-beater shape	42%	Suitable for mega watt application
2.	(Islam *et al.* 2007)	Darrieus rotor straight bladed	23%	Simple construction
3.	(Ponta *et al.* 2007)	Darrieus rotor variable geometry oval trajectory	57%	Unique design
4.	(Sharpe *et al.* 2010)	Cross flex wind turbine	38%	Useful in high rise building
5.	(Gorelov *et al.* 2008)	Darrieus-Masgrowe (two tier rotor)	40%	Self start at low wind speed
6.	(Wakui *et al.* 2000)	Combined Savonious and Darrieus rotor	35%	Self start
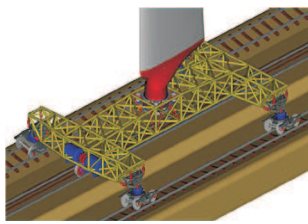
(a) Variable-geometry oval-trajectory wind turbine
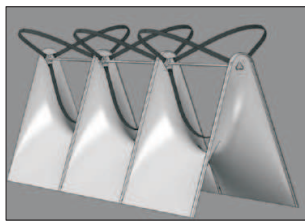
(b) Crossflex wind turbine

(c) Darrieus-Masgrowe two tier rotor

Figure 1.2 Various existing VAWT wind turbines

to the reason that most of the time the blade remains perpendicular to the wind direction which means the inflow wind remains constant in VOGT, whereas a traditional Darrieus rotor blade subject to the variable flow both in magnitude and angle of incident along the path. Secondly, a VOGT configuration increases the area swept by the blade (which depends on the blade height and the trajectory width across the direction of the incoming wind), with a smaller increment in the path length compared to a circular trajectory of traditional Darrieus rotor. It is a highly expensive solution and involves very complemented design procedure due to rail trajectory. A VOGT is not practically feasible in a small-scale wind turbine and also not suitable for urban application where space contains is very tight.

Figure 1.2 (b) shows the Crossflex wind turbine which has a very good aesthetic design and perfectly suitable for building integration along with improved efficiency. The blade design incorporates the low solidity and light weight structure forming highly flexible blades. The inherent advantages of flexibility induces a twisting in the blade during high wind speed conditions which helps improve the aerodynamic performance by optimized flow conditions. Crossflex is the only turbine available for high rise buildings, and despite its many advantages over the traditional Darrieus egg beater shaped wind turbine still, there is an issue of self start. Also, the maximum

efficiency is achieved at high wind speed $> 14m/s$. Figure 1.2 (c) shows the two tier Darrieus-Msgrowe wind turbine by Gorelov et. al. (Gorelov *et al.* 2008). This turbine has an efficiency of the nearly same as the traditional Darrieus rotor; however, a problem of self start has been solved by increased solidity. The question of use in building integration still exists with all above wind turbine configurations except for the Cross flex wind turbine configuration (Sharpe *et al.* 2010), but its maximum efficiency can be achieved at wind speed $> 14m/s$.

In the present PhD project, the problem of a low efficiency of the H-Darrieus straight-bladed VAWT is addressed. The problem of self start with the VAWT can be solved with a proper selection of an airfoil. A VAWT efficiency is proportional to the lift force which in turn corresponds to the lift coefficient of selected airfoil. An increases in the lift coefficient directly increases the power efficiency which is the main focus of this PhD project. The lift coefficient of an airfoil is a characteristic that depends on the shape and the Reynolds number at which it is operating. In a VAWT, it is known that they operates at a very low Reynolds number so by considering Re=200,000 an airfoil is selected which is suitable for this condition. The aim is to improve the efficiency significantly by keeping simplicity in the blade design. A multi-element airfoil technology used in the aviation industry is the economical and most practically feasible solution to the problem (Buhl 2009), (Lew 2011), (GE 2011). Hence a two-element airfoil blade design is incorporated in the VAWT blade design. The challenge involved in this case is the proper selection of an airfoil and the design of a two-element airfoil. Wind tunnel testing of the two-element airfoil is performed to determine the aerodynamic characteristics, mainly lift and drag coefficients. The experimental set-up of $D^2A - VAWT$ is done to test the performance in outdoor environment, and the numerical model is validated. An active blade pitch control mechanism is designed for $D^2A - VAWT$ which is another source of complexity and has been implemented, and specific test results are discussed extensively.

1.5   Research background

The VAWTs have more advantages than the HAWTs in urban and remote location and this has attracted the interest of researchers in the last decade and has resulted in the new configurations of VAWTs designs reviewed in (Eriksson *et al.* 2008) and (Bhutta *et al.* 2012). The main difference in the configurations of the VAWT from the recent development can be found on the website (Seao2). The performance of a VAWT is basically determined by aerodynamic load models in which the flow around the wind turbine blades is analysed. The flow field around the VAWT was first addressed by (Templin 1974). This method is termed as the Single Stream Tube Method (SSTM) originally developed for curved blade VAWT. The SSTM method is based on the approach of propeller or windmill actuator disk theories in which the induced velocity assumed to be constant and directly related to the wind turbine drag. This method overestimates the power output at stalling region of the airfoil, and the maximum rotor efficiency (approximately 0.2) is achieved at low value of the design solidity. Subsequently, the SSTM was improved for the Multiple Stream Tube Model (MSTM) by dividing swept the volume of the turbine as a series of adjacent stream tubes (Strickland 1975). MSTM uses the Glauert's blade element theory and the time average stream wise momentum equation. A theocratical model for defining a flow physics around VAWTs is given in Chapter 4. Further, the MSTM was improved by dividing

the rotor into two halves: upwind zone and downwind zone. The reduction of induced velocity at the downwind zone was later introduced in (Paraschivoiu 1981) which was named DMSTM. In the mid 1980s a lot of work was done on prediction of the performance of the Darrieus rotor aerodynamics at the Bombardier Aeronautical Chair Research Group, and computer programs were developed (Paraschivoiu 1984). A Stream tube model and a 3D viscous flow model were based on steady incompressible flow conditions, which were not sufficient enough to predict correct aerodynamic loads.

There are very few articles which use computational fluid dynamics simulation to predict the correct performance. A 3D simulation of a VAWT using CFD software is performed, and results are validated by a wind tunnel test in recent research (Castelli *et al.* 2011). Still, the power efficiency is observed to be quite low. There is a scope for researching in aerodynamics of airfoil and rotor design to improve the power efficiency of VAWTs. In general, a VAWT consists of three blades with a straight, curved, helical or spiral geometry to improve the efficiency. Aerodynamic blade design helps improve the efficiency. Therefore, the aerodynamic characteristics (lift and drag coefficients) of airfoils are very important to obtain correctly for maximum power output from the VAWT. The NACA series symmetric airfoils are mainly used for VAWT blade design. In a study conducted at TU Delft (Claessens 2006), a new airfoil was designed with refer to NACA0018 airfoil. Du-06-W200 airfoil was designed with an increase in thickness by 2% and in the camber by 0.8%, which improved the power coefficient by 8% at a tip speed ratio of 3.

Despite great variety in the VAWT configurations, they all suffer from low starting torque, low lift force which results low efficiency. To achieve the highest possible power coefficient, a high lift airfoil design configuration is proposed in the current PhD research. High lift coefficients for airfoils are obtained by multiple element airfoil technology used in the aviation industry. The working principle of a multiple element airfoil is nicely addressed in (Smith 1975). In the current PhD research, two airfoils are used to design a VAWT blade. 2D CFD simulations are performed for double-element airfoil and validated with wind tunnel testings. The prototype of proposed design of a VAWT is manufactured, and testing of the new design is done. The design incorporates the active blade pitching mechanism to change the blade pitch angle.

The proposed design configuration of VAWT is termed $D^2A - VAWT$ in the current PhD project. The research includes a review of airfoil designs for use in VAWTs and design of different VAWTs.

1.6   Thesis outline

Chapter 1 '*Introduction*' : A review of historical and modern wind energy convertors is given in section 1.1. A short explanation of the importance of a VAWT compared to a HAWT is also described. Section 1.2 focus on polical influence on development of VAWTs and the current government policies. Section 1.3 summarizes problems in understanding flow physics around a VAWT and technological challenges of a small VAWT. The existing solutions to these challenges are described in section 1.4. A research background of the development of the vertical axis wind turbine is discussed in section 1.5, and in section 1.6 PhD thesis outline is given.

Chapter 2 '*Wind Turbine Theory*': A method of double actuator disk theory is explained in section 2.1 used to describe the aerodynamics of VAWT. Section 2.1 describes the blade element moment method for VAWT. A comparison of HAWT and a VAWT is given in section 2.3. Further, section 2.4 gives various methods to improve the efficiency of the H-Darrieus VAWT with numerical examples of each method. A comparative study of different methods such as number of blades, airfoil shape, two-element airfoil and the active blade pitch control for efficiency improvement is discussed. Finally, a concluding remarks are of the chapter 2 are mentioned in the section 2.5.

Chapter 3 '*The Multi-Element Airfoil*': A review of multi-element airfoil technology is given in section 3.1 with possible adaption in a wind turbine application. The technology is well-know in the aviation industry and has not been practically implemented into the wind turbine area. However, use of multi-element airfoil in application to wind turbine have been recently initiated. Section 3.2 focuses on the airfoil selection and the two-element airfoil arrangement and explained the design used in this PhD thesis. Section 3.2 describes the wind tunnel testing and results are also be discussed. In a section 3.4 a performance of a two-element airfoil is determined by a CFD simulation, and a validation of a CFD model is carried out by a wind tunnel experiment on the test specimen. Section 3.5 concludes the outcome of Chapter 3 and completion first milestone of this PhD thesis.

Chapter 4 '*Aerodynamic Load Modeling*': Section 4.1 describes the different aerodynamic models used in the performance evaluation of VAWT. Also, numerical example of all models is given. Section 4.2 describes the mechanical model of $D^2A - VAWT$ with details of geometric parameters of the experimental set-up. An aerodynamic load model is derived for $D^2A - VAWT$ by using the double multiple stream tube method (DMSTM). Section 4.3 the gives results of the numerical simulation of $D^2A - VAWT$ for performance evaluation, and it is validated by experimental results. Section 4.4 gives the concluding remarks of the design of $D^2A - VAWT$ and its performance improvement due to implementation of a two-element airfoil.

Chapter 5 '*Pitch Controller*': This chapter is dedicated to the pitch control design for VAWT. Section 5.1 gives a review of the pitch control mechanism used for a VAWT. A design of an active blade pitch control mechanism for VAWT is critical due to the rotor speed and the actuator complexities. Therefore, it is separately addressed in section 5.2. Improvement in the efficiency of a $D^2A - VAWT$ due to active blade pitch controller is numerically determined and explained in section 5.3. Finally, concluding remarks of Chapter 5 are summarized.

Chapter 6 '*Conclusion and Future Research*':Finally, concluding remarks from this thesis are given and future research work is mentioned.

Necessary details such as theories, mathematical expressions, nomenclatures are documented in the appendices followed by the list of references.

CHAPTER 2
Wind turbine theory

Efficiency of a wind energy convertor is the amount of kinetic energy of the wind flow which can be practically extracted. This quantity is given by a dimensionless number or in terms of percentage. According to the Betz's limit theoretically 59.4% of the kinetic energy of the wind flow can be converted to mechanical energy. However, in practice the maximum achievable energy possible is up to 45%, claimed by manufactures of the mega watt wind turbine (Hansen 2008). It is important to know the efficiency of a HAWT and a VAWT for a comparative study. There are different methods of determination of efficiency, and they have all been experimentally validated. A momentum method and blade element method are very popular in HAWTs and VAWTs [(Hansen 2008), (Paraschivoiu 2009)]. The aim of this chapter is to derive the equations for efficiency calculation and compare the efficiency of the HAWT and a VAWT with an numerical example. Finally conclusions on the importance of the efficiency of wind energy convertors, and summarized objective of the PhD thesis are given.

2.1 Double actuator disk momentum theory for VAWT

In vertial axis wind turbines, the wind passes twice through the rotor swept area and the induced velocities differ on the upstream and the down stream half of the swept surface. The VAWT can be represented by two disks in tandem at each level of the rotor according to the Lapin's concept (Lapin 1975) as shown in Figure 2.1. The first disk represents the upstream half of the surface swept by the blades, and the second disk represents the down stream half of the rotor. In the actuator disk theory, the induced velocity on the upstream half of the rotor V_1 is constant and similar for V_2 on the down-stream surface. With this assumption, the drag coefficients C_{D_1} and C_{D_2} are calculated for the upstream and down-stream halves of the blade rotation. The drag coefficient may also be calculated by a momentum theory, then compared to those derived from the blade theory. When both theories converge, an iterative procedure is used to obtain the solution. Once the induced velocities on each disk and the drag coefficients are known, we can determine the loads and the performance of the Darrieus rotor.

In the momentum theory, it is assumed that the flow is inviscid, steady, one dimensional and without swirl (Newman 1983). With the above assumptions, (Newman 1983), showed that the maximum power coefficient for the double disks is $C_{pmax} = 16/25 = 0.64$ compared with the single disk Betz limit $16/27(0.593)$.
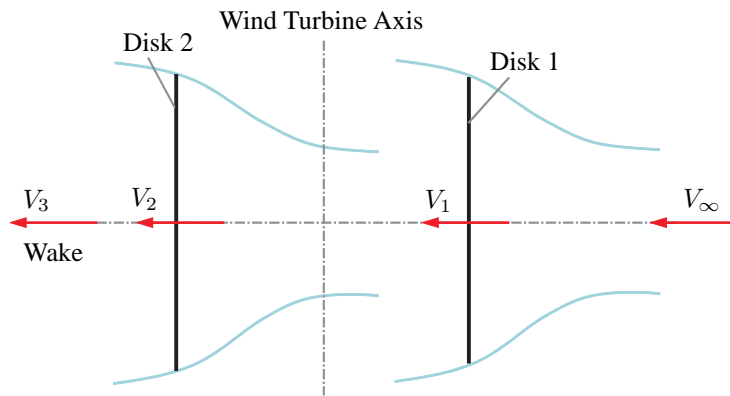
Figure 2.1 A pair of actuator disk in tandem.

The static pressure and the velocity in the approaching undisturbed stream are ρ_∞ and V_∞ respectively. In Figure (2.2) the streamline pattern is illustrated.
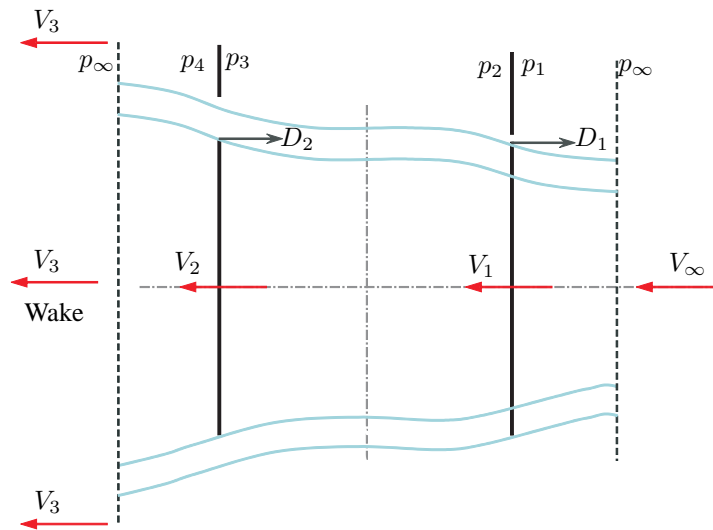
Figure 2.2 Streamline pattern across a pair of actuator disk

Let A be the total area of each disk, V the induced velocity in the first disk and V_1 the induced velocity through the second actuator disk. The pressure drops on the first actuator disk from p_1 and p_2 and the resulting drag is denoted by the D_1. Similarly, the drag on the second actuator disk D_2 is a result of the pressure drop from p_3 to p_4 (Fig. 2.2). The momentum equation is applied to two control volumes shown in Fig 2.3 (the annulus control volumes 1 and 2) and the control volumes 3, 4, 5 in Fig 2.4.
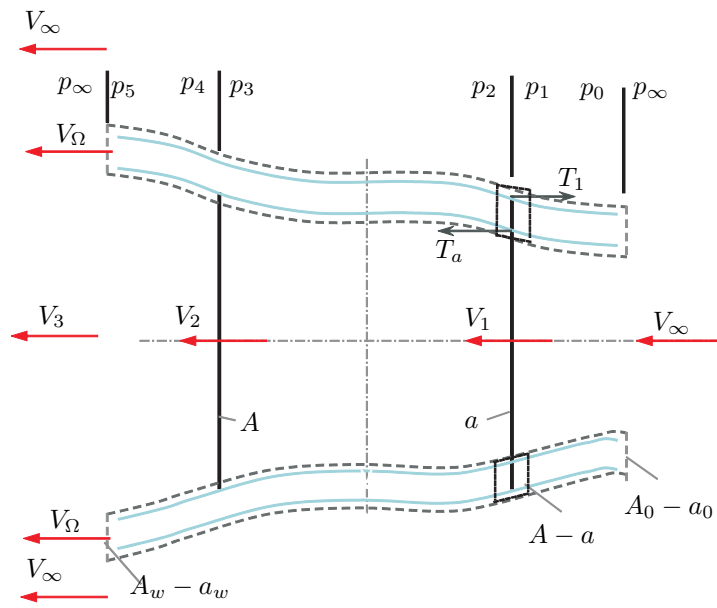
Figure 2.3 Annulus control volume 1 and 2
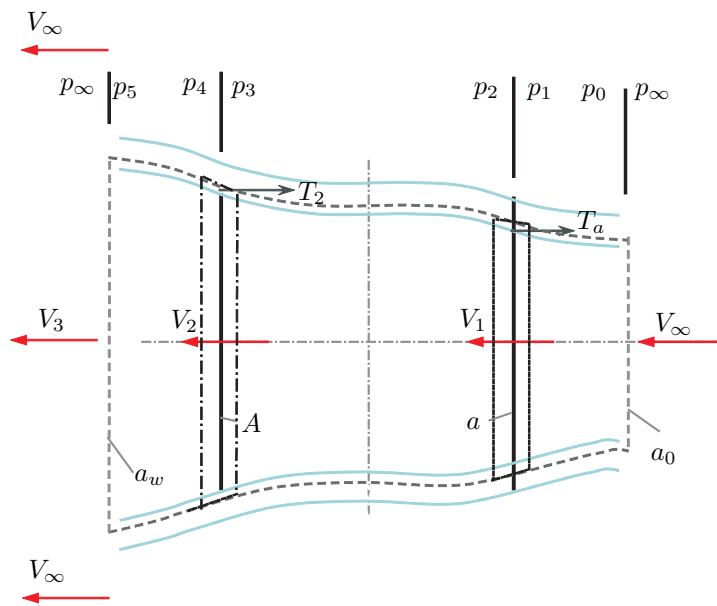
Figure 2.4 Annulus control volume 3,4, and 5

Control volume 1

Continuity equation:

$$\rho \left(A_0 - a_0 \right) V_\infty = \rho \left(A - a \right) = \rho \left(A_w - a_w \right) V_\infty \tag{2.1}$$

Bernoulli's equation:

$$p_\infty + \frac{1}{2}\rho\,V_\infty^2 = p_1 + \frac{1}{2}\rho\,V_1^2 \tag{2.2}$$

$$p_2 + \frac{1}{2}\rho\,V^2 = p_\infty + \frac{1}{2}\rho\,V_\Omega^2 \tag{2.3}$$

Momentum equation:

$$T_1 - T_a = \rho\,(A - a)\,V_1\,(V_\infty - V_\Omega) \tag{2.4}$$

Control volume 2

Momentum equation:

$$(p_1 - p_2)\,(A - a) = T_1 - T_a \tag{2.5}$$

Control volume 3

Continuity equation:

$$\rho\,a_0\,V_\infty = \rho\,a\,V_1 = \rho\,A\,V_2 = \rho\,a_w\,V_3 \tag{2.6}$$

Bernoulli's equation from 0 to 1:

$$p_\infty + \frac{1}{2}\rho\,V_\infty^2 = p_1 + \frac{1}{2}\rho\,V_1^2 \tag{2.7}$$

$$\tag{2.8}$$

from 2 to 3:

$$p_2 + \frac{1}{2}\rho\,V_1^2 = p_3 + \frac{1}{2}\rho\,V_2^2 \tag{2.9}$$

$$\tag{2.10}$$

from 4 to 5

$$p_4 + \frac{1}{2}\,\rho\,V_2^2 = p_\infty + \frac{1}{2}\,\rho\,V_3^2 \tag{2.11}$$

Momentum equation:

$$T_a + T_2 = \rho\,A\,V_1\,(V_1 - V_3) \tag{2.12}$$

Prasad V.D. Chougule

Control volume 4 and 5

Momentum equation:

$$(p_1 - p_2)\, a = T_a \tag{2.13}$$

$$(p_3 - p_4)\, A = T_2 \tag{2.14}$$

Drag coefficient of the upstream actuator disk

By combining equations 2.4 and 2.5, we get:

$$p_1 - p_2 = \rho\, V\, (V_\infty - V_\Omega) \tag{2.15}$$

and from equation 2.2 we get:

$$p_1 - p_2 = \frac{1}{2}\, \rho\, (V_\infty^2 - V_\Omega^2) \tag{2.16}$$

by combining equations 2.15 and 2.19:

$$V = \frac{V_\infty + V_\Omega}{2} \tag{2.17}$$

$$\tag{2.18}$$

From equations 2.19 and 2.13, we obtain:

$$T_a = \frac{1}{2}\, \rho\, (V_\infty^2 - V_\Omega^2)\, a \tag{2.19}$$

Substituting the value of V_Ω from equation 2.17, and the value of a from equation 2.6, we obtain:

$$T_a = 2\, \rho\, (V_\infty - V_1)\, A \tag{2.20}$$

Substituting the results obtained in equation 2.6, and knowing that $T_1 = D_1$ results in:

$$D_1 = 2\, \rho\, A\, (V_\infty - V_1)\, V_1 \tag{2.21}$$

Taking into account 2.6 and 2.13 and substituting 2.20 in 2.5.
Defining the drag coefficient C_{D_1} as:

$$C_{D_1} = \frac{D_1}{\frac{1}{2}\, \rho\, V_\infty^2\, A} \tag{2.22}$$

in other form, we obtain:

$$C_{D_1} = 4 \frac{V_1}{V_\infty} \left(1 - \frac{V_1}{V_\infty}\right) \tag{2.23}$$

as the drag coefficient of the upstream actuator disk.

Drag coefficient of the down-stream actuator disk

If we substitute equations 2.20, 2.13 and 2.6 into the momentum equation 2.12 of control volume, (Fig.2.4), we get:

$$V_3 = V_2 \pm \left[V_2^2 + 4V_1\left(V_1 - V_2 - V_\infty\right) + V_\infty\left(2\,V_2 + V_\infty\right)\right]^{1/2} \tag{2.24}$$

Konwing that $T_2 = D_2$ and the combining equations 2.20 and 2.12 we obtain:

$$D_2 = \rho\,A\,V_2\left(2\,V_1 - V_\infty - V_3\right) \tag{2.25}$$

defining the drag coefficient C_{D_2} as:

$$C_{D_2} = \frac{D_2}{\frac{1}{2}\,\rho\,V_\infty^2\,A} \tag{2.26}$$

and combining it with the equation 2.24 results in:

$$C_{D_2} = 2\frac{V_2}{V_\infty}\left(2\frac{V_1}{V_\infty} - \frac{V_2}{V_\infty} + \left[\left(\frac{V_2}{V_\infty}\right)^2 + 2\frac{V_2}{V_\infty} + 4\frac{V_1}{V_\infty}\left(\frac{V_1}{V_\infty} - \frac{V_2}{V_\infty} - 1\right) + 1\right]^{1/2} - 1\right) \tag{2.27}$$

as the drag coefficient of the down-stream actuator disk. We thus obtain the drag coefficient for each actuator disk. Note that the drag coefficient of the upstream actuator disk C_{D_1} is a function of only $\frac{V_1}{V_\infty}$ and that the down-stream C_{D_2} is a function of $\frac{V_1}{V_\infty}$ and $\frac{V_2}{V_\infty}$.

The overall drag of the wind turbine is the summation of the drag coefficient of the upwind and downwind actuator disks. Thus the coefficient forms;

$$C_D = C_{D_1} + C_{D_2} \tag{2.28}$$

There are some theoretical limitations to the values of C_{D_1} and $\frac{V_1}{V_\infty}$. We can invert equation 2.23 and obtain the velocity ratio $\frac{V_1}{V_\infty}$ as a function of the drag coefficient C_{D_1}

$$\frac{V_1}{V_\infty} = \frac{1}{2} + \frac{1}{2}\sqrt{1 - C_{D_1}} \tag{2.29}$$

The maximum theoretical value of C_{D_1} is 1.0 at $\frac{V_1}{V_\infty} = 0.5$.

Prasad V.D. Chougule

2.2 Blade element momentum method for VAWT

The classical BEM model from (Glauert 1935) is used in case of a vertical axis wind turbine with change in the momentum theory which is based on double actuator disc theory. The Blade Element Momentum method couples the momentum theory with the local events taking place at the actual blades. A diagram of the velocity the airfoil fluid flow is given in the follwing figure.
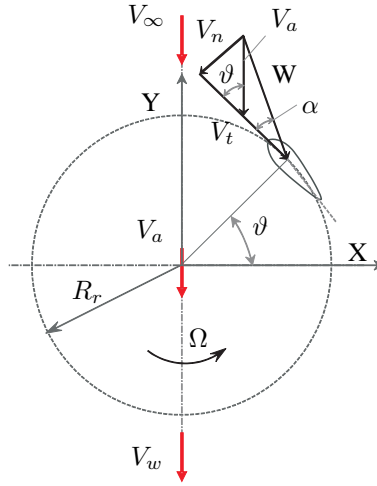
Figure 2.5 Velocity components for blade 1

Flow characteristics

The velocities at the inlet of the rotor and the outlet of the rotor are different as can be seen in Figure (2.5). Inlet velocity is the free-stream velocity represented by V_∞ and outlet velocity is the wake velocity V_w. The tangential velocity component $V_t(\vartheta)$ and the normal velocity $V_n(\vartheta)$ component acting on the rotor blade can be expressed as (Darrieus):

$$\left.\begin{aligned} V_t(\vartheta) &= R_r\,\Omega + V_a\cos(\vartheta) \\ V_n(\vartheta) &= V_a\sin(\vartheta) \end{aligned}\right\} \tag{2.30}$$

A force diagram of blade element is given in Figure 2.6.

Referring to Figure 2.6 , the angle of attack α can be expressed as:

$$\alpha(\vartheta) = \tan^{-1}\left(\frac{V_n(\vartheta)}{V_t(\vartheta)}\right) \tag{2.31}$$

Substituting the values of $V_t(\vartheta)$ and $V_n(\vartheta)$ from equation 4.3, and we get, angle of attack as
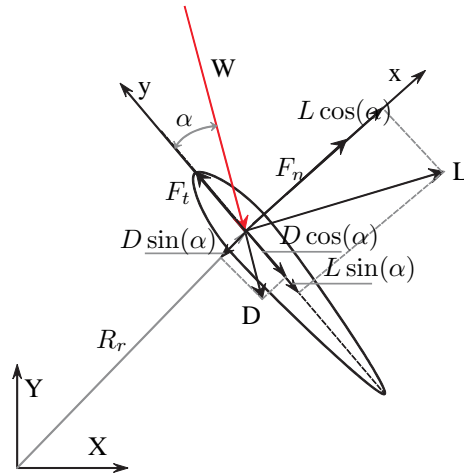
Figure 2.6 Force diagram of airfoil

follows:

$$\alpha(\vartheta) = \tan^{-1}\left[\frac{\sin(\vartheta)}{\frac{R_r\,\Omega}{V_a} + \cos(\vartheta)}\right] \tag{2.32}$$

Variation of local relative flow velocity

The variation of the local relative flow velocity W can be given as follows:

$$W(\vartheta) = \sqrt{V_t^2(\vartheta) + V_n^2(\vartheta)} \tag{2.33}$$

Reynolds number is defined as:

$$Re = \frac{c\,W}{\nu} \tag{2.34}$$

Lift and drag coefficients of of the blade element are given as follows (Darrieus):

$$\left.\begin{aligned}
c_L &= \frac{dL}{\frac{1}{2}\,\rho\,W^2\,c\,dh}\\[2mm]
c_D &= \frac{dD}{\frac{1}{2}\,\rho\,W^2\,c\,dh}
\end{aligned}\right\} \tag{2.35}$$

Blade element forces

The directions of lift (L) and drag (D) forces and their tangential ($F_t(\vartheta)$) and normal ($F_n(\vartheta)$)

force components are shown in Figure 2.6. The tangential force coefficient ($C_t(\vartheta)$) is basically given by an addition of tangential components of lift and drag forces. The normal force coefficient ($C_n(\vartheta)$) is the difference between the normal components of lift and drag forces. The expression of tangential force coefficient ($C_t(\vartheta)$) and normal force component ($C_n(\vartheta)$) are given as:

$$\left.\begin{aligned} C_t(\vartheta) &= c_L \sin\alpha + c_D \cos\alpha \\ C_n(\vartheta) &= c_L \cos\alpha - c_D \sin\alpha \end{aligned}\right\} \tag{2.36}$$

The lift (c_L) and drag (c_D) coefficients in equation (2.36) are obtained from an experiment for the particular Reynolds number. The tangential forces (dF_t) and normal forces (dF_n) of the blade element can be defined as follows,

$$\left.\begin{aligned} dF_t(\vartheta) &= \frac{1}{2}\,\rho\,c\,dh\,C_t\,W^2 \\ dF_n(\vartheta) &= \frac{1}{2}\,\rho\,c\,dh\,C_n\,W^2 \end{aligned}\right\} \tag{2.37}$$

where dh is the height of the blade element and ρ is the air density.

Shaft torque and power

$$dM = dF_t\,\Omega \tag{2.38}$$

$$C_p = \frac{\bar{M}\,\Omega}{\frac{1}{2}\,\rho\,A\,V_\infty^3} \tag{2.39}$$

where $\bar{M}$ is the total shaft torque of the rotor depnding on the azimuthal angle of the rotor.

$$\bar{M} = \frac{1}{2\pi} \int_0^{2\pi} \int_0^N \int_0^H dM\,\Omega \tag{2.40}$$

Blade element

$$dF_x = dF_t\,\cos(\vartheta) + dF_n\,\sin(\vartheta) \tag{2.41}$$

$$d\bar{F}_x = N\,2\frac{\Delta\vartheta}{\pi}\,dF_x \tag{2.42}$$

$$C_{TH} = \frac{d\bar{F}_x}{\frac{1}{2}\,\rho\,V_\infty^2\,dA_s} \tag{2.43}$$

$$dA_s = dh\,r\,d\vartheta\,\sin\vartheta \tag{2.44}$$
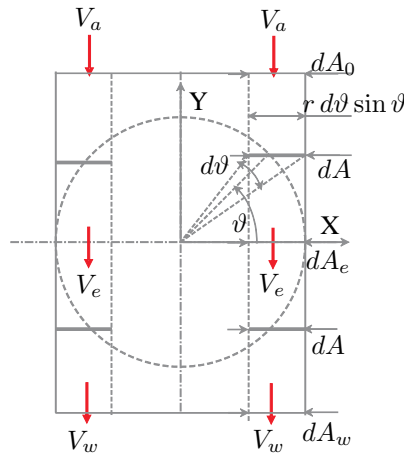
Figure 2.7 Blade element method for VAWT

Momentum theory

$$a = \frac{V_a}{V_\infty} \tag{2.45}$$

$$dF_x = 2\,\rho\,dA_s\,V_a(V_\infty - V_a) \tag{2.46}$$

$$
\begin{aligned}
C_{TH} &= \frac{dF_x}{\frac{1}{2}\rho\,V_\infty^2\,dA_s} \\
&= \frac{2\rho\,dA_s\,V_a(V_\infty - V_a)}{\frac{1}{2}\rho\,V_\infty^2\,dA_s} \\
&= 4a(1-a)
\end{aligned} \tag{2.47}
$$

Glauert correction factor:

$$C_{TH} = \frac{26}{15}(1-a) + \frac{4}{15} \tag{2.48}$$

The blade element momentum method for a VAWT has the follwoing limitations:

♦ The circular path is simplified in two actuator disks.

♦ The momentum equilibrium is applied only in 1-D (axial direction).

♦ The axial expansion is generally neglected or not correctly or completely implemented.

♦ The turbulent wake state correction is taken from HAWT corrections.

♦ No (or weak) interaction between stream tubes.

♦ Tip losses correction is of doubtful application for VAWT.

◆ Complex geometry not resolvable from a fluid dynamic point of view.

◆ Unsteady fluid dynamic effects are of difficult implementation.

2.3   Comparision of HAWT and VAWT

Horizontal axis wind turbines and vertical axis wind turbines can be compared in many different aspects in terms of construction, cost, efficiency and application. The present PhD work focuses on simple construction, low cost and high efficient technological development of VAWT considering small power production.

Construction: HAWT mainly consists of three blades with a rotor axis parallel to the wind flow direction. HAWT has a yaw mechanism to keep the rotor plane in to the wind flow direction to optimize the power production. A blade pitch mechanism is needed to extract more power output. Both systems are expensive and complicated. The VAWT considered in this PhD thesis consists of three straight blades in which rotor axis lies perpendicular to the wind flow. Due to a low operating speed the VAWT is quiet and can be used in an urban area without being trouble to neighborhood. Also, the aesthetic look of the VAWT makes it attractive.

Cost: The cost of the VAWT is almost 50% less than the HAWT, which makes it more attractive as electricity bills are constantly increasing and the demand for an off-grid electricity system has increased in last two decades (Malcolm 2003). The VAWT suits perfectly in this economical situation and in the advancement of technology.

Efficiency: Efficiency of the HAWT is almost double than that of the VAWT, which makes the VAWT quite unsuccessful. But in this PhD thesis, a new design is proposed which improves the efficiency of the VAWT and makes it more promising than HAWT. The common measure of the efficiency of a rotor is the power coefficient C_p. It is the fraction of the total kinetic energy passing trough a certain swept area that is captured by the rotor, which is given as:

$$C_p = \frac{P}{0.5\,\rho\,A\,V^3} \tag{2.49}$$

where P is the power captured, ρ is the density of air, A is the swept area, and V is the wind speed. There are certain limits on this fraction of the kinetic energy that can be captured, and they depend on the type of wind turbine. As per Betz limit with a horizontal axis wind turbine can convert only 59% of kinetic energy into mechanical energy (Betz 1966). Figure 2.1 shows the performance coefficients typical of several of the main types of wind turbines. The C_p value is plotted against the tip speed ratio which is a non-dimensional term measuring the wind speed and is defined as the ratio of speed of the blade tip to the ambient wind speed.

In Figure 2.8 a comparison of aerodynamic coefficients of the common types of wind turbines from (Hau and Renouard 2006) originally from (Wilson and P.B.S.Lissaman 1974) are given. The maximum C_p value measures the maximum efficiency, but most wind turbines do not operate
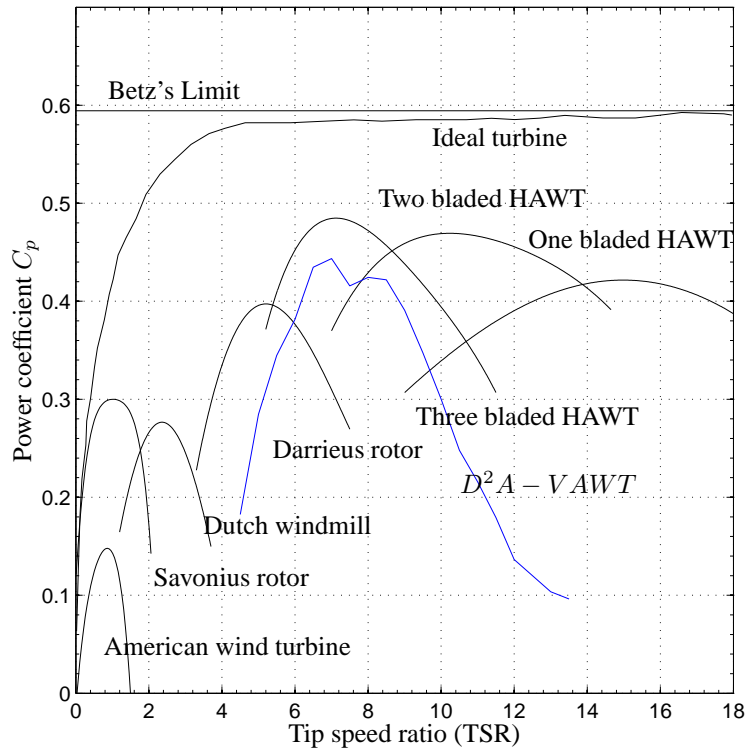
Figure 2.8 Aerodynamic efficiency of wind turbines with proposed $D^2A - VAWT$ represented by red solid line (Mau (2006))

at the optimum tip speed ratio all of the time but over a range of wind speeds and a range of tip speed ratios. Therefore, the width of the curves in Figure 2.8 is also important; a very broad curve indicates that the machine can be efficient over a wide range of wind speeds. It should be noted that if the rotor rpm is constant then the tip speed ratio is inversely proportional to the wind speed.

Machines such as the Savonius and the American wind turbines have relatively low maximum C_p values and are limited to low tip speed ratios. This means that for a given wind speed, the rotors will turn relatively slowly. This, in turn, implies that the torque in the drive shafts will be higher since torque is equal to power divided by rotational speed; this is advantageous for applications such as water pumping.

Figure 2.8 is a fairly accurate indication of maximum power coefficient. The peak C_p values of current HAWTs are close to 0.50 whereas the maximum C_p values that have been recorded for most VAWTs are in the range of 0.35 to 0.40. (However, C_p values of up to 0.46 were claimed for the Sandia 17-m prototype (Maydew and Klimas 1981). Thus, the HAWT technology has at

least a 20% advantage in power capture by this measure. However, the peak C_p is not the only measure of overall economics.

In Figure 2.8 the power coefficient of the proposed $D^2A - VAWT$ is shown by solid blue line. Transnational three bladed VAWT with single airfoil design has power coefficient of under 0.23 whereas the proposed $D^2A - VAWT$ with double-element airfoil could reach power coefficient upto 0.43 without pitch control in place.

2.4 Methods to improve efficiency of wind turbine

2.4.1 Rotor solidity

Rotor solidity is the first essential parameter to be considered in the VAWT design. Rotor solidity defines the optimal operating speed of the rotor which is given by a dimensionless number σ defined as ratio of turbine blade area to the swept area S.

$$\sigma = \frac{N\,c}{D} \tag{2.50}$$

where N is the number of blade, c is the chord length, and D is the rotor diameter. High value of solidity gives a peak power output at a low rotational speed. Here, it is very important to define the number of blades in the VAWT design. It is been understood that the number of blades for the VAWT (three blades) is the best for optimal power production (Castelli *et al.* 2012), (Paraschivoiu 2009).
Figure 2.9 shows the effect of solidity on the aerodynamic efficiency of the rotor determined by CFD method (Castelli *et al.* 2012). It can been seen from the Figure 2.9 that the higher the solidity lower the power production is. Also, if the rotor solidity is less, then the operating range of the VAWT increases which makes it noisy during operation. It means a rotor solidity must to be addressed first. A numerical simulation is performed for three different configurations of the VAWT which includes three, four and five blades. An NACA0025 airfoil profile is used for this numerical simulation.

2.4.2 Shape of airfoil

Airfoils are broadly classified into symmetric and non symmetric airfoils. Many of such airfoils have been designed and optimised for flight operation in different physical conditions. Usually airfoils designed for low altitude gliders are essentially symmetric in nature with a high thickness compared to the one used for high altitude and faster aircrafts. There has been very few airfoils which have been specifically designed for a VAWT application. A flow physics around these aircraft and the VAWT resembles. Therefore a symmetric airfoil can be modified and used for the VAWT blade design. Recently, a study has been done by (Mohamed 2012) in which twenty such symmetric and non symmetric airfoil are analysed by a 2D CFD simulation to see which one is better for a VAWT application.
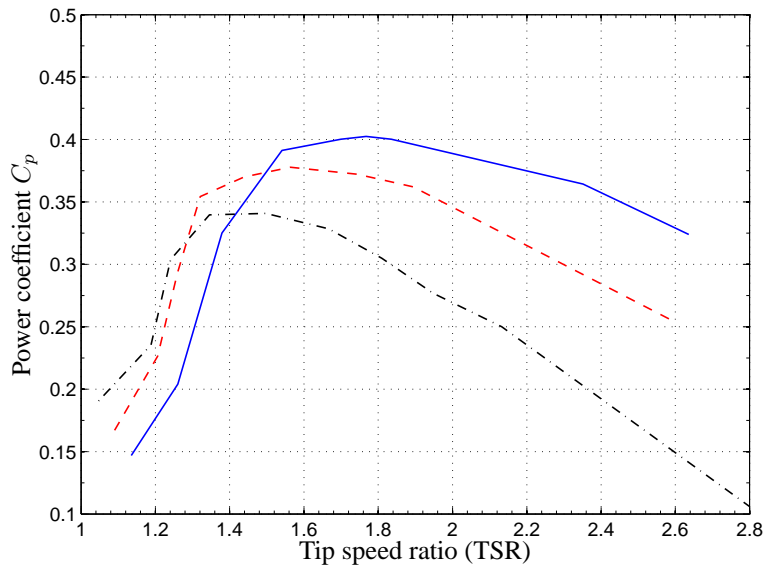
Figure 2.9 Effect of solidity on power coefficient (Castelli 2012) .
——— : Three blades.   – – – : Four blades .   – - – - – : Five blades

Five different series of profiles are studied mainly the symmetric NACA00XX, and the non sym-
metric NACA63XXX, S Series, A Series and FX Series are studied. A simulation is performed
for a rotor with the solidity $\sigma = 0.1$ and in the range of tip speed ratio 2 to 10. It can be pointed
out from study by (Mohamed 2012) that, the use of an NACA's symmetric either non symmetric
profile is not the best choice. The S series profile S-1046 shows promising results in this study
with maximum power coefficient $C_p = 0.4051$.

From Figure 2.10, the H-Darrieus VAWT is less efficient than the HAWT based on an NACA00XX
and NACA63XXX series airfoil shapes in the design. However, it is interesting to see that the
airfoil shapes S-809,S-1046, FX71L150, FXL142 and FXLV152 are showing higher efficiency
than the traditionally used airfoil shapes as in the case of H-Darrieus VAWT with a solidity
$\sigma = 0.1$. Increased power efficiency for S-series, FX-series comes with the decrease in the oper-
ating range of the VAWT. In other words, for symmetric airfoil stall occurs later than in the case
of a non-symmetric airfoil. This means symmetric airfoil helps to delay the stall situation which
is not good in wind turbines. However, the less operating range, i.e the tip speed range, means
maximum power coefficient can be achieved at low wind speed which is the biggest advantage
of non symmetric, S series and FX series airfoils. The delaying of stall can be achieved by a
method explained in subsection 2.4.4 of this chapter: 'Multi element airfoil' which is the most
attractive part of this PhD thesis.
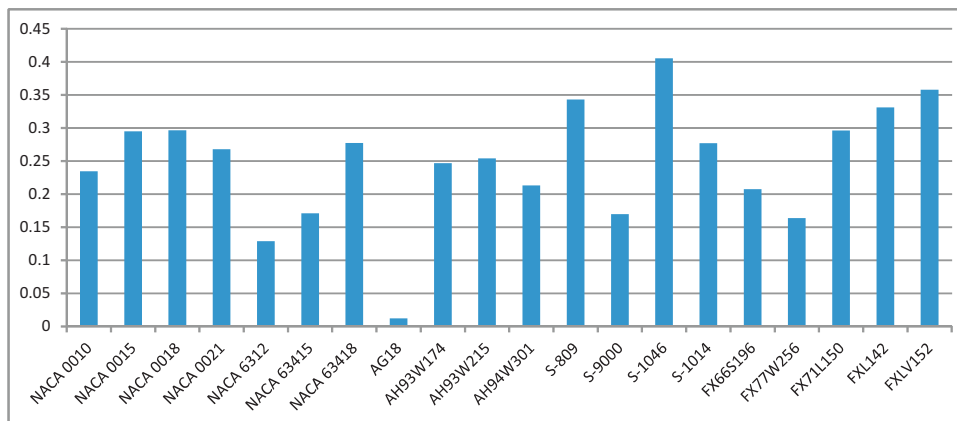
Figure 2.10 Power coefficienct of VAWT depends on different airfoil shape (Mohamed 2012)

.

2.4.3 Blade pitch control

Blade pitching in a VAWT has been understood and well studied since 1990s. The three different methods of blade pitch control mechanism are given in (Lazauskas 1992). Also, a comparison between these three methods is explained with respect to the complexities in the design and the cost. The sinusoidal forced pitch control mechanism comes under the active pitch control whereas the self-acting stabilized pitch control and self-acting mass stabilized pitch control come under the active blade pitch control type. The passive control mechanisms are more commonly found due to its low cost compared to the the active blade pitch control system. The active blade pitch control system is a complicated and an expensive control elements. Due to the development in electronics and its cost the active pitch control system has been implemented by some researchers in order to study the importance of the active pitch control. These research projects have been documented and published, and their improvement in the power coefficient of a VAWT due to active blade pitch control and can be found in (Miau *et al.* 2012) and (Duncker *et al.* 2010). In report (Duncker *et al.* 2010), an individual pitch control, and a collective pitch control have been compared, and it was found that the individual pitch control improved the efficiency and helped to start the turbine at a lower tip speed ratio. In other words, maximum power coefficient can be obtained at lower tip speed ratio as can been seen in the Figure 2.11.

Implementation of collective blade pitch control is simple and cheaper, but from the performance of a VAWT it is found that the improvement in the efficiency is not considerable. Whereas the performance advantages of individual pitch control were promising and the system utilizing individual pitch control was selected by the author. In this PhD thesis, an active blade pitch control mechanism and sinusoidal blade pitch control are compared. The focus is on individual blade pitch control in which an optimized pitch angle is calculated for optimized power output for $D^2A - VAWT$, as well as due to simplicity of sinusoidal pitch control mechanism is also addressed.
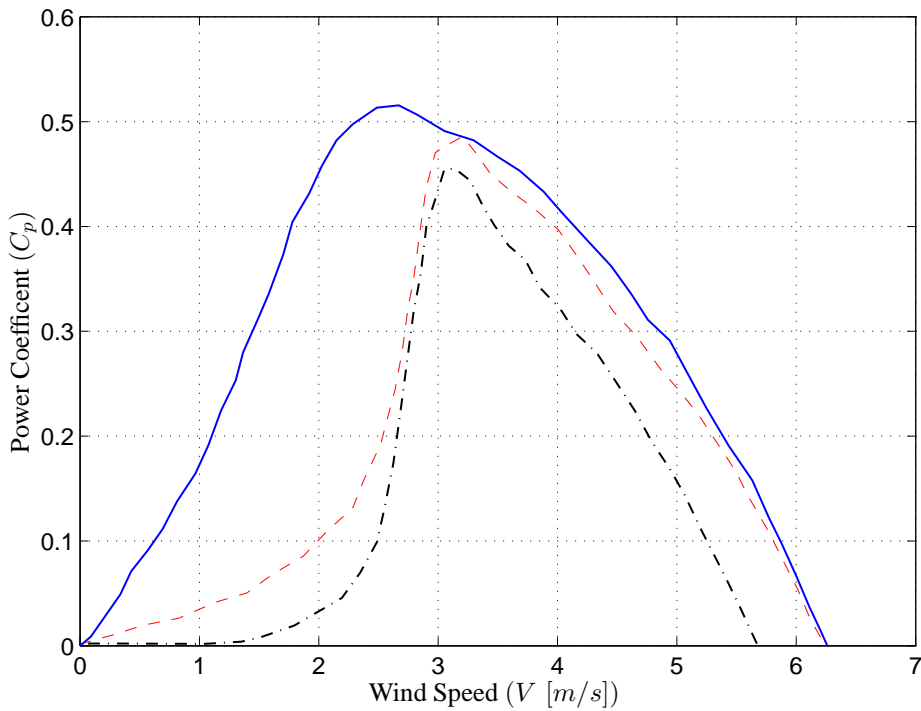
Figure 2.11 Power coefficient of VAWT at different pitch control types (Duncker 2010).
——— : Individual pitch control.   − − − :Collective pitch control.   − − − − −: Without pitch control

2.4.4   Multi-element airfoil

In a VAWT, the airfoil used has not been specifically designed. However, the study performed by (Mohamed 2012) showed that the thin airfoils have a high power efficiencies. A summary of the results from the use of low speed airfoils can be found in technical report by (Williamson *et al.* 2012). Maximum power coefficient is achieved at a high tip speed ratio as discussed in the section 'Shape of Airfoil' in this chapter. A high power coefficient comes with drawback of VAWT operating with the high tip speed ratio, and also the airfoil stalling occurs at a low angle of attach which affects the total power output of the VAWT.

Therfore, in this PhD thesis a multi-element airfoil is used for high lift and delay in the stall angle. The main purpose is to increase the lift of the airfoil; therefore, it is also called high lift airfoil. Multi-element airfoil is well studied and documented in the aviation industry for a century now. It is the novelty of this PhD thesis to introduce a two-element airfoil design in a straight-bladed VAWT. In two-element airfoil two different airfoils fixed to each other with a specific position and orientation. A detailed theory and design of the two-airfoil design is given in (James 1977). Figure 2.12 shows the typical lift coefficient for a single and two-element airfoil.
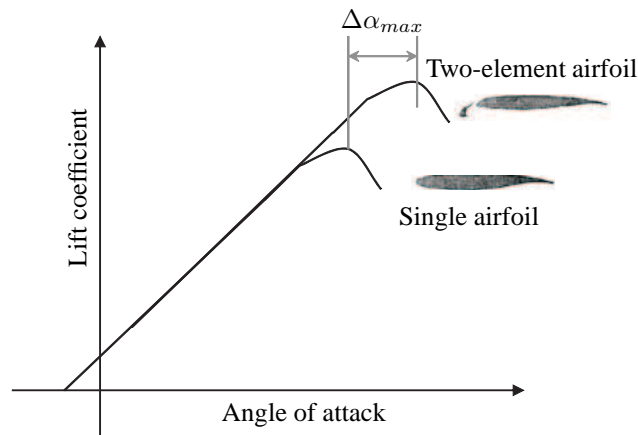
Figure 2.12 Lift coefficient for single and double-element airfoil (Dam 2002)

It is an advantages to have a two airfoil design instead of the traditional single airfoil design in a VAWT. However, it has not yet been proven that the method will actually work for a VAWT. The main reason for this is the application of high lift airfoil in an aircraft, but a wind turbine has totally different flow physics. A detailed review of high lift airfoil and its applicability in a wind turbine is given in Chapter 3. The central focus of this PhD thesis is to prove that the two-element airfoil design increases the power efficiency of the straight-bladed VAWT.

2.5 Concluding remarks

Wind turbine devices have been developed for the last 30 years. A lot of development has specifically been seen in the horizontal axis wind turbines due to their commercial success compared to the vertical axis wind turbine. Theoretically VAWT can extract maximum power coefficient of 0.64. But, it has never attracted by commercial point of view to develop a wind turbine. Egg better type VAWT had went through commercial failure due to the vibration issues of a VAWT and main bearing wear-out problem, and a cyclic loading pattern make it unpopular and the VAWT remains undeveloped.

In this PhD thesis, the focus is on small-sized wind turbines and how the efficiency can be improved. There has been less investment in developing the small-sized wind turbines since the 1980s. But now the scenario has changed, and new designs of wind turbine have been developed since the beginning of this century. Therefore, many patented technologies have claimed to have about improved the efficiency and made better fits for certain applications etc.

In this Chapter 2 a theoretical power efficiency of a VAWT has been derived with a blade element momentum method for the double-actuator disc theory. However, there are some drawbacks of using blade element method for a VAWT, which have still not been resolved. In this chapter, instead of going into the details of computational physics to understand the flow around a VAWT

the focus is on methods to improve an efficiency by adopting multi element airfoil into the rotor design. It is understood that the airfoil should be thin to get the maximum power coefficient in a high tip speed ratio condition, but an airfoil should be thin to operate a VAWT at a low tip speed ratio. Individual blade pitch control is advantageous compared to the collective pitch control.

Innovative two-element airfoil blade design has been used for a VAWT and an experimental testing of airfoil is carried out to determine the performance of a VAWT. The advantages of using two-element airfoil over one airfoil have been discussed in this chapter. It has been documented that the two-element airfoil design works for a large-scale HAWT. The effect of a delaying stall angle due to the two-element airfoil is very advantageous for a VAWT which increases total power output. Whereas increase in lift coefficient gives higher power coefficient. However, in the case of the VAWT it is more critical due to the low operating tip speed ratio. A detailed review of the feasibility of using two-element airfoil for a VAWT is carried out in Chapter 3.

CHAPTER 3
The Multi-Element Airfoil

A multi-element airfoil is also called the high-lift system in the aviation industry. It is a requirement of an aircraft to generate high lift during take-off. The flow physics in a take-off situation of an aircraft is quite similar to VAWT flow physics. The flow physics varies enough to change the effect of a multi-element airfoil on the lift characteristics. Therefore, it is important to understand the development of high-lift systems for aircraft. This chapter is dedicated to a review of the 'multi-element airfoil' and its design with 'double-element airfoil' for use in the VAWT blade. The numerical simulation is performed for the selected double-element airfoil and validated with the wind tunnel testing results. It has been a challenging task right from the selection of an airfoil to the validation of 2D CFD simulation results with wind tunnel testing results.

3.1   Introduction to multi-element airfoil flow physics

A review and the progress in a multi-element high-lift systems can be found in an article by (Dam 2002). This article also focuses on the aerodynamic design of multi-element high-lift systems for transport airplanes. The high-lift system is a complex system in an airplane which makes them expensive, for this reason nowadays focus has shifted towards simplified design of a multi-element airfoil. It is also discussed in this article about the necessity of the high-lift system, design objectives and a constraints. Historically, multi-element airfoil aerodynamics were studied and documented in a number of publications: (Obert 1993),(Abbott *et al.* 1945),(Abbott and Doenhoff 1949),(Cahill 1949)(Young 1953) until 1970s. Later on A.M.O. Smith (Smith 1975), (Smith 1972) created the theoretical basis of the high-lift airfoil.

Flow physics of a multi-element airfoil system

(Smith 1972) and (Smith 1975) have described the aerodynamics of the high-lift system in the early 1970s. In this subsection, a summary of the flow physics explained by A.M.O. Smith is given. In the multi-element, a gap between the airfoils creates the following physical effects as per (Smith 1975):

1. The circulation of a forward element (a slat airfoil) accounts for the reduction in a pressure peak on the down-stream element (a main airfoil). This is called a *slat effect* which delays the stall angle.

2 The loading of a forward element increases due to a disturbance of the flow at the trailing edge of the forward element. This is called *circulation effect*.

3 The high speed flow over a trailing element allows the flow to leave the forward element at a higher rate. This *dumping effect* reduces the pressure recovery of the forward element.

4 *Off-surface pressure recovery*, in which the deceleration of the wake generated by a slat element occurs in an efficient manner than the recovery in contact with the wall.

5 Each element has a fresh boundary layer which originates on that element. A thin, turbulent boundary layer can withstand stronger pressure gradients than a thick one and is less likely to separate.

In an attached flow condition, a thin boundary layer is formed due to the viscous effects which is presented by Prandtl, (Prandtl and Tietjens 1957). A standard potential flow theory in which an incompressible flow is governed by the inviscid theory is applicable for wind turbine at wall of the airfoil in the boundary layers. An effect of the viscosity which is needed to be taken into account, even for the flow where the effect of the viscosity is confined to an extremely thin layer at the solid surfaces, which can be solved by the Kutta condition. Therefore, after the solution of the inviscid, an incompressible airfoil is obtained flow around a single airfoil in which the lift almost linearly increases with the angle of attack, up to very high lift coefficients c_L of the magnitude 4π with zero lift in 2D inviscid flow condition. In reality, the high-lift is not achievable due to the effect of viscosity.

The deceleration of the flow starts the separation of the flow from the airfoil surface, and the boundary layers are no longer thin, and the simple potential flow methods using the airfoil shape cannot be used to determine the forces on the airfoil. Also, the airfoil surface roughness significantly reduces the maximum obtainable lift coefficient which seldomly exceeds c_L of magnitude 2.5 for 2D airfoil simulation.

The potential flow solution of the multi-element airfoil configuration corresponds well to the single airfoil cases. Therefore, a small amount of the stress can be applied on the boundary layer in order to develop the high-lift i.e. preventing a stall. As pointed out by Smith (Smith 1975), these scenarios can be analyzed with an inviscid solution such as the panel method as long as the flow is not stalling. Therefore, the boundary layer solution in one form or another is needed when developing a high-lift configuration and/or airfoil shape.

The boundary layer flow simulation of the multi-element airfoil is strongly dependent upon the location of the flow separation and the type of flow transition. There are five types of flow mechanisms which can cause: i)stream wise instability, ii)inflectional instability, iii)laminar separation, iv) cross-flow (CF) instability, v) attachment-line instability, and vi) contamination by the turbulent shear layers emanating from the up-stream elements. All these flow mechanisms are influenced by a 2-dimensional high-lift system instead of an attachment-line instability which takes place in a 3-dimensional high-lift system.

3.2   Airfoil

From chapter 2 it can be seen that, the airfoil is the key in the blade design of a VAWT configuration. In the flow physics, an airfoil surface roughness is also important. Therefore in this section the selection of airfoil and the design of the double-element airfoil is carried out.

3.2.1   Selection and design of a single airfoil

Selection of a proper airfoil for the VAWT is very important at initial stage of the design process. (Mohamed 2012) summarizes that the operating range for a symmetric airfoil is wider than the non-symmetric airfoil. That means that stall is observed at smaller angle of attack in case of a non-symmetric airfoil. There are a few other airfoils which operate at the low Reynolds number, mainly they are S1210, S1213 (Selig *et al.* 1995) and S1223 (Selig and Guglielmo 1997), (Giguere and Selig 1997). These airfoils have the high-lift at a low Reynolds number from $Re = 200,000$ to $Re = 500,000$. Recently, a new airfoil for a small horizontal axis wind turbine has been designed by focusing a low wind speed startup which is called *airfish* AF300 (Singha *et al.* 2012). The author has mentioned that, this airfoil works for Reynolds number ranging from $Re = 38,000$ to $Re = 205,000$, which means, it is a very low wind speed condition. AF300 is designed by addition of 1% to 3% in the trailing edge of the airfoil S1223 and 1% to 5% thickness in trailing edge of the airfoil S1210.

(Mohamed 2012) indicates that an S1046 airfoil has highest power coefficient, so its obvious to select this profile for the design. However, there is one thing to be considered which is that the Reynolds number at which this airfoil performs well is related to the tip speed ratio (TSR). Also, in the selection and design of the airfoil one must consider other parameters such as the airfoil lift-to-drag ratio (c_L/c_D) also known as glide ratio, endurance parameter, thickness, pitching moment, stall characteristics, and sensitivity to the roughness are all important factors, amongst others.

In a VAWT, the airfoil shape contributes in the generation of a lift coefficient by creating suction on upper surface of the airfoil. In this process, a drag is also being generated which is not desirable for the maximum power output of the wind turbine. To get the maximum torque and a power output from wind turbine, it is important to have an airfoil which will generate the high-lift and the high lift-to-drag ratio.

Initially in this PhD project, an airfoil designed at Delft University of Technology, Netherlands called the DU06-W200 is used for a wind tunnel testing (Claessens 2006). DU06-W200 is originally obtained from NACA0018 airfoil by addition of 2% thickness and a camber increase. The thickness of the base airfoil is increased to give more structural strength to the blades; however, it has not been justified with its need for the VAWT. In reality, the thick airfoil has the disadvantages of lowering the maximum lift coefficient even though it works at higher tip speed ratio. The increase in the power coefficient becomes 5% as compared to the use of the NACA0018 airfoil in a VAWT blade design. It was the starting point for this PhD thesis and, therefore, a DU06-W200 airfoil was initially selected for the design of a double-element airfoil. The wind tunnel results

for the double-element airfoil using a DU06-W200 airfoil eventually published, see Appendix A.

It has been found that,the DU06-W200 airfoil is not the best choice for the VAWT blade design even though it solves the problem of self-start. Therefore, a new S1210 airfoil has been studied due to the high-lift coefficient at a low Reynolds number. Further, the S1210 airfoil is used in this PhD thesis, and a double-element airfoil design is proposed. The basis for this design is a primary experiment carried out in the wind tunnel and then followed by 2D CFD simulations. The selection of a S1210 airfoil is done due to its maximum lift and higher lift-to-drag ratio. The aerodynamic characteristics of S1210 airfoil at different Reynolds number are given in Figure 3.1.
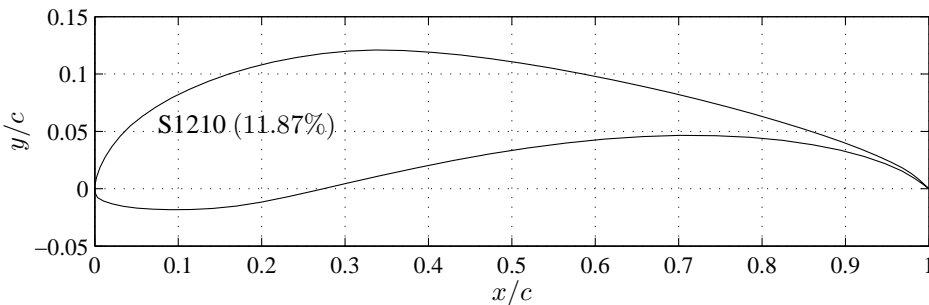
Figure 3.1 S1210 airfoil (Selig et. al 1995)

A plot of the lift coefficients versus angle of attack is given in Figure 3.2. The plot of lift coefficient versus the drag coefficient is given in Figure 3.3. These plots are redrawn from (Selig *et al.* 1995) by using Engauge digitizer software tool,(Engage Digitizer).
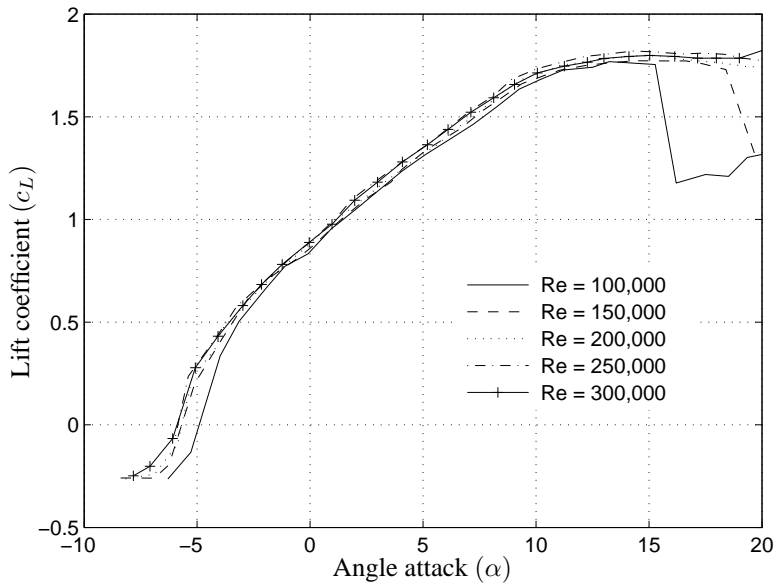
Figure 3.2 S1210 airfoil c_L (Selig et. al 1995)
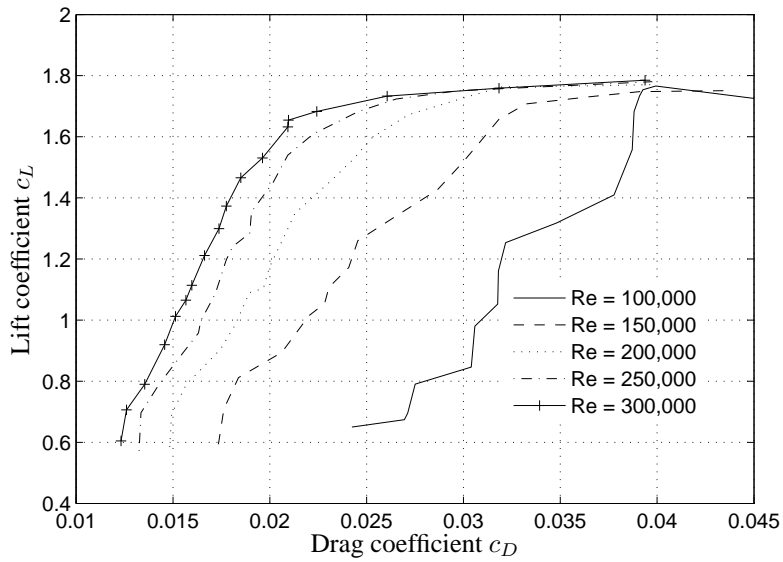
Figure 3.3 S1210 airfoil lift and drag coefficient (Selig et. al 1995)

3.2.2   Design of double-element airfoil

Usually airfoils designed by the National Advisory Committee of Aeronautics (NACA) are used for conventional VAWT blade design. However, these airfoils are designed for low altitude aeroplane application and are not suitable for VAWT blade design. A common practice in the design of an airfoil for the VAWT is to modify available NACA symmetric airfoils or other airfoils which satisfy the operating condition of the VAWT. In the VAWT application, the Reynolds numbers are very low, so the airfoils that are good at low Reynolds number are suitable to design the blade, such as S1210 airfoil, and S1223 airfoil (Singha *et al.* 2012). The S1210 airfoil performs better for low Reynolds number and has the best combination of lift coefficient (c_L) and the high glide ratio. Therefore, S1210 airfoil is used as the base airfoil in a double-element airfoil blade design for a proposed $D^2A - VAWT$. Figure 3.4 shows the division of a S1210 airfoil into the main and the slat airfoil.
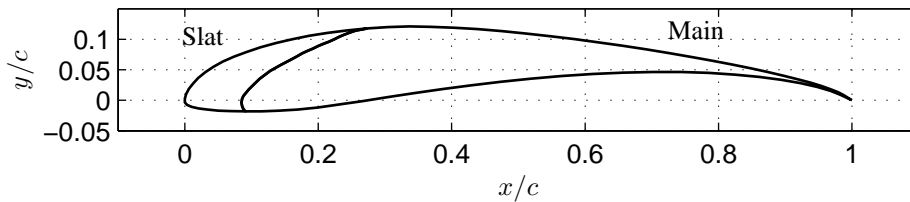
<div align="center">**Figure 3.4** Division of a S1210 airfoil</div>

In the design of a double-element airfoil, the chord length of a slat airfoil is kept in between 25% to 35% of the chord length of a base airfoil(c=100 mm). The chord length is decided based upon the test specimen requirements of the Aerolab wind tunnel (Aerolab 1974). The main and slat airfoil obtained in Figure 3.4 are further oriented as per design guidelines given by Buhl,(Buhl 2009) and by Gaunaa et al, (Gaunaa *et al.* 2010). In a double-element airfoil, the position and the orientation of a slat airfoil and respect to the main airfoil is expressed by three parameters. The first two parameters describes the position of the trailing edge (TE) of a slat airfoil along the local $x - direction$ (x_{TE}) and along the local $y - direction$, (y_{TE}), respectively. The third parameter is the slat angle (β_s) representing the orientation of a slat airfoil defined in Figure 3.5. It is the angle between the chord length of a slat airfoil with the local $x - direction$ and it is positive in the nose-up direction.

3.3   Wind tunnel testing

A wind tunnel testing is performed in this work to:

♦ determine the optimal angle of a slat airfoil (β_s) with respect to the main airfoil.

♦ determine the lift and a drag coefficient of the double-element airfoil.
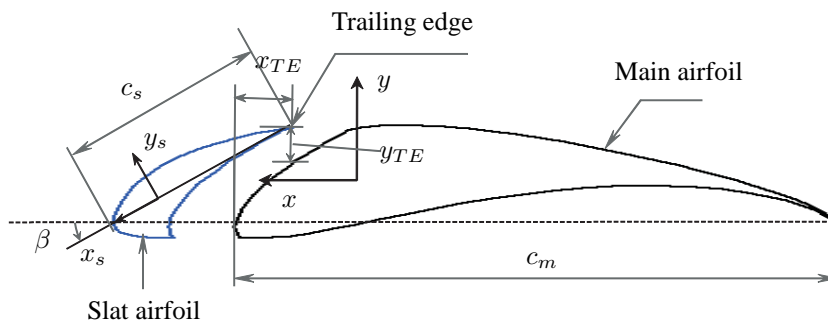
Figure 3.5 Double-element S1210 airfoil

♦ validate the 2D CFD simulation results.

The dimensions of the wind tunnel used in this experiment are 305 mm width, 305 mm height and 610 mm length (Aerolab 1974). The range of the wind speed achievable is 4.5 m/s to 60 m/s. The wind tunnel used in this work has a limitation on the angle of attack which can be adjusted in the range of $-22°$ to $+22°$ due to the size of the wind tunnel. Therefore, a 2D CFD simulation result obtained within this range of the angle of attack is compared with the wind tunnel test results. The mounting arrangement for a double-element airfoil in the wind tunnel is shown in Figure 3.6, a photograph of a double-element airfoil inside the wind tunnel.

Figure 3.6 DU06-W200 double-element airfoil in the wind tunnel

The slat airfoil is bolted with a main airfoil by two side links fixed to the main airfoil, and a linear adjustment is provided by a slot on the link end so that, the position parameter x_{TE} can be adjusted. The y_{TE} position can be adjusted by rotating the links around main airfoil. The third parameter β_s is set by an angular position of a slat airfoil with respect to two side links parallel to the chord length of the main airfoil. The main and the slat airfoil blades are manufactured by 3D printing technology, and plastic material is used. The optimum length of the double-element

airfoil blade is 250 mm for this wind tunnel and is represented by h length of the double-element airfoil test blade.

The main and the slat airfoils are manufactured individually, and fixed to each other by side links as shown in Figure 3.7. Figure 3.7.a shows the top view of the double-element S1210 airfoil and Figure 3.7.b shows the bottom view of the double-element S1210 airfoil. A single airfoil is formed by joining a slat airfoil with the main airfoil and later used as a single airfoil test specimen in Aerolab wind tunnel. Then experiments are performed to find out the lift and the drag coefficients for a single and a double-element airfoil.
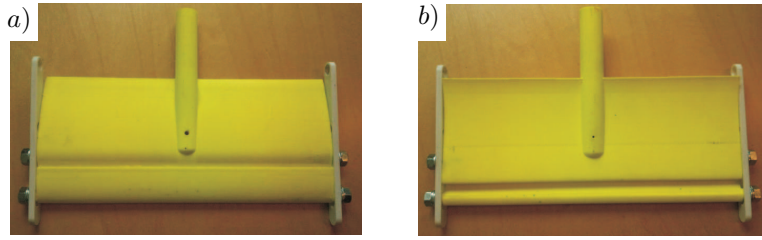
Figure 3.7 Double-element S1210 airfoil test specimen

The Aerolab wind tunnel has a data display and an acquisition system through which, the normal force N_f and the tangential force A_f acting on the double-element airfoil are obtained and stored in a text format. These forces are then converted to experimental lift force L_f and the drag force D_f by the following equation:

$$\left. \begin{aligned} L_f(\alpha) &= N_f\,cos(\alpha) - A_f\,sin(\alpha) \\ D_f(\alpha) &= N_f\,sin(\alpha) + A_f\,cos(\alpha) \end{aligned} \right\} \tag{3.1}$$

Finally, the experimental lift coefficient $c_{L_{expt}}$ and an experimental drag coefficients $c_{D_{expt}}$ are obtained:

$$\left. \begin{aligned} c_{L_{expt}} &= \frac{L_f}{\frac{1}{2}\,\rho V_m^2\,(c_m + c_s)\,h} \\ c_{D_{expt}} &= \frac{D_f}{\frac{1}{2}\,\rho V_m^2\,(c_m + c_s)\,h} \end{aligned} \right\} \tag{3.2}$$

Figure 3.8 shows the experimental lift coefficient of a single airfoil (SA) and a double-element airfoil (DA) for various Reynolds numbers.

At different Reynolds number, it is interesting to see that, the maximum lift coefficient for a single and double-element airfoil is increases, and also the stall angle is increased due to effect of the slat airfoil in front of the main airfoil. The tabular values represent the maximum lift coefficient for a single and double-element airfoil for different Reynolds number, and the difference in a stall angle is calculated and concluded with observations.

Prasad V.D. Chougule
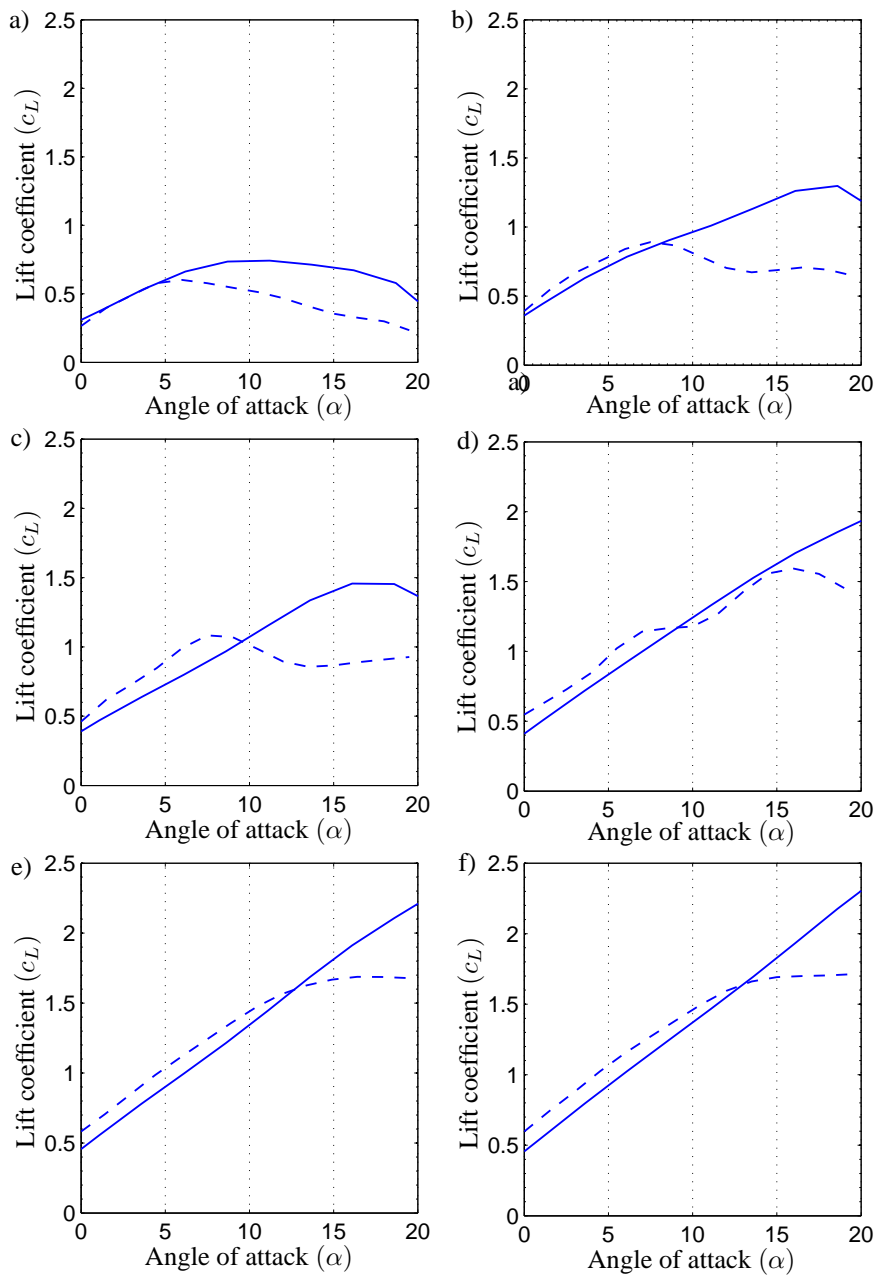
Figure 3.8 Wind tunnel test results for single and double-element airfoils :
a) Re = 40,000 . b) Re = 55,000 . c) Re = 75,000. d) Re = 100,000. e) Re = 200,000. f) Re = 240,000
– – – : Single S1210 airfoil   ——— : Double-element S1210 airfoil

Table 3.1 The maximum experimental lift coefficient of a single (SA) and a double-element (DA) S1210 airfoil.

Re	$\alpha_{max}(SA)$	$c_{L_{max}}(SA)$	$\alpha_{max}(DA)$	$c_{L_{max}}(DA)$	$\Delta\alpha_{max}$	$\Delta c_{L_{max}}$
40,000	6°	0.6015	11.2°	0.7425	5.2°	0.1410
50,000	7.5°	0.8907	18.6°	1.257	11.2°	0.3663
75,000	7.5°	1.083	16.1°	1.457	8.6°	0.3740
100,000	16°	1.593	20°	1.935	—	—
200,000	16.4°	1.687	20°	2.200	—	—
240,000	19.5°	1.712	20°	2.310	—	—

In Table 3.1, α_{max} represents the stall angle in the wind tunnel test. The difference of the stall angle between a single and double-element airfoil at Re = 50,000 is 11.2° which is very interesting, and it reduces to 8.6° for Re=100,000. From this it can be concluded that the S1210 double-element airfoil arrangement performs very well in the range of Re= 50,000 to Re 100,000 by delaying the stall angle. Whereas, the difference of the maximum lift is gradually increasing which produces the extra power output. In case of VAWT the delay of the stall angle contributes more into improvement of the total power output than that of the increase in the maximum lift coefficient. At the high wind speed conditions the effect of a slat airfoil on main airfoil has been less than in the low wind speed conditions. The S1210 airfoil has characteristics of the high lift coefficient at a low Reynolds number which supports the previous conclusion from the wind tunnel results.

The lift coefficient curve of a single airfoil at $Re \geq 200,000$ remains the same with a very less increment in the maximum value, which indicates further increase in the Reynolds number will not improve the maximum lift coefficient value. The double-element airfoil lift coefficient at $Re \geq 200,000$ is increasing and a stall condition of an airfoil is yet to reach at 20° angle of attack. The maximum lift coefficient of a single airfoil is increased by 40% at $Re = 200,000$ for the angle of attack 20° in the double-element airfoil. At an angle of attack below 12° the lift coefficient curves of the double-element airfoil follows sagging nature in the curve, as compared to a single airfoil lift coefficient curve. Therefore, wind tunnel results show that, the double-element airfoil is effective at $Re \geq= 200,000$ for a S12010 airfoil.

Figure 3.9 represents the glide ratio for a double-element airfoil at a different Reynolds numbers. It is advantageous that, the slope of this curve is low which shows a very low decrease in the lift coefficient after the stall angle.

The lift and a drag coefficient obtained in the wind tunnel testing and from 2D CFD simulations are further used in performance evaluation of a proposed $D^2A - VAWT$.

3.4   2D CFD Simulation

In this study, a 2D geometry is meshed using ANSYS ICEM CFD. The domain is a circle of radius 4 m, which corresponds to 40 times the chord length on the main airfoil (20cm). It is
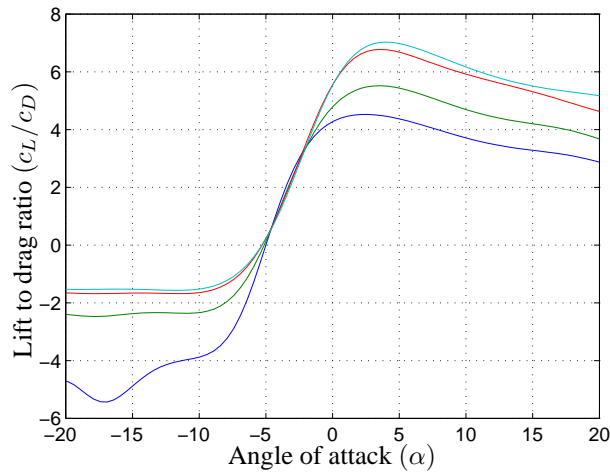
Figure 3.9 Experimental lift to drag ratio (Glide ratio) at different Reynolds numbers :
——— :Re = 100,000 ——— :Re = 150,000 ——— :Re = 200,000 ——— : Re = 230,000

a structured Hexa mesh. The first cell height from boundary surface is 3 μm. It grows with a ratio of 1.2, and smooth transition is maintained between smaller boundary quad elements and much larger elements away from airfoil surfaces. The boundary layer is captured properly using O-Grid blocking topology within ICEM CFD in a C shape pattern. Usage of C shaped O gird helped us not only to capture the boundary layer around airfoil, but also to capture the wake zone with finer sized mesh element behind the airfoil. First grid is fixed to a distance of $1 X 10^{-6} m$ to ensure a y+ less than 1, in order to properly resolve the boundary layer close to the wall surface and obtain accurate reports of the drag and lift coefficient (domain and boundary layer). The structured mesh with a circular air domain is used as different angles of attack are simulated given more flexibility on the mesh generation and increasing the convergence in the solution. The cell count is 0.15 millions.
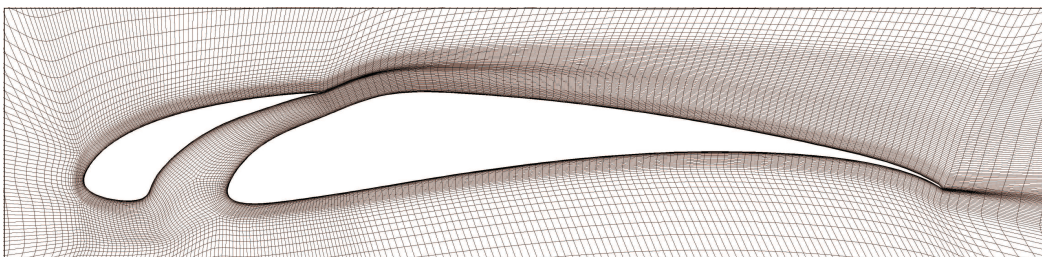
Figure 3.10 Grid for double-element S1210 airfoil

Air is considered as an isothermal and incompressible gas with constant density in solver setting. A single set of momentum equations is solved. Mass balance is ensured by continuity equation

and force balance is ensured by momentum equation set in the solver. In order to simulate turbulence, the Spalart Allmaras(1 equation) model is used. The Strain/Vorticity based SA Production mode is activated under this viscous model. The reason for that, it predicts wall forces quite accurately, and was developed basically for aerospace lift and drag studies. On top of that, this model is chosen because it is computationally efficient and it has been used to correctly simulate airfoil. In order to solve the system of governing partial differential equations, discretization of the continuity equation and Reynolds average Navier-Stokes equation (RANS) is formulated by using a Finite Volume Method with an algebraic segregated solver as implemented in ANSYS Fluent. The continuity and momentum equations need to be linked, which is attained by the SIMPLE (Semi-Implicit Method for Pressure-Linked Equations) algorithm.

In addition, the iterative solver is sped up due to an Algebraic Multigrid (AMG) technique that yields better convergence rate. All simulations in this work are performed under steady-state conditions. Under relaxation, factors of 0.2 and 0.6 respectively are applied on pressure and momentum parameters for bit slower but accurate prediction of physics involved. The run is continued till the coefficients of lift and drag attains steady values which in turn ensure a converged solution.

At the airfoil walls, boundary conditions are assumed to be no-slip boundary. The no-slip condition is the appropriate condition for the velocity component at the wall since the fluid in contact with the wall is stationary. At domain boundary, Velocity Inlet type boundary condition is applied, where the free stream velocity is set and the angle of attack is changed between $+40°$. and $-40°$. Multiple simulations are performed at different angle of attack for Re = 200,000. Figure 3.11 shows the lift and drag coefficient of double-element airfoil obtained from CFD simulations and compared with wind tunnel results.

In the Figure 3.11.a for lift coefficient of 2D CFD model fits very well with experimental data from $\alpha = -10°$ to the $\alpha = 20°$. The deviation occurs due to the difference in wind tunnel setup and the 2D CFD simulation model. The main reason for the deviation of the lift coefficient and a drag coefficient at $\alpha > 20°$ is because the wind tunnel wall boundaries start showing the effect on the flow. Secondly, The CFD simulations are performed in 2 dimension model which is not the case in wind tunnel. The open space or so called non confined domain is chosen for simulation at $\alpha > 20°$ and at $\alpha < -20°$. The wind tunnel results are utilized to calculate power output from proposed $D^2A - VAWT$ in Section 4. Due to the limitation of angle of attack in wind tunnel, 2D CFD results are used to estimate the lift and a drag coefficients beyond $22°$. In reality, the flow around the airfoil will be non confined so, the 2D CFD simulations are performed in this domain and the stall angle for a double-element S1210 airfoil is found to be $\alpha_{stall} = 30°$. It is found from Figure 3.2 and Figure 3.11.a that, the difference between the stall angle of a single S1210 airfoil and the proposed double-element S1210 airfoil is $\Delta\alpha = 15°$

3.5 Concluding remarks

In this chapter, a review the multi-element airfoil system is carried out. The benefits of using a multi-element airfoil in the VAWT blade design are discussed. A low Reynolds number, a high
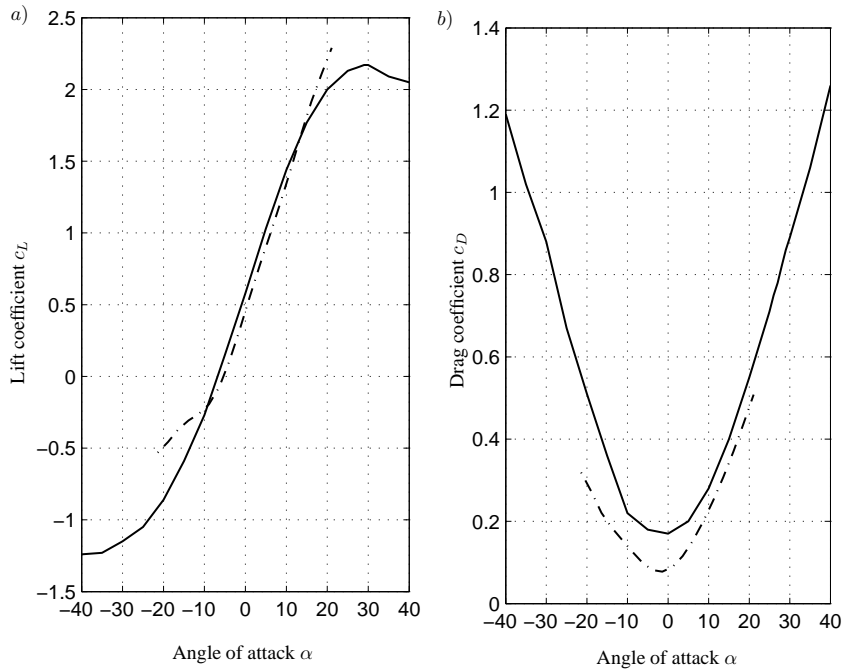
Figure 3.11 Validation of 2D CFD model with wind tunnel tests at Re=200,000 :
a) Lift coefficient . b) Drag coefficient.
$-\cdot-\cdot-$: Wind tunnel results   ——- :2D CFD results (ANSYS Fluent)

lift airfoil is selected to design a double-element airfoil. A simple way of dividing a single airfoil into a double-element airfoil is given, based on the literature of two- element airfoil flow physics and experimental method. It is certainly a rough estimate of slat and main airfoil sizes due to very limited or almost zero available research work on two-element airfoil for $Re < 500,000$ particularly used in a wind energy application. In this PhD thesis, the size of an airfoil, the position, and the orientation of the slat airfoil with respect to the main airfoil are decided based on the wind tunnel experiments performed with a selected first airfoil (DU06-W200) and a second S12010 airfoil. In the first wind tunnel testing, a sever blockage effect and wall effect were observed. Also, the thickness of an airfoil selected had been un-necessarily was more than that of the required thickness. So, finally a thin airfoil S12010 was selected which performs well at low Reynolds number $Re < 200,000$.

A wind tunnel test for a single S1210 airfoil and a double-element S1210 airfoil has been performed for various Reynolds numbers. It is observed from the wind tunnel tests that, the use of a double-element airfoil instead of a single airfoil has increased the lift coefficient and delayed the stall angle which is very advantageous in the VAWT. A delay in stall angle certainly increases the power output and keeps the VAWT performance at an optimal level. An increase in the maximum lift coefficient for $Re > 55,000$ has been very prominent which, indicates that, at the low

wind speed the double-element airfoil performance has been considerable, and the turbine can start producing power at low wind speed. However, it is also observed that, there is decrease in the lift coefficient of a double-element airfoil under the angle of attack at which the single airfoil stalls. This phenomenon is not explainable at this stage. The wind tunnel test results are further used to validate the 2D CFD model for the double-element airfoil. The wind tunnel tests showed promising results. Therefore, it was decided to perform 2D CFD simulations to obtain the lift and a drag coefficient for certain range of angle of attack.

The 2D CFD simulation results are then validated with a wind tunnel results up to $\alpha = 20°$ and 2D CFD model is used to obtain the lift and the drag coefficients for double-element airfoil for an angle of attack in the range of $\alpha = -40°$ to $\alpha = 40°$. The validation of a 2D CFD model has been a critical part of this chapter and hence, careful steps were taken during the modeling. It is observed that, the results under such low Reynolds numbers were influenced by meshing technique and quality of the mesh. Therefore, a mesh quality had been ensured at the critical area between the slat and the main airfoil by refined mesh. After all these precautions in meshing, the 2D CFD simulations are in good agreement with the wind tunnel results. The exact wind tunnel environment was simulated to match the test conditions with the 2D CFD simulations. The 2D CFD simulations are in an acceptable range. However, it will be a very accurate validation, if the 3D CFD simulation is performed. A best compromise between the expense of 3D CFD simulation and quality of 2D CFD simulation data obtained in this work was made. Finally, 2D CFD data was accepted for further work in this PhD thesis.

The aerodynamic characteristics of the double-element S1210 airfoil for an angle of attack in the range of $\alpha = -20°$ to $\alpha = +20°$ are obtained in this chapter by wind tunnel tests and from 2D CFD simulation, the data is determined in the range of $\alpha = -40°$ to $\alpha = +40°$. These characteristics are further used in the calculation of performance of the referential VAWT, and proposed $D^2A - VAWT$ by using aerodynamic models is explained in the next chapter.

CHAPTER 4
Aerodynamic Load Modeling

Prediction of aerodynamic loads on the VAWT is given by various models such as: i)Stream tube model, ii) Vortex model, iii) Lifting line model, and iv) local circulation model. Amongst all these models, a stream tube model is computationally less time consuming. A multiple stream tube model (MSTM) and double multiple stream tube model (DMSTM) are used in this PhD research. The DMSTM model is the focus of this chapter, and the formulae are the derived for proposed $D^2A - VAWT$. A schematics of the proposed $D^2A - VAWT$ and its aerodynamic load model is given in the chapter. Further, the performance of the proposed $D^2A - VAWT$ is determined based on the DMSTM by using aerodynamic characteristics of the double-element S1210 airfoil.

4.1 DMSTM for $D^2A - VAWT$

DMSTM is the more accurate method for the stream tube models. DMSTM is based on the momentum theory and the Blade element method. DMSTM needs to be applied with the Glauert correction factor as well. A rotor is divided into two halves namely upstream and downstream of the rotor. Further, the rotor is represented by a series of multiple stream tubes, and velocities of the fluid flow are calculated for each stream tube by assumption of inviscid and incompressible fluid flow. The geometric parameters of the $D^2A - VAWT$ are given in the Table 4.1.

Table 4.1 Geometrical parameters of $D^2A - VAWT$

Description	Symbol	Value	Unit
Height of Rotor	H	6.2	m
Diameter of Rotor	Dr	1.22	m
Single airfoil chord length	c	0.10	m
Main airfoil chord length	c_m	0.114	m
Slat airfoil chord length	c_s	0.0445	m
Main airfoil thickness	t_m	0.0135	m
Slat airfoil thickness	t_s	0.0034	m
Slat TE position x-direction	x_{TE}	0.012	m
Slat TE position y-direction	y_{TE}	0.004	m
Slat Airfoil angle	β_s	-20	°

In Table 1, TE corresponds with the trailing edge. A double multiple stream tube model for $D^2A - VAWT$ is represented in Figure 4.1.
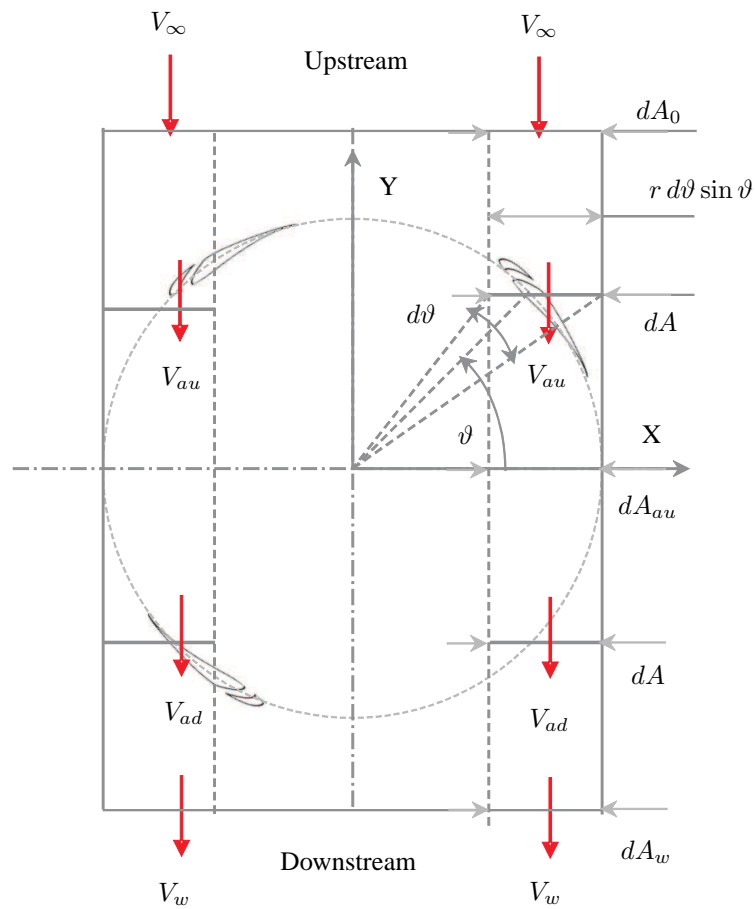
Figure 4.1 DMSTM for $D^2A - VAWT$

4.1.1 Mechanical model

The schematic of the 2-Dimensional view of the $D^2A - VAWT$ is represented in Figure 4.2. MA1 and SA1 are notations used for the main airfoil and the slat airfoil respectively which represents the blade 1. Similarly SA2 and MA2 both denotes the blade 2, and SA3 and MA3 both denotes the blade 3. Ω is the rotor angular speed, and ϑ_g is the fixed geometric angle between the main and slat airfoil and is same for all three blades. Azimuthal angles ϑ_1, ϑ_2 and ϑ_3 represents the azimuthal angle of blade 1, blade 2 and blade 3 respectively.
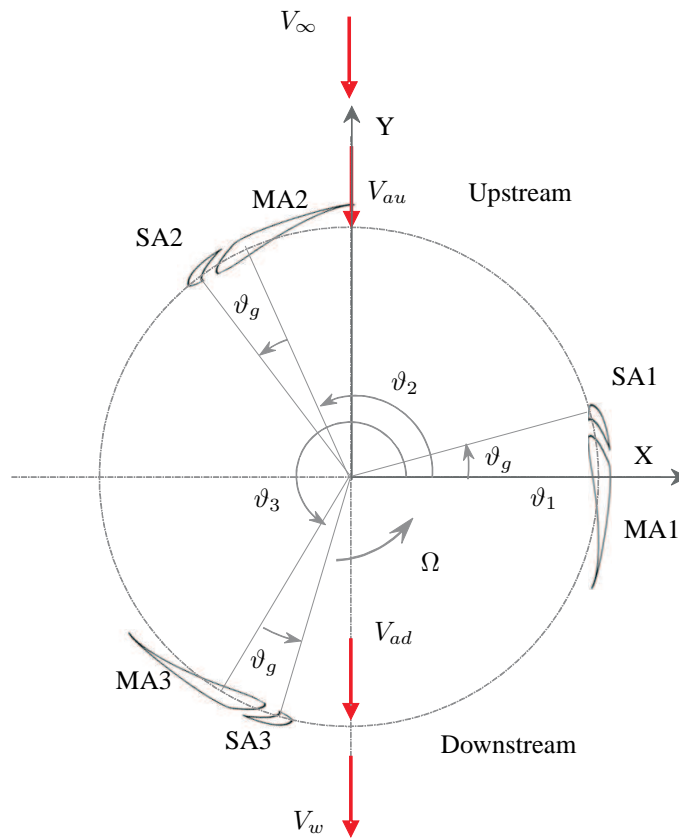
Figure 4.2 Schematic diagram of proposed $D^2A\ VAWT$

4.1.2   Aerodynamic model

The aerodynamics of VAWT and the flow around the rotor are mainly studied with the multiple actuator disc theory(Newman 1983). The Velocity components at various locations in the flow area are interesting and calculated by the momentum theory and the blade element theory. The double multiple stream tube method (DMSTM) proposed by (Paraschivoiu 1981) is used. In DMSTM, the flow field outside the rotor is divided into two subfields placed; upstream and downstream of the rotor. The fluid flow is considered to be inviscid and incompressible for the calculation of the induced velocity through the each stream tube.

Since the flow field is divided into two halves it is necessary to derive the local angle of attack, local relative velocity for upstream and downstream of the rotor individually. To obtain these quantities, an index j is used where $j = u$ and $j = d$ correspond to upstream and downstream half of the flow region, respectively. The up stream induced velocity V_{au} is given by the equation

as follows:

$$V_{au} = a_u \, V_\infty \tag{4.1}$$

where a_u is the up stream axial induction factor, and V_∞ is the free stream velocity and $V_{au} < V_\infty$. A reduction in wind induced velocity exists down stream of the rotor and is denoted by V_{ad} which is given as follows:

$$V_{ad} = a_d \, (1 - 2 \, a_u) \, V_\infty \tag{4.2}$$

where a_d is the down stream induction factor, V_{ad} corresponds to down stream induced velocity which holds relation $V_{ad} < V_{au}$. The calculation of the induction factor is based on the one-dimensional momentum theory and is explained later on in this thesis.

Once the induced velocities are calculated, the aerodynamic forces can be obtained by airfoil free body diagrams. The geometric parameters and aerodynamic forces acting on the double-element S1210 airfoil are given in Figure 4.3. $X - Y$ represents the global co-ordinate system of proposed $D^2A - VAWT$ and is located at the center of the rotor. The local co-ordinate system of the main airfoil is represented by $x - y$, whereas $x_s - y_s$ represents the local co-ordinate system of a slat airfoil. Aerodynamic characteristics and geometric parameters of the slat airfoil are represented by the suffix 's' and with lower case alphabet letters. β_s is the angle between the main airfoil chord and the slat airfoil chord which is called as a slat angle. Entities which are associated with index j in Figure 4.3 and Figure 4.4 are correspond to the blade 1 in the upstream and downstream flow fields respectively. α_j and α_{sj} are the angles of attack of the main and slat airfoils. W_j and w_j are the relative wind velocity of the main airfoil and the slat airfoil.

4.1.3   Aerodynamics of main airfoil

Variation of angle of attack

Figure 4.4 shows the velocity diagram for the main airfoil of blade 1. The inlet velocity is the free stream velocity represented by V_∞ and outlet velocity is the wake velocity V_w.

The tangential velocity component V_{t_j} and the normal velocity V_{n_j} component of main airfoil in up stream and down stream half of the rotor can be expressed as the following (Darrieus):

$$\left. \begin{aligned} V_{t_j} &= R_r \, \Omega + V_{a_j} \cos(\vartheta_{1j}) \\ V_{n_j} &= V_{a_j} \sin(\vartheta_{1j}) \end{aligned} \right\} \tag{4.3}$$

R_r is the radius of the rotor, and ϑ_{1j} is the azimuth angle of blade 1. Referring to Figure 4.4, the angle of attack $\alpha_1 j$ can be expressed as the following:

$$\alpha_{1j}(\vartheta_{1j}) = \tan^{-1} \left(\frac{V_{n_j}}{V_{t_j}} \right) \tag{4.4}$$
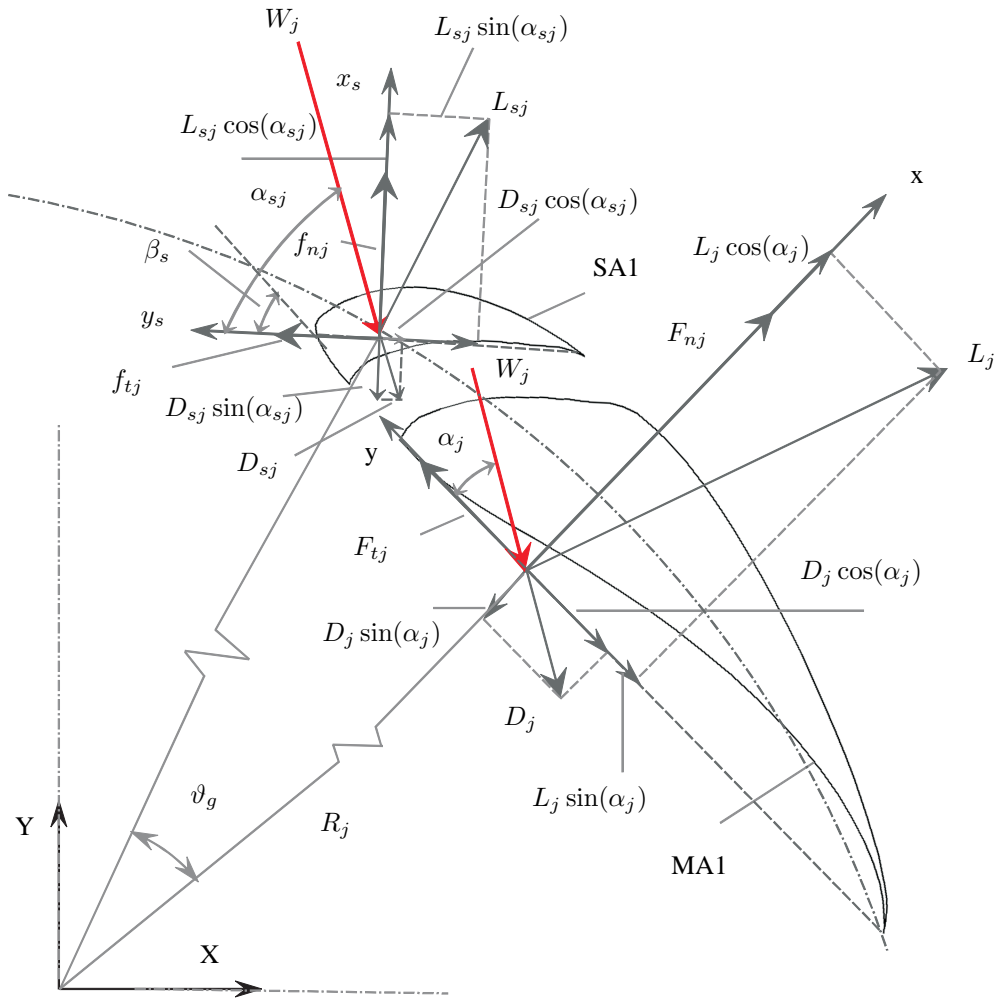
Figure 4.3 Aerodynamic forces on proposed $D^2A - VAWT$

Also, Figure 4.4 shows that the flow angle φ_{1j} is same as the angle of attack α_{1j} which forms a relation as follows:

$$\varphi_{1j}(\vartheta_{1j}) = \alpha_{1j}(\vartheta_{1j}) \tag{4.5}$$

Substituting the values of V_{t_j} and V_{n_j} from equation 4.3, a new equation can be written as follows:

$$\varphi_j(\vartheta_{1j}) = \tan^{-1}\left[\frac{\sin(\vartheta_{1j})}{\frac{R_r\Omega}{V_{a_j}} + \cos(\vartheta_{1j})}\right] \tag{4.6}$$
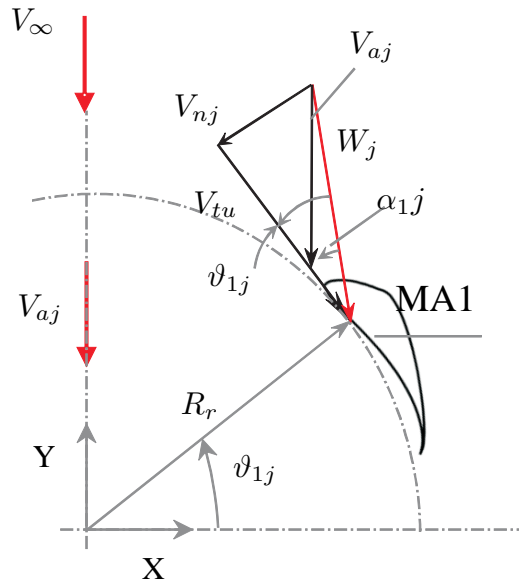
Figure 4.4 Velocity component for main airfoil of blade 1

The variation of local relative flow velocity W_j can be given as follows:

$$W_j(\vartheta_{1j}) = \sqrt{V_{t_j}^2 + V_{n_j}^2} \tag{4.7}$$

Local Aerodynamic Loads

The directions of lift (L_j) and drag (D_j) forces per unit length and their tangential ($F_{t_j}(\vartheta_{1j})$) and normal ($F_{n_j}(\vartheta_{1j})$) force components are shown in Figure 4.3. The tangential force coefficient ($C_{t_j}(\vartheta_{1j})$) is basically given by an addition of tangential components of lift(L_j) and drag (D_j) forces. The normal force coefficient ($C_{n_j}(\vartheta_{1j})$) is the difference between the normal components of lift(L_j) and drag(D_j) forces. The expression of tangential force coefficient ($C_{t_j}(\vartheta_{1j})$) and normal force component ($C_{n_j}(\vartheta_{1j})$) are given as follows:

$$\left.\begin{aligned} C_{t_j}(\vartheta_{1j}) &= c_{L_j} \sin\varphi_j + c_{D_j} \cos\varphi_j \\ C_{n_j}(\vartheta_{1j}) &= c_{L_j} \cos\varphi_j - c_{D_j} \sin\varphi_j \end{aligned}\right\} \tag{4.8}$$

c_{L_j} and drag c_{D_j} represents the lift and drag coefficients in equation (4.8) for main airfoil.

Prasad V.D. Chougule

Force coefficients are given as follows:

$$
\left.
\begin{aligned}
CF_{t_j} &= C_{t_j}\left(\frac{W_j}{V_\infty}\right)^2 \\[2em]
CF_{n_j} &= C_{n_j}\left(\frac{W_j}{V_\infty}\right)^2
\end{aligned}
\right\}
\tag{4.9}
$$

The tangential forces (F_{t_j}) and normal forces (F_{n_j}) can be defined as follows:

$$
\left.
\begin{aligned}
F_{t_j}(\vartheta_{1j}) &= \frac{N s c H}{S}\int_0^H CF_{t_j}\,dH \\[1em]
F_{n_j}(\vartheta_{1j}) &= \frac{N s c H}{S}\int_0^H CF_{n_j}\,dH
\end{aligned}
\right\}
\tag{4.10}
$$

where $S = H\,2\,R$ is the rotor frontal area. H is the total height of the rotor.

Torque and Power

By integrating along the blade length, a total torque on complete blade as a function of azimuthal angle is obtained as follows:

$$
T_j(\vartheta_{1j}) = \frac{N}{2\pi}\int_0^H C_{t_j}(\vartheta_{1j})\,W_j{}^2\,dH
\tag{4.11}
$$

where N is the number of blades and R_r is the radius of the rotor. Therefore, the total torque on both halves of the rotor is given by integrating over azimuthal angle as follows:

$$
T_j = \frac{1}{2}\,\rho\,c\,R\int_m^n T_j(\vartheta_{1j})\,d\theta_1
\tag{4.12}
$$

In equation (4.12) for $j = u;\ m = 0, n = \pi$ and for $j = d;\ m = \pi, n = 2\pi$. The torque coefficient and hence power coefficient are given as follows:

$$
\begin{aligned}
CT_j &= \frac{T_j}{\frac{1}{2}\,\rho\,V_\infty\,S\,R} \\[1.5em]
C_{p_j} &= \frac{R\,\omega}{V_\infty}\,CT_j
\end{aligned}
\tag{4.13}
$$

The power coefficient contribution from main airfoil is the weighted sum of the upstream power coefficient C_{p_u} and downstream power coefficient C_{p_d} which is denoted by C_p as follows:

$$
C_p = C_{p_u} + C_{p_d}
\tag{4.14}
$$

Reynolds Number

It is well known (Paraschivoiu 2009) that vertical axis wind turbines operate under low Reynolds number, and that the performance of airfoil degraded as Reynolds number is lower. So it is important to determine the Reynolds number at the blade chord in selection of airfoil for use in vertical axis wind turbines. Therefore, a local Reynolds number R_e of the blade 1 at different azimuthal angle ϑ_{1j} is expressed by the equation, (Paraschivoiu 1984):

$$R_e(\vartheta_{1j}) = \frac{\rho\, c_m\, W_j(\vartheta_{1j})}{\mu} \tag{4.15}$$

where R_e is the rotor Reynolds Number, μ is the air viscosity. The Reynolds number varies with relative velocity which depends on the azimuthal angle at each blade. It is observed from the plot of Reynolds number versus azimuthal angle and relative velocity versus azimuthal angle that the variation of Reynolds number is relatively less. Hence it is assumed in this work that the Reynolds number is constant over the VAWT rotor.

Induction Factor Determination

The induction factor is determined by iterative method in which the induction factor for up stream and down stream half of the rotor a_u and a_d is initially set to 1.0. After that, the numerical simulation is run to determine the function related to up stream and down stream half of the rotor, which is given as,(Paraschivoiu 1984):

$$F_{1j} = \frac{N\, c}{8\,\pi\, R_r} \int_{ll}^{ul} \left(C_{nj}\, \frac{\cos \vartheta_{1j}}{|\cos \vartheta_{1j}|} - C_{tj}\, \frac{\sin \vartheta_{1j}}{|\cos \vartheta_{1j}|} \right) \left(\frac{W_j}{V_{aj}} \right)^2 d\vartheta_{1j} \tag{4.16}$$

In equation (4.16) integration limits are as follows:

$$
\begin{aligned}
for\ \ j &= u : \quad ll = 0 \ , ul = \pi \\
for\ \ j &= d : \quad ll = \pi \ , ul = 2\,\pi
\end{aligned}
\tag{4.17}
$$

Finally, a new value of induction factor in up stream and down stream a_j is given by:

$$a_j = 1 - \frac{F_j}{\pi} \tag{4.18}$$

In equation (4.18), a_u corresponds to up stream induction factor, and a_d corresponds to down stream induction factor.

4.1.4   Aerodynamics of slat airfoil

Aerodynamic loads acting on the slat airfoil of blade 1 are derived in this section. In Figure 4.5, the azimuthal angle of the slat airfoil of blade 1 (ϑ_{s1}) is seen to be dependent on the azimuthal
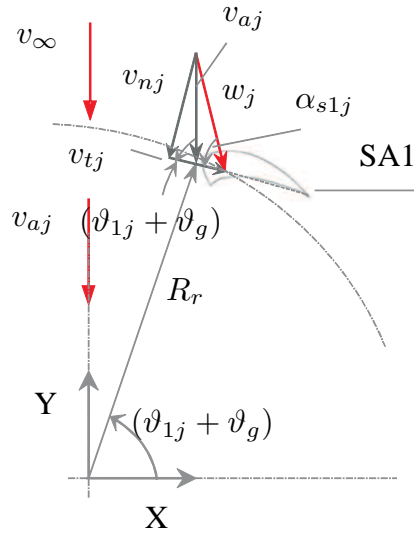
Figure 4.5 Velocity component for slat airfoil of blade 1

angle (ϑ_{1j}) of main airfoil of blade 1. The angle of a slat airfoil (ϑ_{s1_j}) in up stream and down stream half of the rotor can be expressed in following equation:

$$\vartheta_{s1j} = \vartheta_{1j} + \vartheta_g \tag{4.19}$$

For blade 2 and blade 3, the azimuthal angle is given by the same equation (5.1). Therefore, in what follows all equations are derived for blade 1, in which the azimuthal angle of the main airfoil is denoted by ϑ_{1j} and azimuthal angle of the slat airfoil is represented by ϑ_{s1j}. It is noted that ϑ_{1j} and ϑ_{s1j} vary in the range from 0 to π in upstream and from π to 2π in downstream half of the rotor. The fixed azimuthal angle ϑ_g is the angle between main and slat airfoil and is the same for all blades. The slat airfoil position and the orientation are fixed, relative to main airfoil in local frame of main airfoil ($x - y$). The change of position causes increase in radius of rotor which is neglected in the following formulation due to a small change in R_r. Further, the tangential velocity component v_{t_j} and the normal velocity component v_{n_j} for upstream and downstream of rotor are given as follows:

$$\left. \begin{array}{l} v_{t_j} = R_r\,\Omega + v_{a_j}\cos(\vartheta_{s1}) \\ v_{n_j} = v_{a_j}\sin(\vartheta_{s1}) \end{array} \right\} \tag{4.20}$$

where v_{a_j} represents the induced velocity of a slat airfoil in up stream and in down stream half of the rotor. By substituting v_{t_j} and v_{n_j} from the equation (4.20), and from Figure 4.5, the angle of attack α_{s1j} can be expressed as:

$$\alpha_{s1j}(\vartheta_{s1j}) = \tan^{-1}\left(\frac{V_{n_j}}{V_{t_j}}\right) \tag{4.21}$$

Also, in Figure 4.5 the flow angle φ_{1j} is same as the angle of attack α_{1j} which forms relation as follows:

$$\varphi_{s1j}(\vartheta_{s1j}) = \alpha_{s1j}(\vartheta_{s1j}) \tag{4.22}$$

Therefore, a new equation for flow angle of a slat airfoil is given as follows:

$$\varphi_{s1_j}(\vartheta_{s1}) = \tan^{-1}\left[\frac{\sin(\vartheta_{s1})}{\frac{R_r\,\Omega}{v_{aj}} + \cos(\vartheta_{s1})}\right] \tag{4.23}$$

The variation of local relative flow velocity w_j can be given as follows:

$$w_j(\vartheta_{1j}) = \sqrt{v_{t_j}^2 + v_{n_j}^2} \tag{4.24}$$

The directions of lift L_{sj} and drag D_{sj} forces and their tangential $f_{t_j}(\vartheta_{s1})$ and normal $f_{n_j}(\vartheta_{s1})$ force components are shown in Figure 4.3. The expression for tangential force coefficient $c_{t_j}(\vartheta_{s1})$ and normal force component $c_{n_j}(\vartheta_{s1})$ are given as:

$$\left.\begin{array}{l} c_{t_j}(\vartheta_{s1}) = c_{Ls_j}\,\sin\varphi_{s1} + c_{Ds_j}\,\cos\varphi_{sj} \\[2mm] c_{n_j}(\vartheta_{s1}) = c_{Ls_j}\,\cos\varphi_{s1} - c_{Ds_j}\,\sin\varphi_{sj} \end{array}\right\} \tag{4.25}$$

c_{Ls_j} and c_{Ds_j} represent the lift and drag coefficients of slat airfoil. The tangential and normal force coefficients of the slat airfoil are given as follows:

$$\left.\begin{array}{l} cf_{t_j} = c_{t_j}\left(\dfrac{w_j}{V_\infty}\right)^2 \\[5mm] cf_{n_j} = c_{n_j}\left(\dfrac{w_j}{V_\infty}\right)^2 \end{array}\right\} \tag{4.26}$$

The tangential forces (f_{t_j}) and normal forces (f_{n_j}) can be defined as follows:

$$\left.\begin{array}{l} f_{t_j}(\vartheta) = \dfrac{Ns\,c_s\,H}{S}\displaystyle\int_0^H cf_{t_j}\,dH \\[5mm] f_{n_j}(\vartheta) = \dfrac{Ns\,c_s\,H}{S}\displaystyle\int_0^H cf_{n_j}\,dH \end{array}\right\} \tag{4.27}$$

By integrating along the blade length, a total torque on complete blade as a function of azimuthal angle is obtained as follows:

$$t_j(\vartheta_{s1}) = \frac{N}{2\pi}\int_0^H c_{t_j}(\vartheta_{s1})\,w_j{}^2\,dH \tag{4.28}$$

Prasad V.D. Chougule

where N is the number of blades and R_r is the radius of the rotor. Therefore, the total torque on both half of the rotor is given by integrating over azimuthal angle as follows:

$$t_j = \frac{1}{2} \rho \, c_s \, R \int_m^n t_j(\vartheta_{s1}) \, d\theta_{s1} \tag{4.29}$$

In equation (4.29) for $j = u; m = 0, n = \pi$ and for $j = d; m = \pi, n = 2\pi$

The torque coefficient and hence theoretical power coefficient are given as (Betz 1966):

$$\begin{aligned} ct_j &= \frac{t_j}{\frac{1}{2} \rho \, V_\infty \, S \, R} \\ c_{p_j} &= \frac{R \, \omega}{V_\infty} \, ct_j \end{aligned} \tag{4.30}$$

The power coefficient of whole rotor for a slat airfoil is the weighted sum of upstream power coefficient c_{p_u} and downstream power coefficient c_{p_d} which is denoted by c_p as follows:

$$c_p = c_{p_u} + c_{p_d} \tag{4.31}$$

The total power coefficient of the rotor (main and slat airfoil) can be calculated by summation of the power coefficient of the main airfoil obtained by equation (4.14) and the power coefficient of the of the slat airfoil obtained by equation (4.31).

4.2   Numerical simulation

A numerical model discussed in this chapter is validated with the reference wind turbine. Here the detailed geometric parameters of the reference wind turbine are given.

4.2.1   Parameters and Input used for simulation

A reference 1-kW Windspire standard wind turbine has geometric parameters mentioned in Table 4.2:

Table 4.2 Geometrical Parameters of reference 1-kW Windspire wind turbine

Description	Symbol	Value	Unit
Height of Rotor	H	6.2	m
Diameter of Rotor	Dr	1.22	m
Airfoil shape	DU06-W200		
Chord length	c	0.127	m
Thickness of airfoil	t	0.0254	m
Solidity of rotor	σ	0.3122	

More details of the reference wind turbine can be found in (Huskey *et al.* 2009) and (Energy 2010). The reference wind turbine experimental results show the relation of the wind speed versus the rotor rotational speed, and power coefficient is given in Table 4.3:

Table 4.3 Performance data of reference 1-kW Windspire wind turbine

Sr. No.	V_∞	Ω	TSR	C_p
1	0.5	0	0	-10.60
2	1.0	0	0	-1.68
3	1.5	1	0.0426	-0.51
4	2.0	3	0.0958	-0.22
5	2.5	9	0.2298	-0.11
6	3.0	20	0.4256	-0.06
7	3.5	42	0.7662	-0.03
8	4.0	80	1.2769	0.02
9	4.5	137	1.9438	0.06
10	5.0	177	2.2602	0.09
11	5.5	204	2.3681	0.11
12	6.0	228	2.4262	0.12
13	6.5	255	2.5048	0.13
14	7.0	279	2.5174	0.14
15	7.5	291	2.4773	0.15
16	8.0	312	2.4900	0.16
17	8.5	331	2.4863	0.17
18	9.0	344	2.4404	0.18
19	9.5	353	2.3724	0.19
20	10.0	359	2.2921	0.19
21	10.5	355	2.1586	0.18
22	11.0	352	2.0431	0.18
23	11.5	348	1.9321	0.17
24	12.0	326	1.7345	0.16
25	13.0	318	1.5618	0.14
26	13.5	321	1.5181	0.13
27	14.0	299	1.3636	0.12

The power efficiency and total power output of a proposed $D^2A - VAWT$ of the same rotor solidity of magnitude 0.31 and operating conditions are obtained. The rotor height H and the rotor diameter D_r for a proposed $D^2A - VAWT$ remain the same as a reference Windspire 1-kW wind turbine (Energy 2010). The lift and drag coefficients of the main and slat airfoil of double-element airfoil are used as the input to the numerical simulation. Table 4.4 gives the values of these coefficients.

The aerodynamic characteristics of large angle of attack for $DU06 - W200$ and $S1210$ are given in Appendix E.

Table 4.4 Aerodynamic characteristics of double-element S1210 airfoil

Angle of attack	Lift Coefficient			Drag Coefficient		
α	$c_{L_{slat}}$	$c_{L_{main}}$	$c_{L_{overall}}$	$c_{D_{slat}}$	$c_{D_{main}}$	$c_{D_{overall}}$
-40	-2.76	-0.91	-1.24	3.84	0.60	1.19
-35	-3.01	-0.83	-1.23	3.62	0.44	1.02
-30	-3.20	-0.72	-1.17	3.37	0.29	0.85
-25	-3.25	-0.56	-1.05	3.04	0.15	0.676
-20	-3.08	-0.36	-0.86	2.61	0.046	0.51
-15	-2.62	-0.14	-0.59	2.08	0.034	0.36
-10	-1.68	0.04	-0.27	1.31	0.02	0.22
-5	-0.90	0.38	0.15	0.986	0.00	0.18
0	0.12	0.69	0.58	0.59	0.07	0.17
5	1.32	0.97	1.03	0.27	0.18	0.20
10	2.55	1.19	1.44	0.09	0.32	0.28
15	3.66	1.35	1.77	0.05	0.48	0.40
20	4.51	1.44	2.00	0.14	0.63	0.55
25	5.04	1.48	2.13	0.35	0.79	0.71
26	5.11	1.48	2.14	0.40	0.82	0.75
27	5.17	1.48	2.15	0.45	0.86	0.78
28	5.22	1.48	2.16	0.50	0.89	0.82
29	5.25	1.48	2.17	0.56	0.92	0.86
30	5.27	1.47	2.17	0.61	0.95	0.89
35	5.16	1.41	2.09	0.90	1.09	1.06
40	5.00	1.39	2.05	1.19	1.28	1.26

4.2.2   Validation of DMSTM

A validation of the DMSTM model used in this analysis is important before performance evaluation of the proposed $D^2A - VAWT$. The numerical simulation is carried out for the reference 1-kW windspire wind turbine. A simulation of the power coefficient of the rotor over one rotation is carried out at different wind speeds. The power coefficient of the reference 1-kW windspire wind turbine is calculated with DMSTM, and the DMSTM is validated with the experimental results available. The VAWT is known to be subject to the high angle of attack compared to the HAWT. Therefore it is interesting to plot the angle of attack versus the azimuthal angle of the blade. It is noted that the upwind zone of the rotor ranges from $0°$ to $180°$, and the downwind zone of the rotor ranges from $180°$ to $360°$.

Figure 4.6.b shows the plot of normal force of the blade 1. There is a variation in the normal force in upwind and downwind zone. It can be observed from the Figure 4.6 that for low TSR the angle of attack is high and normal force is low. A normal force does not contribute in the torque generation so it is advantageous to have a high angle of attack to keep the low normal force, but it is not good idea. Due to the high angle of attack the airfoil enters in its stall reason which is not good for extracting maximum power, and VAWT enters in the dynamic stage of its operation. Further, to understand the importance of the angle of attack a tangential force and rotor torque behavior are plotted in Figure 4.7:
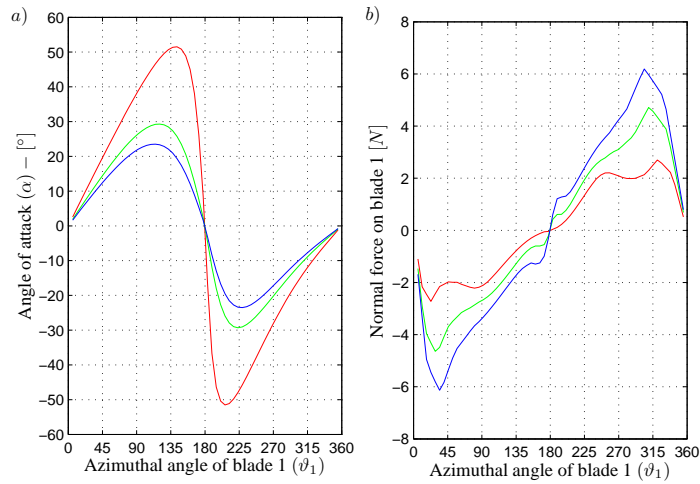
Figure 4.6 Angle of attack and normal force variation over azimuthal angle:
a) Angle of attack. b) Normal force .
——— : TSR = 1.27   ——— : TSR = 2.04   ——— : TSR = 2.50
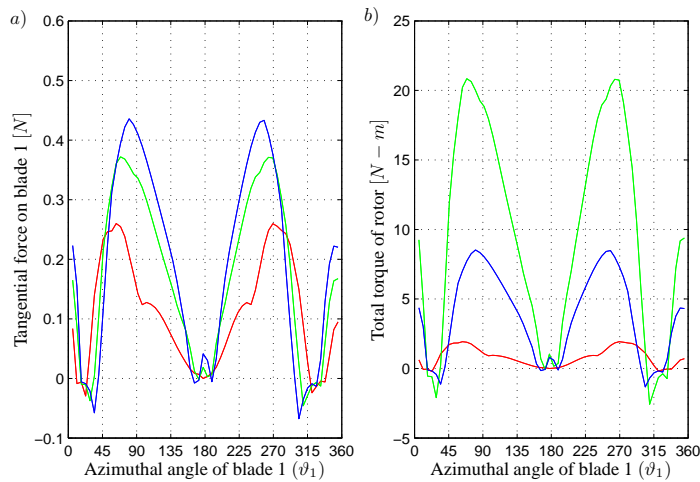
Figure 4.7 Tangential force and rotor torque variation over azimuthal angle :
a) Tangential force. b) Total torque .
——— : TSR = 1.27   ——— : TSR = 2.04   ——— : TSR = 2.50

In Figure 4.7 for the low TSR the tangential force and the rotor torque are lower, which indicates that the lower TSR is not good for VAWT. For TSR of magnitude 2.5, the rotor torque is lower than the rotor torque at TSR of magnitude 2.04; this indicates that the TSR 2.04 is the optimal

magnitude at which the reference VAWT performance will be maximized.

Figure 4.8 shows the combined power coefficient in upwind and downwind zone of the rotor and the total power output prediction for reference 1-kW wind turbine.
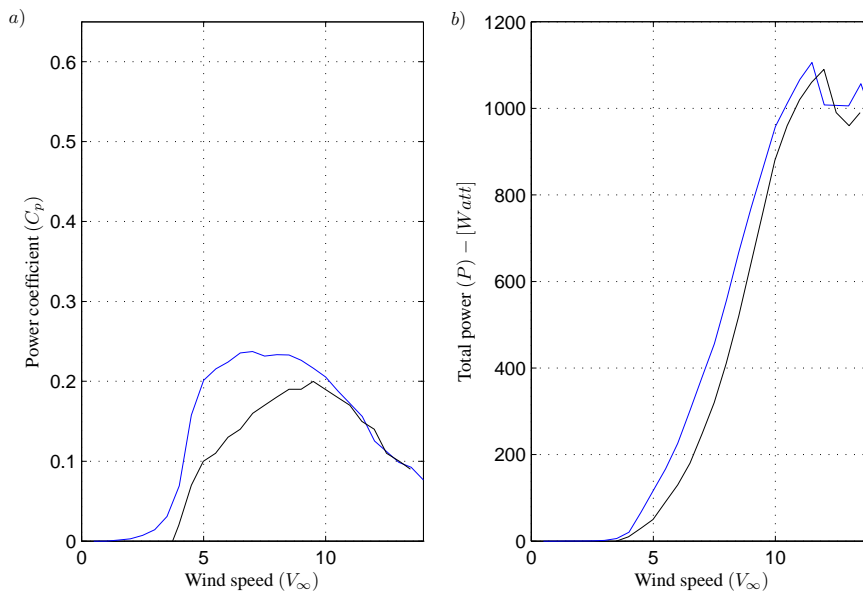
Figure 4.8 Validation of DMSTM with reference 1-kW Windspire wind turbine:
a) Power coefficient. b) Power output.
——- : Measurement results of reference Windspire.
——- : DMSTM results for reference Windspire

The maximum power coefficient of the reference VAWT at $V_\infty = 9.5\ m/s$ is 0.2, whereas the power coefficient calculated from the DMSTM model is 0.22. There is very little difference at this wind speed; however, the DMSTM model predicts the maximum power coefficient of 0.24 at wind speed of magnitude 7 m/s. The DMSTM model over predicts the maximum power confident by less than 10% which is in the acceptable range. The predicted power output shows that the wind turbine starts producing power at lower wind speeds than the experimental results, and which is also found in the numerical study carried by, (Paraschivoiu 1984). After validation of the DMSTM, it is convenient to analyze the performance of the proposed $D^2A - VAWT$. The results of DMSMT for proposed $D^2A - VAWT$ are given in next section and discussed.

4.2.3 Results and discussion

In the calculation procedure angle of attack is determined for the angular position of the individual blades, and then a aerodynamic lift and drag coefficients are interpolated from available data

for double-element S1210 airfoil. Later on, the aerodynamic forces such as the normal force and the tangential forces are determined for different angular positions of the rotor. To calculate the total power output from the proposed $D^2A - VAWT$ the total torque by rotor is calculated as a function of angular position. The numerical simulation is carried out for various wind speed conditions mentioned in Table 4.3. A performance contribution from the slat airfoil and a main airfoil blade of a double-element S1210 is individually determined. The numerical results for TSR of magnitude 2.04 are considered and plotted here. The aerodynamic characteristics of slat, main airfoil and overall aerodynamic characteristics mentioned in Table 4.4 are used. The variation of the angle of attack and the normal forces on blade 1 with respect to the azimuthal position is shown in Figure 4.9. The maximum angle of attack in upwind zone of the rotor occurs at $120°$ and in the downwind zone it occurs at $223.5°$ which shows the antisymmetrical variation of the angle of attack. This phenomenon of a higher angle of attack in upwind zone was explained by, (Wilson 1977).
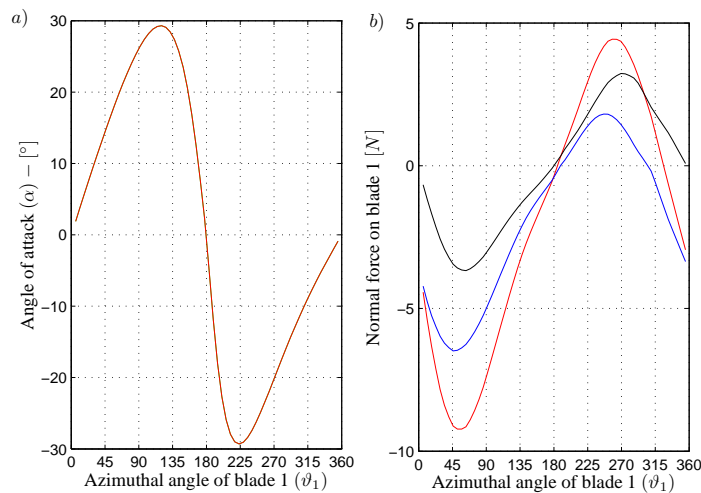
Figure 4.9 Angle of attack and normal force variation over azimuthal angle :
a) Angle of attack. b) Normal force .
——- : Slat airfoil blade ——- : Main airfoil blade ——- : Combined output

The normal forces on blade 1 is shown in Figure 4.9.b. There is a variation in the normal force in upwind zone and downwind zone which is considerably larger compared to the reference wind turbine where it is symmetric. The magnitude of normal force in the upwind zone is almost twice than the down wind zone of the rotor for the proposed $D^2A - VAWT$. The effect of this variation will reflect in the tangential force component, which is plotted in Figure 4.10.a. A tangential force component in the upwind zone is lower than the downwind zone of the rotor, which is a positive direction contributing to the positive torque generation. Figure 4.10.b shows the total torque acting on the rotor with maximum magnitude of 65 Nm for the overall rotor output.
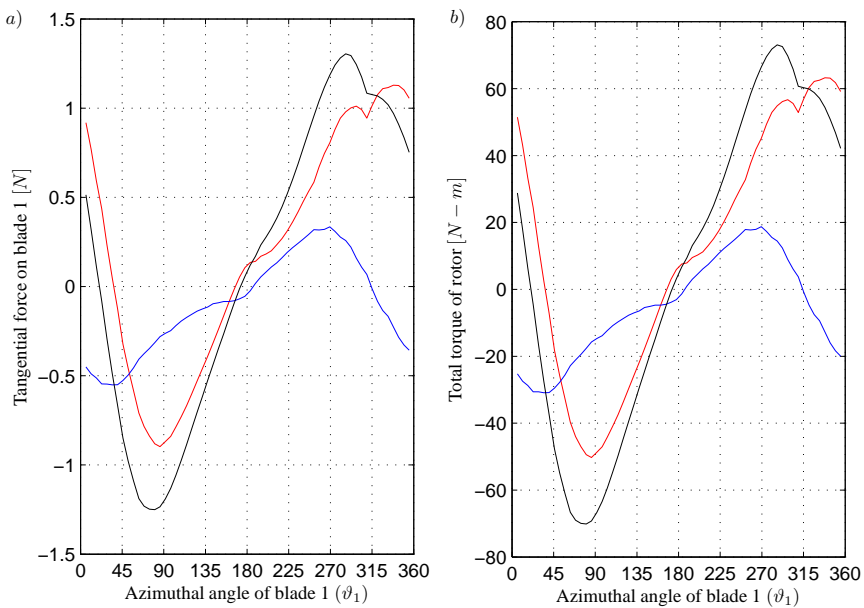
Figure 4.10 Tangential force and rotor torque variation over azimuthal angle.
a) Tangential force. b) Total torque .
———— : Slat airfoil blade ———— : Main airfoil blade ———— : Combined output

The effective torque remains on positive and higher than the negative torque, which ultimately contributes to the power production. The power coefficient and the total power obtained for $D^2A - VAWT$ are plotted in Figure 2.11. The power coefficient by the main, slat airfoil blade and the double-element S1210 airfoil blade are shown in Figure 2.11.a. The maximum power coefficient of the $D^2A - VAWT$ is of magnitude 0.5, which is almost twice the power coefficient of the reference 1-kW Windspire wind turbine. The power coefficient predicted with DMSTM is nearly 10% more than the actual power coefficient which is discussed in the DMSTM validation section of this chapter. A corrected power coefficient can be obtained by deducting 10% of 0.5 which corresponds to 0.45.

A power output is plotted in Figure 2.11.b. An addition of power contribution from the main and slat airfoil blades gives the total power output from the proposed $D^2A - VAWT$. The maximum power is achieved for comparably lower wind speeds than in the case of the reference wind turbine. This indicates that the proposed $D^2A - VAWT$ starts producing power earlier than the reference wind turbine. However, the power coefficient curve shows the double increase in the maximum power coefficient than the reference wind turbine. The power curve shows an increase in total power instead of maximum power output compared to the reference wind turbine. The area under the power curve for the proposed wind turbine is larger which indicates more power output. As a concluding remark it can be mention that, the proposed $D^2A - VAWT$ wind turbine of same size can produce more power output with improved power efficiency due
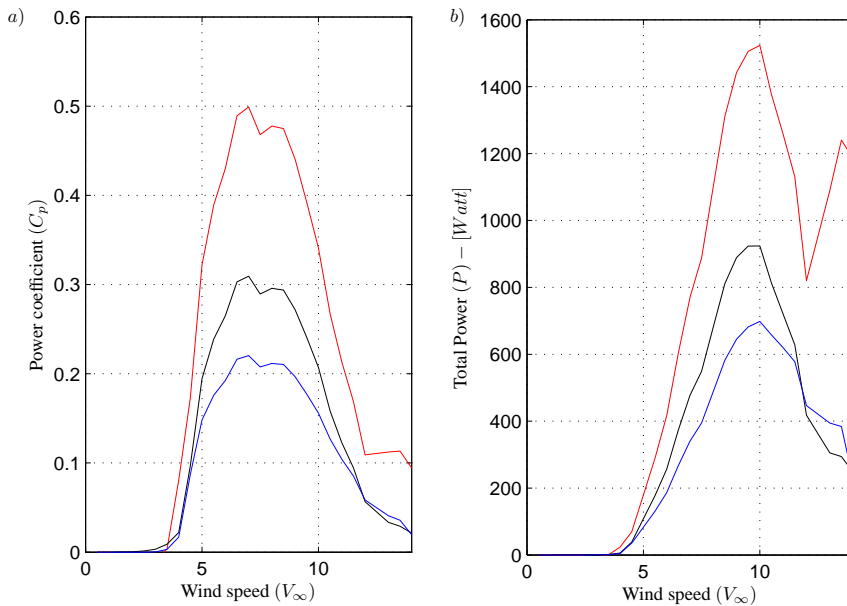
Figure 4.11 Validation of DMSTM with reference 1-kW Windspire wind turbine :
a) Power coefficient. b) Power output.
——- : Slat airfoil blade ——— : Main airfoil blade ——— : Combined output

to increase in the lift coefficient and the delaying the stall angle.

The power coefficient of the wind turbine rotor is often represented as a function of the tip speed ration (TSR). Therefore, the power coefficient of reference 1-kW Windspire wind turbine and the proposed $D^2A - VAWT$ are plotted in Figure 4.12.

It is clear that the proposed wind turbine design has a higher power coefficient and also produce more power output than the conventional three-bladed wind turbine. Scientific results of this work are submitted to an international conference and given in Appendix B.

4.3   Concluding remarks

Aerodynamic models for VAWT are still in the development process which results in a 3D CFD analysis for the VAWT performance prediction in the last decade. However, present DMSTM is quite accurate for performance evaluation of a VAWT and is computationally cheaper than the 3D CFD analysis. A DMSTM for the proposed $D^2A - VAWT$ is implemented in this chapter, and the aerodynamic loads are calculated for a new blade design. It is a rather simple approach, in which aerodynamic characteristics of the slat and main airfoils are individually used to determine
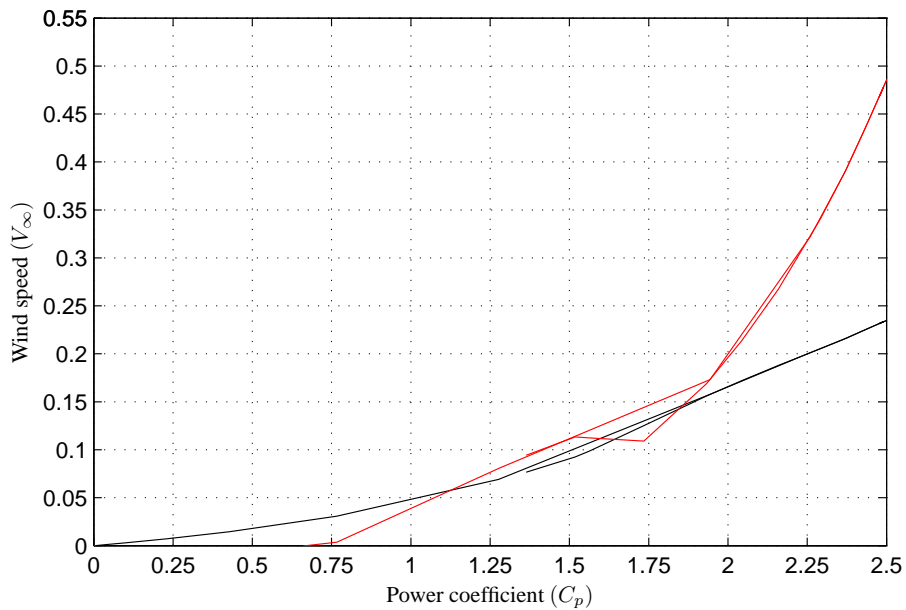
Figure 4.12 Power coefficient versus tip speed of reference and proposed wind turbine :
——— : Reference 1-kW Windspire wind turbine   ——— : Main airfoil blade   ——— : $D^2A - VAWT$

the normal and tangential forces on the blade. Further, a power coefficient from each blade are added to obtain the power coefficient of the double-element airfoil blade.

A numerical example of the reference 1-kW Windspire wind turbine is given, and the DMSTM is validated with the available experimental results. A validation result shows an accuracy within 10%, which is acceptable. Further, the geometric parameters of the reference wind turbine are used to design a proposed $D^2A - VAWT$. Input for the numerical model such as the aerodynamic characteristics of a double-element S1210 airfoil obtained from the combined method of wind tunnel testing and the 2D CFD simulations is used. The performance is calculated based on the validated DMSTM. A proposed wind turbine showed increase in the power coefficient by almost 100% as compared to the reference wind turbine of the same geometrical parameters.

CHAPTER 5
Pitch Controller

A Wind turbine blade is rotated by active or passive forces so as to change the angle of attack to extract the maximum torque. An overview of different methods used for blade pitching are given in this chapter. The aim of chapter 5 is to implement the blade pitching in the aerodynamic load modeling of $D^2A - VAWT$. An Analytical formulation of a pitch angle is derived, and the numerical simulations are carried out to compare the performance of the $D^2A - VAWT$ for active blade pitch control algorithms.

5.1 Overview of controller for VAWT

The power efficiency of a VAWT can be improved by two ways of control methods (Lazauskas 1992):

♦ self acting pitch control also called as passive pitch control.

♦ force pitch control also called as active pitch control.

A Self acting variable pitch mechanism uses aerodynamic forces to actuate self acting devices and works by creating pitching moment about blade pivot (Kirke and Lazauskas 1991). This method is totally based on the individual aerodynamic load balance on each blade. A formulation of the pitch angle is based on the aerodynamic load balance at each blade. To implement this method in practice, it is difficult to design an optimal mechanism which works in the operating range of the VAWT. The mechanism can perform very well at particular wind conditions. It is not yet commercially implemented in the VAWT, but a conceptual design can be found in (Lazauskas 1992). In another mechanism, the passive pitch control system uses mass stabilized or mass spring stabilized blades. In which a mass act as a centrifugal force generator during rotation. One such mechanism is given by (Nahas 1992). In this concept, a blade starts at a higher angle of attack to produce torque at lower speeds. When the rotational speed increases, the mass is forced outwards, and the blade is moved to a reduced angle of attack.

In forced pitch variation, individual blades are actuated by gears or cam actuator devices called Pinson cycloturbine, (Nattuvetty and Gunkel 1982), (Dress 1987) and (Vandenberghe and Dick 1987). This method is also called collective blade pitch because the change of the pitch angle is same for all blades which varies with the azimuthal position of the blade. To implement this

method in practice, it is very simple but the output is negligible compared to the individual blade pitch control method. Changing the angle of attack can also be possible either by the active or passive method. One problem found in this type of mechanism is that blades cannot be configured for high efficiency at high rotational speeds, which results in loss of performance (Sener 1995). A study carried out by Hwang et al. showed that the collective pitch control has generated 30% more power output than the similar wind turbine with fixed pitch control system (Hwang *et al.* 2005). Also, it is found by Kirke and Lazauskas that, the collective pitch control wind turbine has a higher starting torque and efficiency along with large vibration forces (Kirke and Lazauskas 2008).

In the individual blade pitch control method, these problems of large vibration and complexity of design parameters of the collective pitch control system are eliminated. Aerodynamic performance of the individual pitch control system for VAWT showed an increase in performance by 60% as compared with standard VAWT without pitch control (Hwang *et al.* 2005). With this method a pitch angle for each blade is calculated separately by two ways, i) based on sinusoidal input where the pitch angle is directly related to the azimuthal angle of the blade and the magnitude of fixed pitch angle or ii) a pitch angle required for each blade is calculated individually to maximize the VAWT rotor torque.

Active pitch control for VAWT had been critical to implement in past due to the bulkiness of the control devices. Now it has become economically cheaper to design a pitch control mechanism due to modern compact servo actuators only for research projects. Compact actuation devices makes it possible to implement pitch control algorithms such as sinusoidal pitch angle variation, individual pitch angle variation with ease. However it is yet not possible to commercialize the active pitch controlled VAWT due to high cost as compared to HAWT.

5.2   Active blade pitch controller for $D^2A - VAWT$

In this chapter, analytical formulation of the active blade pitch method is given for the $D^2A - VAWT$. The formulation of aerodynamic forces acting on the double-element airfoil is recalculated by implementing the pitch angle mentioned in chapter 4. A pitch angle β_p is the active blade pitch angle obtained in two different algorithms: i) Sinusoidal blade pitch angle and ii) Individual blade pitch angle. These two methods are further compared for power output from the $D^2A - VAWT$.

A blade in the $D^2A - VAWT$ is actively rotated to change the pitch angle about its axis of rotation. In Figure 5.1, the azimuthal angle of the slat airfoil of blade 1 (ϑ_{s1}) is dependent on the azimuthal angle (ϑ_{1j}) of the main airfoil of blade 1. The angle of a slat airfoil (ϑ_{s1_j}) in up stream and down stream can be expressed with:

$$\vartheta_{s1j} = \vartheta_{1j} + \vartheta_g - \beta_{pj} \tag{5.1}$$

For blade 2 and blade 3, the azimuthal angle is given by the same equation, (5.1), by changing
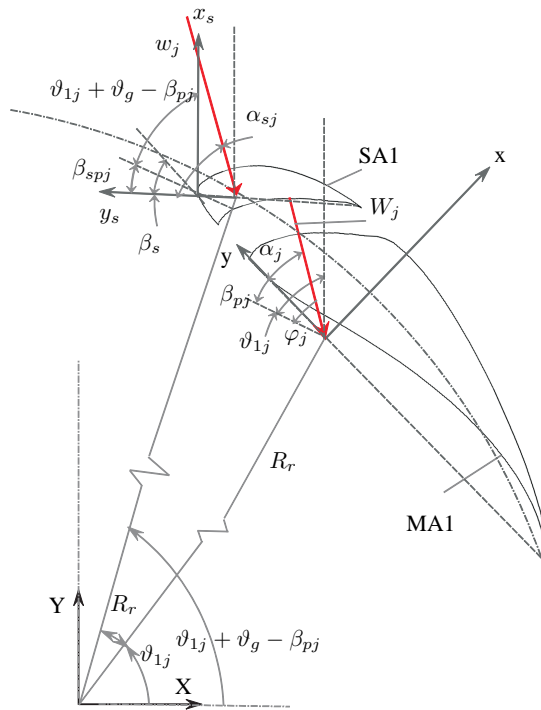
Figure 5.1 Pitch angle representation of double-element airfoil

suffix to 2 and 3 respectively. Therefore, in what follows all equations are derived for blade 1, in which the azimuthal angle of the main airfoil is denoted by ϑ_{1j}, and the azimuthal angle of the slat airfoil is represented by ϑ_{s1}. It is noted that ϑ_{1j} and ϑ_{s1} vary in the range of 0 to π in upstream and π to 2π in down stream. The fixed azimuthal angle ϑ_g is the angle between main and slat airfoil and ϑ_g is the same for all blades. The pitch angle β_{pj} in equation (5.1) is introduced due to the effect of rotation of main airfoil. The slat airfoil position and orientation are fixed relative to the main airfoil in local frame of main airfoil ($x - y$). However, a blade pitch angle of the main airfoil is introduced, which will change the position and orientation of slat airfoil in global fixed frame represented by an $X - Y$ coordinate system. The effect is that, the azimuthal angle ϑ_{s1} of slat airfoil is reduced by size of pitch angle β_{pj}.

α_j and α_{sj} are the angles of attack of the main and slat airfoils. β_{pj} is pitch angle of a main airfoil. β_{spj} is the pitch angle of slat airfoil. W_j and w_j are the relative wind velocity of the main airfoil and the slat airfoil. φ_j and φ_{sj} are the flow angles of the main airfoil and the slat airfoil respectively.

Therefore, a pitch angle is withdrawn from ϑ_s in equation (5.1). The change of position causes an increase in the radius of the rotor, which is neglected in the following formulation due to a small change in R_r.

In Chapter 4, an expression for the flow angle for the main airfoil (MA1) is given by equation (4.5). Due to the addition of the pitch angle, the flow angle changes to new relation which is expressed as follows:

$$\varphi_{1j}(\vartheta_{1j}) = \alpha_{1j}(\vartheta_{1j}) + \beta_{pj}(\vartheta_{1j}) \tag{5.2}$$

where $\alpha_{1j}(\vartheta_{1j})$ is the local angle of attack, and $\beta_{pj}(\vartheta_{1j})$ is the blade pitch angle for blade 1 in upstream and down stream of the rotor respectively.

Similarly, the flow angle for the slat airfoil (SA1), given by equation (4.22), is changed to:

$$\varphi_{s1j}(\vartheta_{s1j}) = \alpha_{s1j}(\vartheta_{s1j}) + \beta_{spj}(\vartheta_{s1j}) \tag{5.3}$$

The blade pitch angle can be expressed by two methods Sinusoidal active pitch angle and individual active pitch angle.

5.2.1 Sinusoidal active pitch angle

In sinusoidal pitch angle a amplitude of the pitch angle is decided based on the stall angle of the airfoil. The double-element S1210 airfoil designed in this study has a stall angle $\alpha_{stall} = 25°$. Therefore the β_0 should be chosen less than the α_{stall}. A sinusoidal variation of the blade pitch angle is given as follows:

$$\beta_{pj} = -\beta_0 \sin(\theta_{1j}) \tag{5.4}$$

β_0 is the amplitude of pitch angle variation, which is equal to or less than the airfoil stall angle. The negative sign indicates that the blade is rotated counterclockwise.

5.2.2 Individual active pitch angle

In individual pitch control, β_{pj} is directly calculated depending on the azimuthal position of each blade and the wind speed and directions, for which the maximum torque is obtained. For different values of blade pitch angle β_{pj}, a total torque for the VAWT rotor is calculated, and the β_{pj} is obtained. The total torque from the main airfoil of each blade can be represented as follows:

$$T_{ij}(\beta, \vartheta_{ij}) = \frac{1}{4\pi} \rho\, c_m\, R \int_m^n \int_0^H \left(c_{L_j} \sin\left(\alpha_{ij}(\vartheta_{ij}) + \beta\right) + \right.$$
$$\left. c_{D_j} \cos\left(\alpha_{ij}(\vartheta_{ij}) + \beta\right) \right) W_{ij}^2\, dH\, d\theta_i \tag{5.5}$$

where $i = 1, 2, 3$ corresponds to the number of blades. In equation (5.5) for $j = u; m = 0, n = \pi$

and for $j = d$; $m = \pi, n = 2\pi$. The pitch angle β is predefined in the range of magnitude $-20°$ to $+25°$ with interval of $1°$, for which the T_{ij} is calculated. The maximum value of T_{ij} is identified, which gives the optimal pitch angle at the particular azimuthal angle and wind conditions for individual blades. This value of optimal pitch angle corresponds to the actual pitch angle $\beta_{pj}(\vartheta_{1j})$ required for the individual blade to extract maximum mechanical power from the VAWT rotor. Further, the value of pitch angle obtained from equation (5.5) is used in equation (5.2).

Similarly, a total torque contribution by a slat airfoil blade is calculated as follows:

$$
t_{ij}(\beta, \vartheta_{sij}) = \frac{1}{4\pi} \rho c_s R \int_m^n \int_0^H \left(c_{Ls_j} \sin\left(\alpha_{sij}(\vartheta_{sij}) + \beta\right) + \right.
$$
$$
\left. c_{Ds_j} \cos\left(\alpha_{sij}(\vartheta_{sij}) + \beta\right) \right) w_{ij}^2 \, dH \, d\theta_i
$$
(5.6)

Further, the value of pitch angle for slat airfoil blade obtained from equation (5.6) is used in equation (5.3).

5.3   Numerical Example

5.3.1   Sinusoidal pitch angle variation

The performance of the proposed $D^2A - VAWT$ is carried out for a sinusoidal pitch angle variation and a individual pitch angle variation. The pitch angle demand from a sinusoidal forcing function given by equation 5.4 is determined. The amplitude of pitch angle $\beta_0 = 17°$. Figure 5.2 shows the flow angle, angle of attack and sinusoidal blade pitch angle versus the azimuthal position of the blade 1 at $TSR = 2.04$.
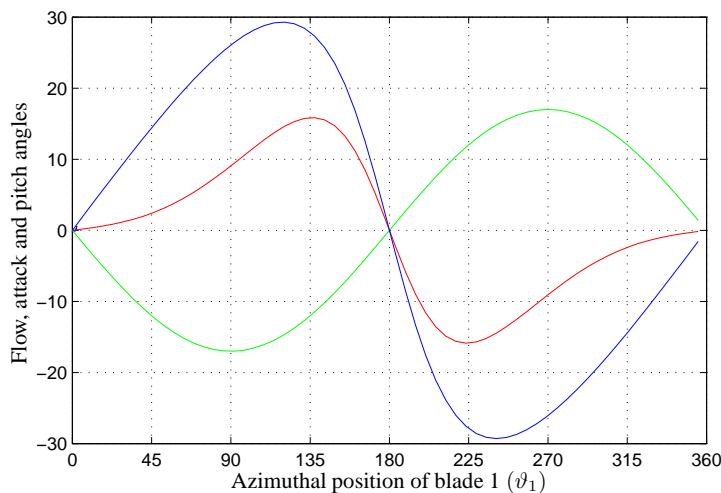
Figure 5.2 Collective pitch angle variation :   ——— : Flow angle (φ_1) ——— : Pitch angle (β) ——— : Angle of attack (α_1).

The flow angle (φ_1) is equal to the angle of attack (α_1) when blade pitch angle (β_1) is zero, which is shown by a blue solid line in Figure 5.2. In collective blade pitch control, the pitch angle is added to the flow angle, then the angle of attack changes at which the aerodynamic characteristics of airfoil are interpolated from experimental lift and drag coefficient data to determine the aerodynamic load on the blade. These aerodynamic characteristics of airfoil with respect to the angle of attack are tabulated in Appendix E. The angle of attack after blade pitch angle is added to the flow angle and shown by a solid red line in Figure 5.2. It can also be observe that the azimuthal angle $120°$ at which maximum flow angle changes to $140°$ due to the addition of the blade pitch angle. It is an indication of the late occurrence of the dynamic stall angle of the airfoil, which fulfills the purpose of the blade pitching.

The performance is plotted in Figure 5.3. There is not much increase in the power coefficient as well as the total power output from the proposed wind turbine. A collective pitch control contributes to an increase in the maximum power coefficient, which narrows down the operating

range of the wind turbine. It is suggested not to implement the collective blade pitch mechanism in wind turbine to get the maximum peak power coefficient. The peak power coefficient only increases the magnitude of peak power. Instead, the performance should be evaluated by the total power production of the wind turbine.
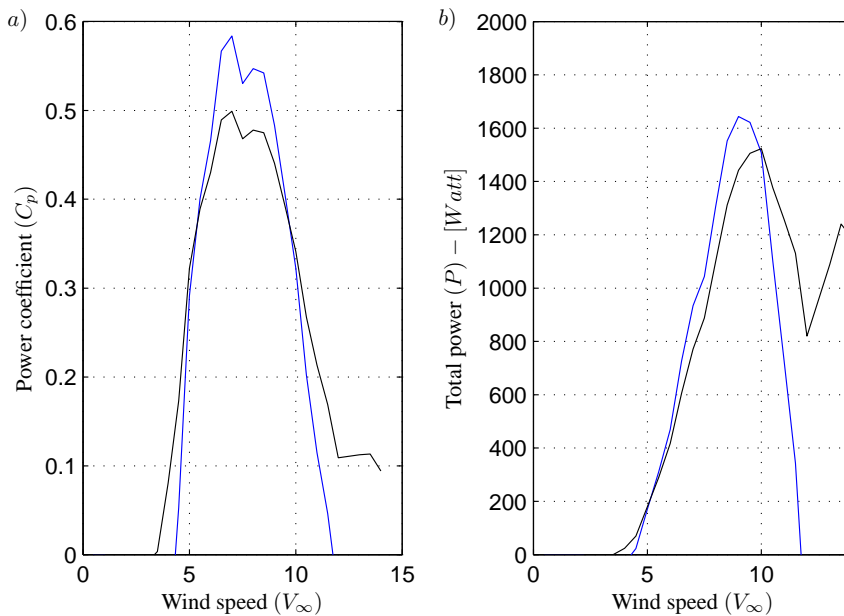
Figure 5.3 $D^2A - VAWT$ performance comparison with sinusoidal pitch control and without pitch control :
a) Power coefficient b) Power output
—— : Without pitch control
—— : With sinusoidal pitch control

5.3.2 Individual pitch angle variation

It is evident from the research carried out by Dunker et al. that, the Individual pitch angle variation shows very good performance improvement (Duncker *et al.* 2010). Therefore, an individual pitch control is implemented for $D^2A - VAWT$, and the pitch angle for each blade is calculated individually at which rotor torque is maximum. For the different wind speeds and rotor rotational speed, numerical simulation is carried out by changing the range of pitch angle from $\beta = -30°$ to $\beta = +30°$. The required pitch demand versus azimuthal angle is plotted for different tip speed ratios in Figure 5.4.

In Figure 5.4 the pitch angle is set to zero at the azimuthal angle of magnitudes $0°$ and $180°$ at which the angle of attack changes its sign. The reason for this is that at these azimuthal angles the pitch angle direction reverses, and the magnitude change that occurs is larger as compared to
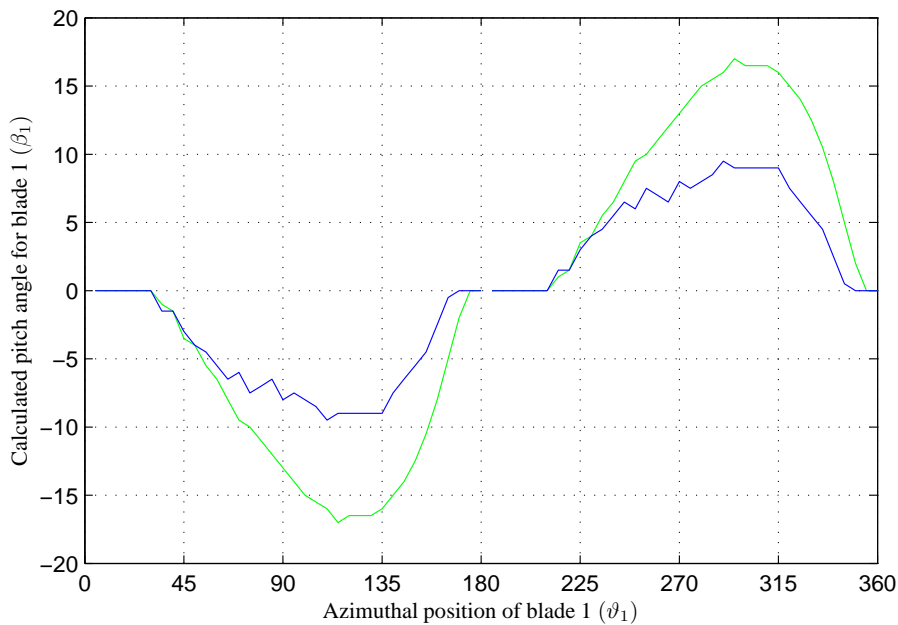
Figure 5.4 Individual blade pitch control demand : ——— : TSR = 2.04 ——— : TSR = 2.50

the gradual increase in the pitch demand at other azimuthal angles. The calculated instantaneous blade pitch angle values are not continuous as can been seen in the plot. These values can further be fitted to a smooth curve when used in reality in experimental analysis.

As it is seen previously, the variation of TSR has an effect on the angle of attack, which replicates in the pitch angle demand also. It can be seen from Figure 5.4 that, the amplitude of pitch demand is equal to $17°$ at $TSR = 2.04$, and it is equal to $9°$ at $TSR = 2.50$. It is advantageous to keep the low amplitude of the pitch angle demand in order to reduce the speed of actuation for the actuator, which is used to change the pitch angle in reality. Low speed of actuation will help in the design of actuators with respect to the actuator size and cost.

Once the pitch demand is calculated, a performance of $D^2A - VAWT$ is determined and is plotted in Figure 5.5. The performance of $D^2A - VAWT$ has considerably improved due to individual pitch control. The individual pitch control is very much an effective method. The self start ability of wind turbine is improved with increase in the maximum value of power coefficient is achieved over larger range of the wind speed. The maximum power coefficient over a larger wind speed range remains steady which results in more power production can be seen in Figure 5.5.b. The total maximum power achievable is 3000 Watts, which is three times the power output from the reference 1-kW Windspire wind turbine of the same rotor size. The peak value of the power coefficient in case of the individual pitch control is less than that of no pitch control. The VAWT rotor torque fluctuation can also be reduced considerably with an individual pitch angle
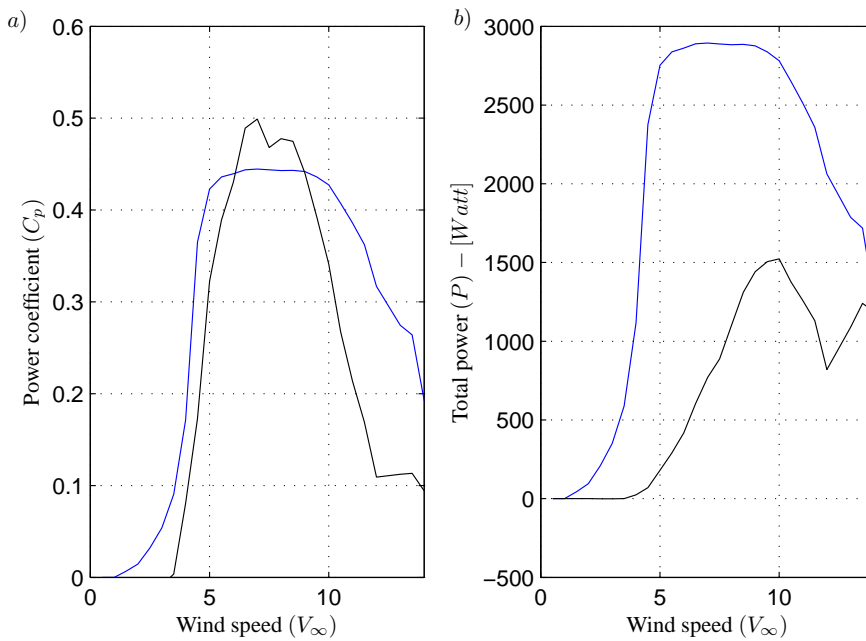
Figure 5.5 $D^2A - VAWT$ performance comparison with individual pitch control and without pitch control:
a) Power coefficient b) Power output
——– : Without pitch control ——– : With individual pitch control

variation at a certain magnitude.

It is common practice to represent the power coefficient as a function of TSR. Therefore, a power coefficient of the reference wind turbine and the proposed $D^2A - VAWT$, with and without pitch control, is plotted in Figure 4.6. A reference 1-kW Windspire wind turbine operates in low TSR. Therefore, a plot is restricted until $TSR = 2.5$. The power coefficient of $D^2A - VAWT$ without pitch control shows better performance at $TSR > 1.8$. It can be justified from the findings of this work that, the double-element airfoil has no effect under low Reynolds number ($Re < 100,000$) explained in Chapter 3. Low Reynolds number corresponds to low wind speed which lead to the low TSR. At $Re > 100,000$, the aerodynamic characteristics show considerable increase in the value and also show delay in the stall angle, which leads to a sudden increase in the power coefficient, which can be observed at $TSR > 2.0$.

A red solid line indicates the performance of pitch controlled $D^2A - VAWT$; until $TSR = 1.5$ the curve shows gradual increase with linear pattern. After this value, the curve starts showing a cubic nature. This can be explained as, to achieve optimized output pitch controller try to avoid peak performance and follows the longer path. It covers a maximum area under the power curve and also widens the operating range. The research outcome of theoretical active pitch control for $D^2A - VAWT$ is eventually published, which can be found in Appendix C and D.
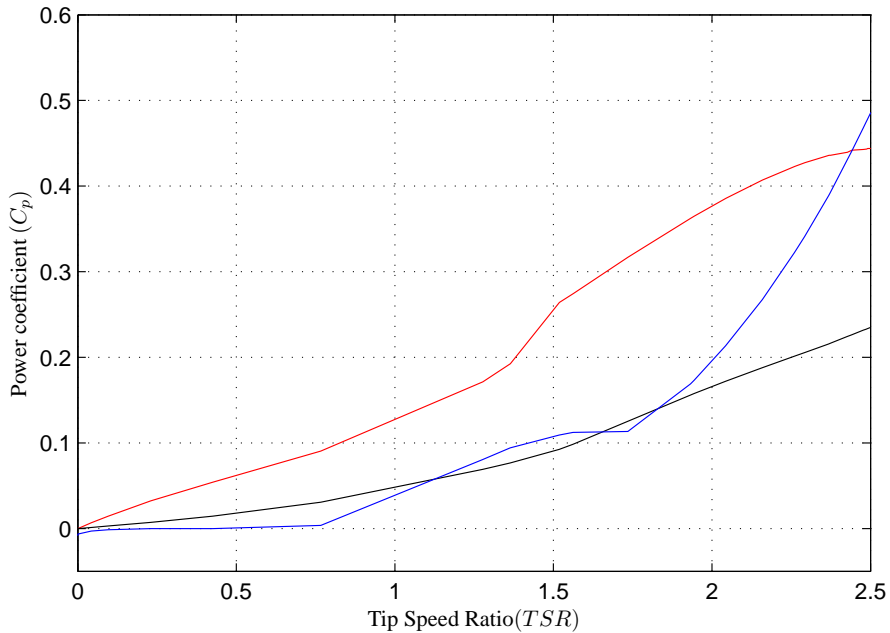
Figure 5.6 Performance of reference wind turbine and proposed $D^2A - VAWT$:
——- : Reference 1-kW Windspire wind turbine
——- : Proposed $D^2A - VAWT$ wind turbine without pitch control
——- : Proposed $D^2A - VAWT$ wind turbine with individual pitch control

5.4   Concluding Remarks

In this chapter, a theoretical analysis of two methods of pitch control are explained for the proposed $D^2A - VAWT$. The sinusoidal pitch angle variation, also called collective pitch angle variation, does not improve the rotor performance that much for the proposed $D^2A - VAWT$. The collective pitch control is advantageous in case of low cost implementation to overcome the low initial torque. It is suggested to use mechanical linkage or a central drive connected with three arms to change the pitch angle to make simple design. This is called passive pitch control mechanism and which is studied in detail and scientific results are published, refer Appendix D.

An individual blade pitching has shown an increase of 100% in the maximum power output. The problem of self start has been solved with the pitch control, and the cut in speed of the rotor changes to $V_\infty = 1.5m/s$. The reference wind turbine and the $D^2A - VAWT$ give maximum power output at wind speeds between $V_\infty = 9m/s$ to $V_\infty = 11.5m/s$. Whereas, $D^2A - VAWT$ with individual blade pitch control has extended its range of operating speed from $1.5m/s$ to $10m/s$.

Implementation of individual pitch control in theory is a comparatively easier task and straight forward. However, it was the aim of this work to determine the performance of the $D^2A - VAWT$ for individual pitch control, which has been satisfied. To design an actuator for future test rig, theoretical analysis is necessary.

CHAPTER 6
Conclusion and Future Research

A PhD project in which innovative design of straight bladed vertical axis wind turbine is proposed to improve power coefficient and the total power output. A need for new design is due the fact that, its straight forward in construction and has a potential to adopt new blade design. However less research is done in respect to vertical axis wind turbine and its problem of self start and lower power efficiency. Therefore, a multi-element airfoil blade design is proposed with modifications in the shape of best available airfoil.

Very few airfoils are suitable for use in vertical axis wind turbine application due to the mixed type of flow physics around the rotor. So it is critical for computation of aerodynamic loads on the airfoil and many aerodynamists will not believe the results without an experimental validation. Also, it is always been challenging tasks to validate computational fluid dynamic simulation results with wind tunnel experiments under this flow conditions. A proper airfoil S1210 is selected as a base airfoil in this research work which come after first try with DU06-W200 airfoil for use in design of double-element airfoil. A method of two-element airfoil blade design is suggested for use in vertical axis wind turbine. A slat airfoil is extracted from the shape of the base airfoil then the remaining portion becomes a main airfoil. A relation of airfoil division is given with respect to the main airfoil chord length. Then the arrangement is defined by main parameters, the slat angle (β_s) and the distance of trailing edge of slat airfoil from the nose of the main airfoil along the chord direction (X_{TE}).

Initially, the wind tunnel testings are carried out on double-element S1210 airfoil for different slat angles β_s and the X_{TE} then an optimal parameters are defined. From the wind tunnel tests the slat angle for S1210 double airfoil found to be optimal at value $\beta_s = 20°$. Due to the limitations of the range of angle of attack numerical simulations of the flow over double-element S1210 airfoil are carried out for optimized parameters $\beta_s = 20°$ and $X_{TE} = 4mm$ at Reynolds number $Re = 200,000$. A validation of 2D Computational Fluid Dynamics results carried out and it showed very good agrement with the wind tunnel results for this case. The accuracy of the 2D CFD results were within 5% for an angle of attack α in the range of $\pm15°$.

The aerodynamics model based on stream tube method is used to predict the performance of the proposed $D^2A - VAWT$. A double multiple stream tube model used in this work is validated

with the reference 1-kW Windspire wind turbine and then model is implemented for $D^2A - VAWT$. A performance of $D^2A - VAWT$ is represented by the power coefficient and the total power output from the rotor. It showed exciting results in which a performance of $D^2A - VAWT$ is enhanced by 100% than the reference wind turbine performance of same size. The purpose of this research work is fulfilled, however it was interesting to see how $D^2A - VAWT$ responds to the blade pitch control.

So in next step active pitch controller is implemented and a theoretical analysis is carried out. In this analysis it is found that, a total power production can be doubled for $D^2A - VAWT$ with individual pitch control mechanism also the cut in speed of the rotor can be considerably reduced down. A problem of self start is disappeared as well. It is found that, it is worth to accommodate the active pitch controller for vertical axis wind turbine to maximize the power production even though it is expensive solution. It is suggested to implement passive pitch control mechanism optimized for specific operating speed of the rotor to make it economical.

In future it is very interesting to measure a performance of $D^2A - VAWT$ in outdoor environment. A variety of different airfoil shapes also can be tested for comparison point of view. A scope of vertical axis wind turbine is immense and can be custom designed for variation applications. one such example can be vertical axis wind turbine which operates on river currents, ocean currents etc. A customized design can be made for suitable in urban environment for high rise building structures. This research work takes the vertical axis wind turbine to its new level of developments.

In my opinion vertical axis wind turbine not just having a scope for small power production but they has got potential on mega watt scale in the range of 10 MW and above for offshore applications. There are couple of project undergoing with concept of floating wind turbine in which a vertical axis wind turbine is used as rotor instead of most popular three bladed horizontal axis wind turbine.

Bibliography

Abbott, I.H. and Doenhoff, A.E.von (1949). *Theory of wing sections*. New York: McGraw-Hill.

Abbott, I.H., von Doenhoff, A.E., and L.S.Stivers (1945, September). Summary of airfoil data. Technica Report TR 824, NACA.

Aerogenerator, UK. (2010). `http://http://www.windpower.ltd.uk`.

Aerolab (1974). Aerolab educational wind tunnel document. Manual, AeroMaryland USA.

Betz, A. (1966). Introduction to the theory of flow machines,.

Bhutta, M.M.A., Hayat, N., Fahrooq, A. U., Ali, Z., Jamil, Sh. R., and Hussian, Z. (2012). Evaluation of different turbine concepts for wind power. *Renewable and Sustainabl Energy Reviews* **16**, 1926—1939.

Buhl, T. (2009, June). Research in aeroelasticity efp-2007-ii. Technical Report R-1698, RISØ.

Cahill, J.F. (1949). Summary of section data on trailing-edge highlift devices. Technica Report 938, NACA.

Castelli, M.R., Betta, S.De., and Benini, E. (2012). Effect of blade number on a straight-bladed vertical-axis darreius wind turbine. *World Academy of Science, Engineering and Technology* **61**, 305Ű–311.

Castelli, M.R., Englaro, A., and Benini, E. (2011). The darreius wind turbine proposal for a new performance prediction model based on cfd. *Energy* **36**, 4919Ű–4934.

Claessens, M. C. (2006). The design and testing of aerofoils for application in small vertical axis wind turbines.

Dam, C.P. Van (2002). The aerodynamic design of multi-element high-lift systems for transport airplanes. *Progress in Aerospace Science* **38**, 101Ű–144.

Darrieus, G.J.M. *Turbine having its rotating shaft transverse to the flow of the current*. United States Patent office.

Denmark, E. (2012, March). Accelarating green energy towards 2020. Danish energy aggrement, General Electric Company Schenectady, New York 12345 US.

Dress, H.M. (1987). The cycloturbine and its potential for broad application. *International Symposium on Wind Engineering*.

Duncker, T., Hall, C., Miles, A., Radosevic, M., Rigby, F., Seccaffien, M., and Thoday, S. (2010). The design, build and test of a small efficiency darreius wind turbine. Level IV Honours Project Project 923, The University of Adelaide.

Energy, EU. (2012). `http://www.ec.europa.eu/energy/renewables/targets_en.htm`.

Energy, Windspire (2010, October). Windspire owners manual 30 ft. standard. Product Installation and Operation Manual 150001 Version 1.18, Windspire Energy Inc.

Engage Digitizer, Digitizing Software Version 4.1. `www.digitizer.sourceforge.net`.

Eriksson, S., Bernhoff, H., and Leijon, M. (2008). Evaluation of different turbine concepts for wind power. *Renewable and Sustainabl Energy Reviews* **12**, 1419—1434.

Eurowind, RE. (2005). `http://www.re-focus.net`.

Gaunaa, M., rensen, N. N. Sø, and Bak, C. (2010, June). Thick multiple element aerofoils for use on the inner part of wind turbine rotors. *Proceeding of the science of making torque from wind*.

GE (2011, April). Wind turbine, aerodynamic assembly for use in a wind turbine, and methods for assembling thereof. Patent EP 2 466 121 A2, General Electric Company Schenectady, New York 12345 US.

Giguere, P. and Selig, M.S. (1997). Low reynolds number airfoils for small horizontal axis wind turbines. *Wind Engineering* **21**(6), 367—380.

Glauert, H. (1935). Airplane propellers in w. f. durand edition. *Aerodynamic Theory* **4**, 169–Ű360.

Gorelov, D.N., Krivospitsky, V.P., and Otero, A.D. (2008). Prospects for development of wind turbines with orthogonal rotor. *Thermophysics and Aeromechanics* **15**, 153—157.

Hansen, M.O.L. (2008). *Aerodynamics of Wind Turbines, 2nd Edition*. Earthscan.

Hau, E. and Renouard, H. (2006). *Wind Turbines : Fundamentals, Technologies, Application, Economics / by Erich Hau, Horst Renouard* (Second Edition ed.). Berlin, Heidelberg: Springer-Verlag Berlin Heidelberg.

Huskey, A., Bowen, A., and Jager, D. (2009, December). Wind turbine generator system power performance test report for the mariah windspire 1-kw wind turbine. Test Report NREL/TP-500-46192, NREL.

Hwang, S., Hwang, C.S., Min, S.Y., Jeong, I.O., Lee, Y.H., and Kim, S.J. (2005). Efficiency improvement of a cyclodidal wind turbine by active control of blade motion. *Flight Vehicle Research Center* **1**(1), 1—9.

Islam, M., k. Ting, D.S, and Fartaj, A. (2007). Desirbale airfoil features for smaller capacity straight-bladed vawt. *Wind Engineering* **31**(3), 165—196.

James, R.M. (1977). Theory and design of two airfoil lifting system. *Computer methods in applied mechanics and engineering* **10**, 13Ű–43.

Kirke, B.K. and Lazauskas, L. (1991). Enhancing the performance of a vertical axis wind turbine using a simple variable pitch systems. *Wind Engineering* **15**(4), 187—195.

Kirke, B.K. and Lazauskas, L. (2008). Variable pitch darrieus water turbines. *Journal of Fluid Science and Technology* **3**(3), 1—9.

Lapin, E.E. (1975). Theoretical performance of vertical axis wind turbines. *ASME Paper* (75-WA/ENER-1).

Lazauskas, L. (1992). Three pitch control systems for vertical axis wind turbines compared. *Wind Engineering* **16**(5), 269Ű–283.

Lew, P. (2011, April). Multi-element wind turbine airfoils and wind turbine incorporating the same. Patent US2011 0255972 A1, US Patent Office.

Malcolm, D.J. (2003, March). Market, cost, and technical analysis of vertical and horizontal axis wind turbines. Technology update, Global Energy Concepts, LLC.

Maydew, R.C. and Klimas, P.C. (1981). Aerodynamic performance of vertical and horizontal axis wind turbines. *Journal of Energy* **5**(3).

Miau, J.J., Liang, S.Y., Yu, R.M., Hu, C.C., Leu, T.S., Cheng, J.C., , and Chen, S.J. (2012). Design and test of a vertical axis wind turbine with pitch control. *Applied Mechanics and Materials* **225**(5), 338Ű–343.

Mohamed, M.H. (2012). Performance investigation of h-rotor darrieus turbine with new airfoil shapes. *Energy* **47**, 522Ű–530.

Nahas, M. (1992). A self starting darrieus type windmill. *Energy* **18**(9), 899—906.

Nattuvetty, V. and Gunkel, W.W. (1982). Theoretical performance of a staright bladed cycloturbine under different operating conditions. *Wind Energy* **6**(3), 110—130.

Newman, B.G. (1983). Actuator disc theory for vertical axis wind turbines. *Journal of Wind Engineering and Industrial Aerodynamics* **15**, 347.

Obert, E. (1993, September). Forty years of high-lift r&d an aircraft manufacturers experience, high-lift system aerodynamics. Technica Report CP 515, AGARD.

Paraschivoiu, I. (1981, February). Double-multiple streamtube model for darrieus rotor.

Paraschivoiu, I. (1984, January). Description of software cardaa and cardaav for the calculation of aerodynamics of darrieus wind turbine. Technical Report IREQ-8RT3010G, Research institute of Hydro-Quebec.

Paraschivoiu, I. (2009). *Wind Turbine Design: with Emphasis on Darrieus Concepts*. Canada: Polytechnic International Press.

Paulsen, U.S., Vitaa, L., Madsena, H.A., Hattelb, J., Ritchiec, E., Lebanc, K.M., Berthelsend, P.A., and Carstensene, S. (2012). 1st deepwind 5 mw baseline design. *Energy Procedia* **24**, 27–Ű35.

Ponta, F.L., Otero, A., and Lago, L. (2011). *Innovative Concepts in Wind-Power Generation: The VGOT Darrieus, Wind Turbines* (Dr. Ibrahim Al-Bahadly ed.). Canada: InTech.

Ponta, F.L., Seminara, J.J., and Otero, A.D. (2007). On the aerodynamics of variable geometry oval trajectory darrieus wind turbines. *Renewable Energy* **32**, 35—56.

Prandtl, L. and Tietjens, O. G. (1957). *Applied Hydro and Aeromechanics* (Second Edition ed.). New York: Dover Publications.

Savonious, S.J. (1931). The s-rotor and its applications. *Mechanical Engineering* **53**(5), 333—338.

Seao2, S. `http://http://www.seao2.com`.

Selig, M.S. and Guglielmo, J.J. (1997). High-lift low reynolds number airfoil design. *Journal of Aircraft* **34**(1), 72—79.

Selig, M.S., Guglielmo, J.J., Broeren, P., and Gigure, P. (1995). *Summary of Low-Speed Airfoil Data*, Volume 1. Virginia Beach, Virginia: SoarTech Publications.

Sener, Y.A. (1995). Investigation of parameters of wind turbine efficiency. *Akara* **1**(1), 4—7.

Sharpe, T., Proven, G., and Otero, A.D. (2010). Crossflex: concept and early development of a true building integrated wind turbine. *Energy and Buildings* **42**, 2365Ű–2375.

Singha, R.K., Ahmeda, M.R., Zullahb, M.A., and Lee, Y-H. (2012). Design of a low reynolds number airfoil for small horizontal axis wind turbine. *Renewable Energy* **42**, 66—76.

Smith, A.M.O. (1972, November). Aerodynamics of high-lift airfoil systems,fluid dynamics of aircraft stalling. CP 102, AGARD.

Smith, M.S. (1975, June). High lift aerodynamics. *Journal of Aircraft* **12**(6), 501—530.

Spera, David A. (2009). *Wind Turbine Technology: Fundamental Concepts in Wind Turbine Engineering* (Second Edition ed.). USA: ASME.

Strickland, J.H. (1975, October). The darrieus turbine : A performance prediction model using multiple streamtube. Technical Report SAND75-0431, Sandia Laboratories.

Templin, R.J. (1974, June). Aerodynamic performance theory for the nrc vertical axis wind turbine. Technical Report LTR-LA-160, N.A.E.

Vandenberghe, D. and Dick, E. (1987). A theoretical and experimental investigation into straight bladed vertical axis wind turbine with second order harmonic pitch control. *Wind Engineering* **11**(5), 237–247.

Wakui, T., Tanzawa, Y., Hashizume, T., and Usui, A. (2000). Optimum method of operating the wind turbine-generator systems matching the wind condition and wind turbine type. *World Renewable Energy Congress* **VI**, 2348—2351.

Williamson, G.A., McGranahan, B.D., Broughton, B.A., Deters, R.W., Brandt, J.B., and Selig, M.S. (2012). Summary of low-speed airfoil data. Technical report, Department of Aerospace Engineering, University of Illinois at Urbana-Champaign.

Wilson, R.E. (1977). Darrieus rotor aerodynamics. *Proceedings of the third biennial conference and workshop on wind energy conversion systems*, 584—594.

Wilson, R.E. and P.B.S.Lissaman (1974, May). Applied aerodynamics of wind power machines. Technical report, Oregon State University, USA.

Young, A.D. (1953). The aerodynamic characteristics of flaps. Technical Report 2622, ARC.

Experimental study of the effect of a slat angle on double-element airfoil and application in vertical axis wind turbine

Ships and Offshore Structures

Experimental study of the effect of a slat angle on double-element airfoil and application in vertical axis wind turbine

Prasad D. Chougule[a], Lasse Rosendahl[b] & Søren R.K. Nielsen[a]

[a] Department of Civil Engineering, Aalborg University, Aalborg, Denmark

[b] Department of Energy Technology, Aalborg University, Aalborg, Denmark
Published online: 14 May 2014.

PLEASE SCROLL DOWN FOR ARTICLE

Taylor & Francis
Taylor & Francis Group

Experimental study of the effect of a slat angle on double-element airfoil and application in vertical axis wind turbine

Prasad D. Chougule[a,*], Lasse Rosendahl[b] and Søren R.K. Nielsen[a]

aDepartment of Civil Engineering, Aalborg University, Aalborg, Denmark; bDepartment of Energy Technology, Aalborg University, Aalborg, Denmark

A design of double-element airfoil is proposed for its use in the vertical axis wind turbine. The double-element airfoil system consists of a main airfoil and a slat airfoil. The design parameters of the double-element airfoil system are given by the position and orientation of the trailing edge of the slat airfoil with respect to the nose of the main airfoil. The position parameters are given by x_{TE} and y_{TE}. The orientation is given by the slat angle β_s; it is the angle between the chord lengths of the slat airfoil with respect to the main airfoil. Various tests were performed using different slat angles at various Reynolds numbers to measure the aerodynamic characteristics, so as to study the slat angle effects. The variation in the slat angle causes a change in the lift coefficient of the double-element airfoil considerably. Therefore, an optimum value of slat angle is determined for the double-element airfoil system designed in this paper. Further, the performance of new design of a vertical axis wind turbine shows considerable increase in the power coefficient and the total power output as compared to the reference wind turbine.

Keywords: double-element airfoil; wind tunnel testing; vertical axis wind turbine design; offshore application

Introduction

The single airfoil design and flow analysis by experimental methods is well known from centuries in the aviation industry, and it has become a key element in wind turbines later on. The design of an airfoil is a very important issue in the aviation and wind turbine industry. The lift coefficient of the airfoil, which improves the performance of an aeroplane, can be increased by using the multi-element airfoil system. The physics of multi-element airfoil in air was explained by Smith in the 1970s (Smith 1975). At that time, the physical phenomenon of multi-element airfoil was correctly introduced, and the effects of slat airfoil in front of main airfoil were understood.

The airfoils used in the high lift system works at Reynolds number Re = 1, 000, 000. With little modifications, these airfoils can be directly used in the design of horizontal axis wind turbine blade (HAWT). However, in case of the vertical axis wind turbine (VAWT), there is a need for special airfoils because the Reynolds number in this case is Re ≤ 500, 000. A recent study is carried out (Bah and Sankar 2013), in which the use of multi-element airfoil is investigated to improve the performance of VAWT numerically. Similarly, an attempt has been made by Gaunaa et al. (2010) and Zahl et al. (2012) to make use of double-element airfoil in HAWT. Findings of these two research work provide guidelines for the design of the double-element airfoil.

The research study also concluded that double-element airfoil is useful to incorporate in multi-rotor design of HAWT (a concept patented by Lew 2011). This concept has become a starting point for the design of double-element airfoil for its use in VAWT at Reynolds number Re ≤ 500, 000. The airfoils used in the design of VAWT can be found in the literature (Mohamed 2012).

In general, NACA symmetric airfoils are used in the design of traditional VAWT blades such as NACA0012, NACA0018, etc. However, in the current work, an airfoil designed at TU Delft is used, named DU06W200 (Claessens 2006). The reason for choosing this airfoil is that it is suitable for low tip speed ratio and has an improved power coefficient as compared to the other symmetric airfoils from the NACA series. Therefore, a DU06-W200 is used as a base airfoil in design of double-element airfoil. Further, two blades of desired length and designed chord length are manufactured by three-dimensional printing technology. These two blades are connected with each other by a link which forms a test specimen. An arrangement is made to change the slat angle of the slat airfoil blade to carry out various tests. This test specimen of double-element airfoil blade is used to perform wind tunnel tests in the Aerolab educational wind tunnel (Aerolab 2010).

The normal and axial forces acting on the double-element airfoil are measured with the data acquisition

---

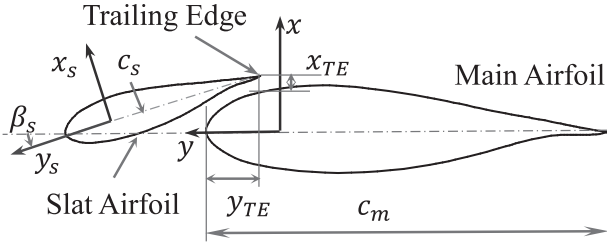*Corresponding author. Email: pdc@civil.aau.dk

Figure 1. Double element DU06-W200 airfoil.

Table 1. Physical properties of air and parameters of double-element airfoil.

Symbol	Value	Unit
ρ	1.21	kg m^{-3}
μ	1.84×10^{-5}	kg m^{-1} s
c_m	0.100	m
c_s	0.050	m
x_{TE}	0.030	m
y_{TE}	0.004	m

system of the wind tunnel. Raw experimental data obtained from the wind tunnel is accurately fitted with the polynomial curve fitting method, and then the lift and drag coefficients are calculated. Further, to this work a double multiple-stream tube method (DMSTM) is used for calculation of induced velocities in the VAWT rotor, and then a blade element method is used to determine the aerodynamic load on the blade (Strickland 1975; Paraschivoiu 2002). A reference 1 kW (Windspire Energy Inc 2010) VAWT is used for the verification of the numerical model based on DMSTM. Then, the power coefficient and the total power output from new VAWT are determined. A comparative study validates that the new VAWT design improves the power coefficient and power output considerably. The new VAWT design can be effectively used on ships and offshore structures to harvest the wind power into electrical energy. It is also interesting to determine the vibrations on the VAWT structure due to ship motion.

In section 'double-element airfoil', the design and terminologies used in a double-element airfoil blade structure are explained. In section 'experimental analysis' information about the wind tunnel test set-up, test variables, validation of test results and outcomes of all tests performed are discussed. Section 'numerical performance analysis' discusses performance of new design of VAWT. The research work is concluded in last section with further research scope.

Double-element airfoil

Double-element airfoil blade structure is constructed by the main and the slat airfoil as shown in Figure 1.

The position of the trailing edge (TE) of slat airfoil and orientation of the slat airfoil with respect to the main airfoil are important design variables. The reason for that is, these two variables cause delay in the stall angle of airfoil and develop the high lift. Two variables representing the position and the orientation of a slat airfoil with respect to the main airfoil are expressed by three parameters. The first two parameters describe the position of the TE of the slat airfoil along the local x-direction (x_{TE}) and along local y-direction (y_{TE}), respectively. In this work, the parameters x_{TE} and y_{TE} are kept constant. The third parameter is the slat angle (β_s), which represents the orientation of a slat

airfoil, which is the angle between the chord length of the slat airfoil (c_s) and the local x-direction. The slat angle is positive in a nose-up direction.

In Gaunaa et al. (2010), it is found that locating the TE of a slat airfoil at 15% of the chord length of a main airfoil (c_m) is an overall good position. In addition, the effective normal distance between the main and the slat airfoil is less. However, a normal distance of less than 5% of c_m is optimal. Therefore, in double-element airfoil blade design, the position and orientation of the slat airfoil with respect to the main airfoil was chosen as per findings in Gaunaa et al. (2010), irrespective of the airfoil shape and its size. These parameters of double-element airfoil can be found in Table 1.

In Table 1, ρ is the air density, μ is the air viscosity, and c_m and c_s are the respective chord lengths of the main and slat airfoil.

It should be noted that the parameters are slightly modified (reduced) to keep the minimum possible normal distance between the TE of the slat airfoil and the upper surface of a main airfoil.

Experimental analysis

Various experiments are performed at different wind speeds which correspond to different Reynolds numbers as follows:

$$\mathrm{Re} = \frac{\rho V_\infty (c_m + c_s)}{\mu} \qquad (1)$$

where u_{expt} is the wind speed during wind tunnel testing. The wind speed (V_∞) which is set during various tests is given in Table 2.

Table 2. Wind tunnel velocity setting.

Sr. No.	1	2	3	4	5	6	7
V_∞ (m^{-1} s)	10	13	15	20	23	25	34

Figure 2. Double element airfoil in wind tunnel. (This figure is available in colour online.)

Wind tunnel test set-up

In this work, a wind tunnel testing is carried out in order to determine

- the lift and drag coefficient and
- the effect of slat angle (β_s) on lift coefficient.

The dimensions of the wind tunnel are 305 mm width, 305 mm height and 610 mm length (Aerolab 2010). The range of wind speed achievable is 4.5–60 m/s. The wind tunnel used in this work has limitation on the angle of attack which can be adjusted in the range of $\pm 22°$. The mounting arrangement for a double-element airfoil in the wind tunnel is shown in Figure 2.

The slat airfoil is bolted together with the main airfoil by two side links fixed to the main airfoil, and a linear adjustment is provided by a slot on link end so that the position parameter x_{TE} can be adjusted. The y_{TE} position can be adjusted by rotating the links about the main airfoil. The third parameter β_s is set by an angular position of a slat airfoil with respect to two side links parallel to the chord length of a main airfoil. The optimum length of the double-element airfoil blade is 250 mm for this wind tunnel and is represented by h length of double-element airfoil blade.

The Aerolab wind tunnel has a data display and an acquisition system through which, the normal force N_f and the tangential force A_f acting on a double-element airfoil are obtained and then stored in a text format. These forces are then converted to an experimental lift force L_f and a drag force D_f by the following equation:

$$L_f(\alpha) = N_f \cos(\alpha) - A_f \sin(\alpha)$$
$$D_f(\alpha) = N_f \sin(\alpha) + A_f \cos(\alpha) \quad (2)$$

Finally, the experimental lift coefficient c_L and experimental drag coefficients c_D are obtained,

$$c_L = \frac{L_f}{\frac{1}{2}\rho V_\infty^2 (c_m + c_s) h}$$
$$c_D = \frac{D_f}{\frac{1}{2}\rho V_\infty^2 (c_m + c_s) h} \quad (3)$$
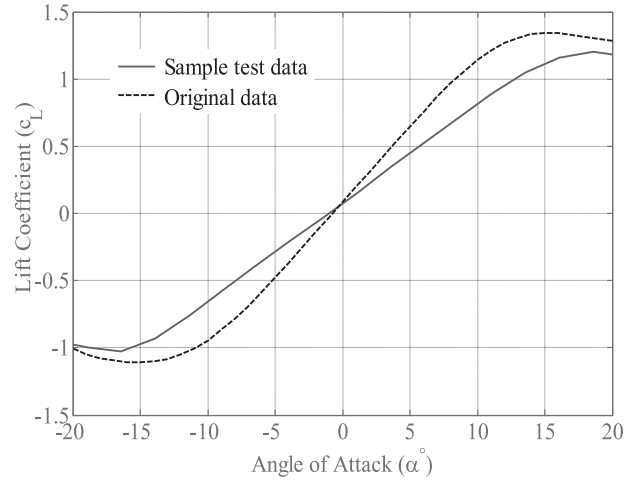
Figure 3. Results of verification test: lift coefficient.

Validation of test results

The accuracy of experimental results is first checked with the sample testing. In this sample, verification test for single DU06-W200 airfoil is carried out at Re = 300,000 and the test results are compared with the available lift coefficient data from Claessens (2006) at Re = 300, 000. Figure 3 shows the lift coefficient versus the angle of attack for DU06-W200 airfoil.

The maximum lift coefficient value for the test specimen is 1.204, which occurs at an angle of attack 18.6°. In the original test results, the maximum lift coefficient value is 1.34, which occurs at the angle of attack of magnitude 17° (Claessens 2006). It is clear that the wind tunnel test carried in this study exists with an error of 10%. These tests are carried in two different wind tunnels which justifies that there is an error in the lift coefficient to some extent. Overall, the test specimen used in this study was not optimised to be used in Aerolab wind tunnel. Also, the results are influenced by the wind tunnel walls, which cause the lower value of lift coefficient as compared to the original values.

In this study, the error of 10% was accepted for due to a reason that the aim of this paper is to determine the optimal slat angle. With this validation test results, further tests are carried out as mentioned in Table 3.

Table 3. Variable in seven different tests.

| Sr. No. | Re | Pitch angle β_s | | | | | |
		10°	16°	20°	25°	30°	45°
1	100,000	×	×	×	×	×	×
2	130,000	×	×	×	×	×	
3	150,000	×		×		×	×
4	200,000	×	×	×	×	×	×
5	230,000	×	×	×		×	
6	250,000	×			×	×	
7	340,000	×				×	

Figure 4. Double-element DU06-W200 airfoil at Re = 200,000: lift coefficient.

Figure 5. Double-element DU06-W200 airfoil at $\beta_s = 20°$: lift coefficient.

In Table 3, ' × ' sign indicates that the test has been done, and an empty space indicates that the test has not been carried out at this Reynolds number for the respective slat angle. The selective tests are performed due to the reason that the test results are very good at certain slat angles, for example, 10°, 20° and 30°. Primary measured data analysis reveals that theses slat angles are of interest in this study.
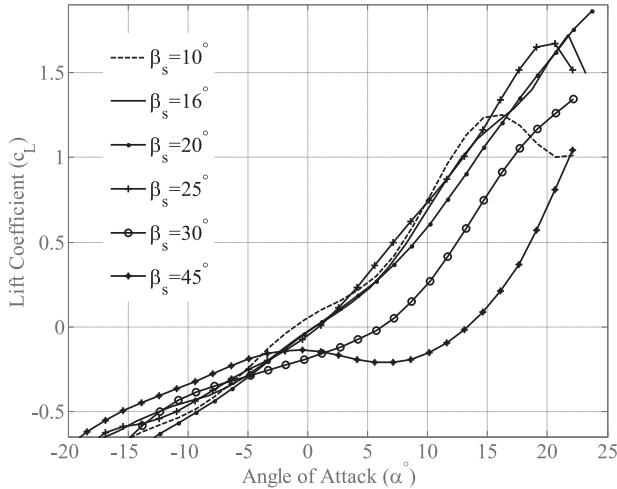
Results and discussion

Figure 4 shows the lift coefficients of the double-element DU06-W200 airfoil at Re = 200,000 for different slat angles.

A lift curve of double-element airfoil at $\beta_s = 10°$, 16° and 20° is gradually increasing for positive angle of attack. The stall angle occurs at 15° and 22° of angles of attack for slat angles $\beta_s = 10°$ and 16°, respectively. A stall angle is the angle of attack of the airfoil at which the lift coefficient starts declining and airfoil enters in dynamic stage.

At $\beta_s = 20°$, the lift curve has not shown any stall behaviour yet until the angle of attack reaches to $\alpha = 24°$. Due to the limitation of the angle of attack adjustment in wind tunnel, it was not possible to increase the angle of attack further. At $\beta_s = 25°$, the lift curve showed a stall angle at $\alpha = 20°$, which indicates that the effect of a slat angle starts declining at this angle. Later on, the slat angle is changed to $\beta_s = 30°$, and the lift coefficient reduces gradually. For the slat angle of $\beta_s = 40°$, it showed similar behaviour of lift curve which confirms that the further increase in the slat angle is not advantageous. From this, it is concluded that the lift coefficient drastically decreases along with the shift in a lift curve towards positive angle of attack at $\alpha = 25°$. It is observed that the slat angle $\beta_s = 20°$ performs better than any other slat angles tested in this experimental study. Therefore, test results at $\beta_s = 20°$ angle are further dis-

cussed in detail with different Reynolds numbers. Figure 5 shows the lift coefficient of double-element DU06-W200 airfoil with slat angle $\beta_s = 20°$ at various Reynolds numbers.
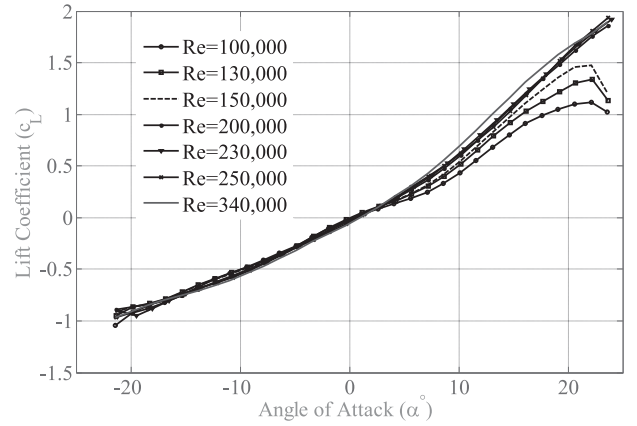
The lift coefficient under Re $< 150,000$ soon enters into the stall behaviour. Also, the variation in the maximum value of the lift coefficient between Reynolds numbers Re = 100,000 and 130,000 is 16%. Similarly, between Reynolds numbers Re = 130,000 and 150,000, it is 10%. It shows the gradual decrease of difference in the maximum lift coefficient of two successive Reynolds numbers. From this, the following conclusion is drawn: at Re = 150,000, there is a large influence of mixed flow conditions, and an airfoil under this Reynolds number does not work properly.

In the range of Reynolds number Re = 200,000 and 250,000, the lift coefficient almost remains unchanged. The double-element airfoil shows stable lift coefficient in this range. Also, the stall angle is not yet appeared which indicates that the airfoil performance is very good at these Reynolds numbers. An experiment is carried out for a higher Reynolds number Re = 340,000 which does not show increase in the maximum lift coefficient. However, it has shown overall improvement in the lift curve by 5% between angle of attack $\alpha = 5°$ and 20° as can be seen in Figure 5.

A drag coefficient is plotted in Figure 6. It is important to observe the behaviour of drag coefficient. The drag coefficient for Reynolds number Re $\leq 150,000$ is very large as compared to other Reynolds numbers. The drag coefficient of maximum magnitude 0.5 for the angle of attack between $\pm 25°$ is in the acceptable range, where the stall angle is not achieved yet at Re $\geq 150,000$. The high value of drag coefficient also explains that the flow is unsteady at the wind tunnel wall. The double-element DU06-W200 airfoil designed in this study performs very well for Re $\geq 150,000$ at slat angle of $\beta_s = 20°$.
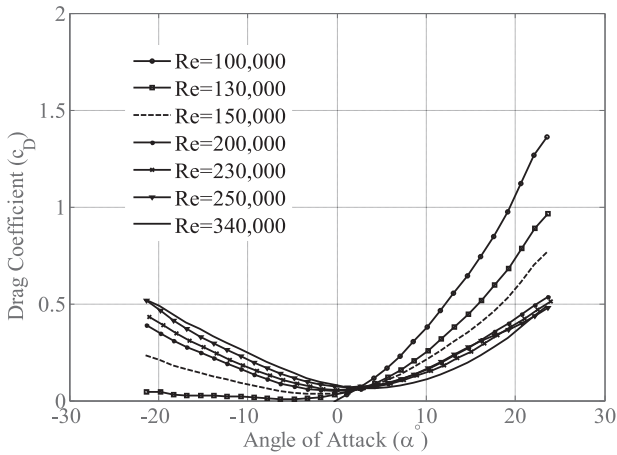
Figure 6. Double-element DU06-W200 airfoil at $\beta_s = 20°$: drag coefficient.

Numerical analysis

A reference Windspire 1 kW wind turbine is considered for comparison with the new design of the VAWT with the double-element airfoil. Parameters of the reference 1 kW wind turbine and double-element airfoil VAWT are given in Table 4.

DMST model

In this study, it is proposed to make use of a double-element airfoil for the construction of a three-blade VAWT. The use of multi-element airfoil in the blade construction has shown increase in the lift coefficient, which is directly proportional to the total power output of the VAWT. The proposed new design of VAWT schematics is shown in Figure 7.

Ω is the rotational speed of the rotor. V_i and V_w are the intermediate and wake velocity. The angle β_s represents the fixed geometrical axis between the main airfoil and a slat airfoil, which is same for all the three blades. Aerodynamics of a VAWT and the flow around the rotor is mainly studied by a multiple actuator disc theory (Newman 1986). The velocity components at various locations in the flow area are of interest, which are calculated by momentum theory and the blade element theory. There are different stream tube methods to describe the VAWT rotor. Such methods are the
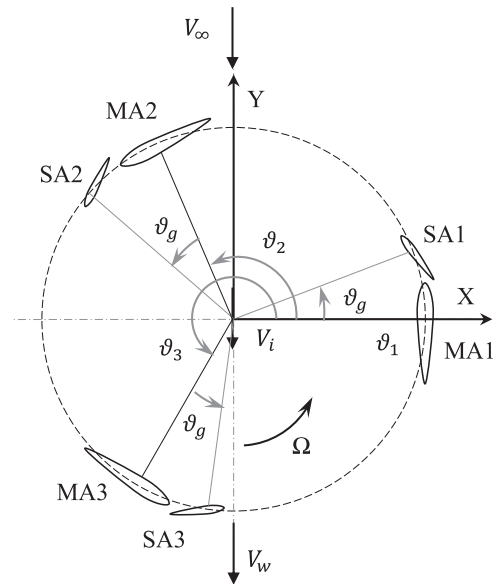
Figure 7. Schematic of VAWT with double-element airfoil in blade design.

single stream tube method, multiple stream tube method and the double multiple stream tube method (DMSTM), where the latter approach offers more precise predictions (Paraschivoiu 1982). In DMSTM, the flow field outside the rotor is divided into two subfields, placed up-stream and down-stream of the rotor. The fluid flow is considered to be inviscid and incompressible for the calculation of the induced velocity through each stream tube. Since the flow field is divided into two halves, it is necessary to derive the local angle of attack, local relative velocity for up-stream and down-stream of the rotor individually. In this study, it is important to determine the aerodynamic loads based on the wind tunnel experimental results and further evaluate the performance of the new VAWT. Author has explained more about numerical modelling which can be referred in Chougule et al. (2013) for more details. To understand the basics of aerodynamic load modelling of VAWT, one can refer to a text book on Darrieus wind turbine design (Paraschivoiu 2002).

Validation of DMST model

In this study, the rotor diameter and the rotor height are same for reference wind turbine and the new wind turbine. The chord length is changed as per double-element airfoil design. The performance evaluation is based on the experimental data available for 1.2 kW Windspire VAWT (Huskey et al. 2009). The wind speed versus rotational speed of the rotor is an input to the numerical calculations.

Figure 8 shows the measured power coefficient and total power curve for the reference Windspire 1 kW wind turbine. The validation of a DMSTM numerical model is carried

Table 4. Geometric parameters of reference and new VAWT.

Description	Symbol	Value
Height of rotor	H	6.100 m
Diameter of rotor	D_r	1.220 m
Single airfoil chord length	c	0.123 m
Main airfoil chord length	c_m	0.085 m
Slat airfoil chord length	c_s	0.035 m
Slat TE position x direction	x_{TE}	0.015 m
Slat TE position y direction	y_{TE}	0.006 m

Figure 8.   Verification of DMSTM. (a) Power coefficient. (b) Power output; —— represents numerical results DMSTM model and – – – represents Windspire measurement.

Figure 9.   Performance of new VAWT. (a) Power coefficient. (b) Power output.

out based on the experimental power output of a reference Windspire 1 kW wind turbine. Based on the data given in Table 1, a total power output from DMSTM numerical model is compared with available experimental data. The maximum power coefficient of the reference wind turbi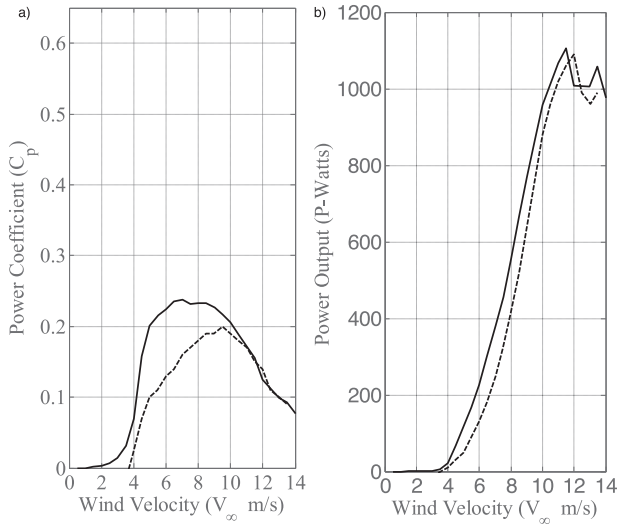ne is 0.20, whereas DMSTM predicts 0.23 with an overestimate of 15%. The validation shows that the order of accuracy of DMSTM model used for numerical simulations is acceptable to predict the power performance of the new VAWT.

Performance of new VAWT

Numerical simulation is performed at Reynolds number Re = 230,000 for new design of VAWT. The power coefficient and the power output for new design are plotted in Figure 9. There is an increase in the maximum power coefficient of the VAWT from 23% to 44% for new design of VAWT. The performance of the new design of VAWT has nearly doubled as compared to the reference wind turbine.

The effect of the high lift and the delay of the stall angle are advantageous in VAWT, because the angle of attack that occurs in the VAWT is comparatively higher than HAWT. Therefore, it can be concluded that the use of a double-element airfoil in VAWT blade design significantly improves the performance of wind turbine. The power efficiency of the reference 1 kW Windspire wind turbine can be increased from 20% to 37.4% in reality. It is worth to note that the peak power output is tremendous as compared to the reference wind turbine power output. This can be disadvantageous for the electrical system component operating at such a peak power output and falls down drastically.

Conclusion

A double-element airfoil blade design is proposed in this work for its use in VAWT. However, the focus of study is to experimentally determine the effect of the slat angle on the lift coefficient of double-element airfoil system. Initially, a verification test is carried out in order to determine the accuracy of the results obtained in this study. An error of 10% is observed in verification test results and the original data of selected airfoil. With the acceptance of this error, further tests are carried out for the double-element airfoil system. The aerodynamic characteristics, mainly the lift and the drag coefficient of a double-element airfoil, are obtained for different Reynolds numbers at different slat angle. A wind tunnel test reveals that a slat angle of magnitude 20° has optimum effect on the lift coefficient curve and it is the most suitable angle for the designed double-element airfoil in this study.

A power coefficient and total power output of new design of VAWT are numerically determined and compared with a reference Windspire 1 kW wind turbine. The power coefficient of the straight-bladed VAWT is improved up to 43%. An effective use of the double-element airfoil in the blade design instead of using a single airfoil has doubled the total power output. There are different airfoils available, which can be utilised in the design of a VAWT blade with the double-element airfoil system. Hence in future, different airfoil shapes will be checked and various combinations of the main and the slat airfoils will be investigated for their use in VAWT.

References

Aerolab. 2010. Aerolab educational wind tunnel. Maryland (MD). http://www.aerolab.com/downloadable-documents/ewtbrochure.pdf

Bah EA, Sankar JJ. 2013. Investigation on the use of multi-element airfoils for improving vertical axis wind turbine performance. 51st AIAA aerospace sciences meeting including the new horizons forum and aerospace expostion; 2013 Jan 7–10; Grapevine, TX. Reston, VA: American Institute of Aeronautics and Astronautics.

Chougule PD, Nielsen SRK, Basu B. 2013. Active blade pitch control for Darrrieus straight bladed vertical axis wind turbine of new design. In: Damage assessment of structures X: 10th International Conference on Damage Assessment of Structures (DAMAS). Zurich-Dumten (Switzerland): Trans Tech Publications Ltd. p. 668–675.

Claessens MC. 2006. The design and testing of airfoils for application in small vertical axis wind turbines [master thesis]. The Netherlands: Delft University of Technology.

Gaunaa M, Sørensen NN, Back C. 2010. The thick multi element airfoil for use on inner part of the wind turbine rotors. Conference proceeding, the science of making torque from wind, Greece; 2010 June 28–30; FORTH, Heraklion, Crete, Greece.

Huskey A, Bowen A, Jager D. 2009. Wind turbine generator system power performance test report for the Mariah windspire 1-kW wind turbine. Golden, CO: National Renewable Energy Laboratory. Technical Report No.: NREL/TP-500-46192.

Lew P. 2011. Multi-element wind turbine airfoils and wind turbines incorporating the same. United States Patent Office, Patent No. US2011/0255972 A1.

Mohamed MH. 2012. Performance investigation of H-rotor Darrieus turbine with new airfoil shapes. Energy. 47:522–530.

Newman BG. 1986. Multiple actuator disc theory for wind turbines. J Wind Energy Ind Aerod. 24:215–225.

Paraschivoiu I. 1982. Double streamtube model for Darrieus wind turbines, Lewis Research Center Wind Turbine Dynamics, NASA. Cleveland, OH: The Smithsonian/NASA Astrophysics Data System, Lewis Research Center. Report No.: N82-23684.

Paraschivoiu I, 2002. Wind turbine design with emphasis on Darrieus concepts. Canada: Polytechnic International Press. ISBN: 978-2-553-00932-0.

Smith AMO. 1975. High Lift Aerodynamics. J Aircr. 12(6):501–530.

Strickland JH. 1975. The Darrieus turbine: a performance prediction model using multiple streamtubes. Albuquerque, NM: Sandia National Laboratory. SAND 75-0431.

Windspire Energy Inc. 2010, Windspire owner's manual, 30 ft. standard, part no. 150001.

Zahl F, Gaunaa M, Sørensen NN, Bak C, 2012. Design and wind tunnel testing of a thick element high lift airfoil. Scientific proceedings of EWEA; 2012 Apr 16–19; Bella Center, Copenhagen, Denmark.

APPENDIX B
Simulation of flow over double-element airfoil and wind tunnel test for use in vertical axis wind turbine

This paper is published in The Science of Making Torque from Wind 2014 (TORQUE 2014).

Simulation of flow over double-element airfoil and wind tunnel test for use in vertical axis wind turbine

Simulation of flow over double-element airfoil and wind tunnel test for use in vertical axis wind turbine

Prasad Chougule
Søren R.K. Nielsen

Department of civil Engineering, Aalborg University, Sohngaardsholmsvej 57, 9000-Aalborg, Denmark.

E-mail: `pdc@civil.aau.dk`; Ph. No. +45 5261 7115

Abstract. Nowadays, small vertical axis wind turbines are receiving more attention due to their suitability in micro-electricity generation. There are few vertical axis wind turbine designs with good power curve. However, the efficiency of power extraction has not been improved. Therefore, an attempt has been made to utilize high lift technology for vertical axis wind turbines in order to improve power efficiency. High lift is obtained by double-element airfoil mainly used in aeroplane wing design. In this current work a low Reynolds number airfoil is selected to design a double-element airfoil blade for use in vertical axis wind turbine to improve the power efficiency. Double-element airfoil blade design consists of a main airfoil and a slat airfoil. Orientation of slat airfoil is a parameter of investigation in this paper and air flow simulation over double-element airfoil. With primary wind tunnel test an orientation parameter for the slat airfoil is initially obtained. Further a computational fluid dynamics (CFD) has been used to obtain the aerodynamic characteristics of double-element airfoil. The CFD simulations were carried out using ANSYS CFX software. It is observed that there is an increase in the lift coefficient by 26% for single-element airfoil at analysed conditions. The CFD simulation results were validated with wind tunnel tests. It is also observe that by selecting proper airfoil configuration and blade sizes an increase in lift coefficient can further be achieved.

1. Introduction

Various types of vertical-axis wind turbines (VAWTs) have been suggested. The most well-known include the Darrieus-type egg beater-shaped VAWT invented in 1931 [1], the Savonius type VAWT invented in 1929, and the H-rotor type design, which appeared after research activity from 1970 to 1980 in the UK. Darrieus VAWTs have recently been documented as an alternative solution for small power production [2]-[3]. Eriksson et al. concluded that VAWTs are more cost-effective than horizontal axis wind turbines (HAWTs) for small power generation [4]. A Darrieus-type VAWT consists of three blades with straight, curved, spiral, helical geometry to improve their power coefficient. In this paper straight bladed VAWT is consider because author wanted to implement self active pitch control mechanism [5].

Bhutta et al. [6] summarized the designs and techniques of VAWTs and compared their performances. VAWTs that operate by a lift force are conventionally designed using a single airfoil in the blade design. There are two main types of airfoils: symmetric and non-symmetric. Symmetric airfoils were developed by the National Advisory Committee of Aeronautics (NACA) for use in low-altitude-flying airplanes. A conventional straight-bladed VAWT design has two

essential drawbacks: i) it shows low power coefficient compared to the horizontal-axis wind turbine (HAWT), and ii) it does not start itself. In this paper, the power coefficient of a conventional VAWT was improved by using a double-element airfoil in the blade design. The operating principle of the multi-element airfoil has been nicely represented by Smith [7]. The purpose of a multi-element airfoil is to increase the lift coefficient and delay the stall angle of a single airfoil [8],[9]. The lift coefficient is directly proportional to the mechanical power output. Therefore, an increase in the lift coefficient of a double-element airfoil should improve the power coefficient of VAWT.

Gaunaa et al. previously tried to determine the aerodynamic characteristics of a double-element airfoil, emphasizing its applicability in the HAWT [10]. They studied the double-element airfoil for high Reynolds numbers of magnitude $Re \geq 1,000,000$. A computational fluid dynamic (CFD) simulation of the flow around a double-element airfoil showed a remarkable increase in lift coefficient. However, VAWT operates at very low range of Reynolds numbers ($Re = 100,000-300,000$). The condition of very low Reynolds number was the most critical part in the flow physics over the airfoil, because the flow behavior was drastically different compared to other conditions and standard flow theories might predict the wrong results. Therefore, care was taken during meshing and a selection of an airfoil providing a high lift coefficient at low Reynolds number.

The size of the slat airfoil with respect to the main airfoil was decided based on the design guidelines given by Buhl [11]. The position and optimal angle of the slat airfoil with respect to the main airfoil were determined by a wind-tunnel experiment, to achieve the maximum lift coefficient. 2D CFD simulation of double-element airfoil is performed in this study and aerodynamic characteristics of the slat airfoil and main airfoil are discussed. A sample test of validation was carried out to compare the 2D CFD over all results with the wind tunnel test.

Section 2 discusses the selection and design of the double-element airfoil. Section 3 gives the wind tunnel experiment carried out with double-element airfoil. Section 4 discusses detail about the 2D CFD modeling and simulation and a sample validation is given. Section 5 contains the conclusion part of the study.

2. Airfoil configuration

A common practice in the design of an airfoil for a VAWT is to modify available NACA symmetric airfoils. These airfoils were designed for low-altitude airplanes, for which the flow conditions nearly correspond to the flow physics around the VAWT. However, these airfoils are not the optimal choice for blade design in VAWTs that operate at low Reynolds numbers. Airfoils that perform well at low Reynolds numbers are more suitable. In this context , the S1210 and S1223 airfoils have proven to be better than the symmetric or non-symmetric NACA airfoils [12]. They were originally designed to obtain high lift at high altitude for a drone, characteristics that can be used in VAWT blade design.

2.1. Airfoil Selection

The airfoil shape contributes in the generation of a lift coefficient by creating suction on upper surface of the airfoil. In this process, a drag is also being generated which is not desirable for the maximum power output of the wind turbine. To get the maximum torque and a power output from wind turbine, it is important to have an airfoil which will generate the high-lift and the high lift-to-drag ratio. Selection of a proper airfoil for the VAWT is very important at initial stage of the design process. In [13] it is summarized that the operating range for a symmetric airfoil is wider than the non-symmetric airfoil. That means that stall is observed at smaller angle of attack in case of a non-symmetric airfoil.

An airfoil designed at Delft University of Technology, Netherlands called the DU06-W200 has shown improvement in the lift coefficient and ability to self- start at low Reynolds number, [14].

An addition of a camber in the airfoil shape has contributed in a self start ability. The thickness of the base airfoil is increased to give more structural strength to the blades; however, it has not been justified with its need for the VAWT. In reality, the thick airfoil has the disadvantages of lowering the maximum lift coefficient even though it works at higher tip speed ratio. The increase in the power coefficient achieved up to 5% as compared to the use of the NACA0018 airfoil in a VAWT blade design.

There are a few other airfoils which operate at the low Reynolds number, mainly they are S1210, S1213 [15] and S1223 [16], [12]. These airfoils have the high-lift at a low Reynolds number from $Re = 200,000$ to $Re = 500,000$. Recently, a new airfoil for a small horizontal axis wind turbine has been designed by focusing a low wind speed startup which is called *airfish* AF300 [17]. The author has mentioned that, this airfoil works for Reynolds number ranging from $Re = 38,000$ to $Re = 205,000$, which means, it is a very low wind speed condition. AF300 is designed by addition of 1% to 3% in the trailing edge of the airfoil S1223 and 1% to 5% thickness in trailing edge of the airfoil S1210.

In this paper, the focus is on the proper airfoil selection for double-element airfoil design. In [13] it is also indicated that an S1046 airfoil has highest power coefficient, so it is obvious to select this profile for the design. However, there is one thing to be considered which is that the Reynolds number at which this airfoil performs well is related to the tip speed ratio (TSR). Also, in the selection and design of the airfoil one must consider other parameters such as the airfoil lift-to-drag ratio (c_L/c_D) also known as glide ratio, endurance parameter, thickness, pitching moment, stall characteristics, and sensitivity to the roughness are all important factors, amongst others. Therefore, a S1210 airfoil has been studied due to the high-lift coefficient at a low Reynolds number. The selection of a S1210 airfoil is done due to its maximum lift and higher lift-to-drag ratio. Further the design of double-element airfoil is carried out.

2.2. Double-element airfoil
In this paper, an S1210 airfoil was selected as the base airfoil for the design of a double-element airfoil. The S1210 airfoil has several characteristics that make it ideal for selection. i) It gives the highest maximum lift coefficient at a low Reynolds number. ii) It stalls smoothly; that is, the lift curve after the stall angle follows a nearly zero slope, represented by a glide ratio of (c_L/c_D). iii) It performs well at low Reynolds number and has the best combination of lift coefficient (c_L) and high glide ratio. c_L and c_D represents the lift and drag coefficients respectively.

The chord length c of the S1210 base airfoil was chosen to be c = 127 mm, based on the test specimen requirements of the Aerolab wind tunnel [18]. Figure 1 shows how the S1210 single airfoil was divided into a double-element airfoil (i.e., into a main airfoil and a slat airfoil). In the design of the double-element airfoil, the chord length of the slat airfoil (c_s) was 35% of
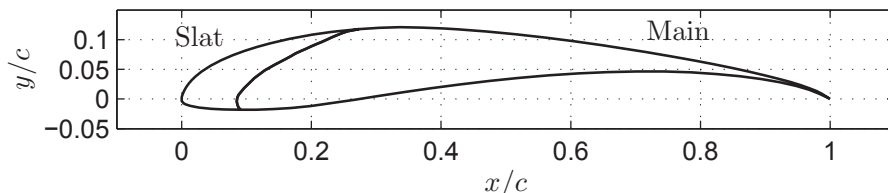
Figure 1. Division of a S1210 airfoil into a double-element airfoil

the chord length of the base airfoil c; thus, c_s (= 44.45 mm)[10],[11]. The main airfoil chord length (c_m) was 90% of c (= 114.3 mm). The design parameters of double-element airfoil, the position and slat angle with respect to the main airfoil are represented in the Figure 2. In the
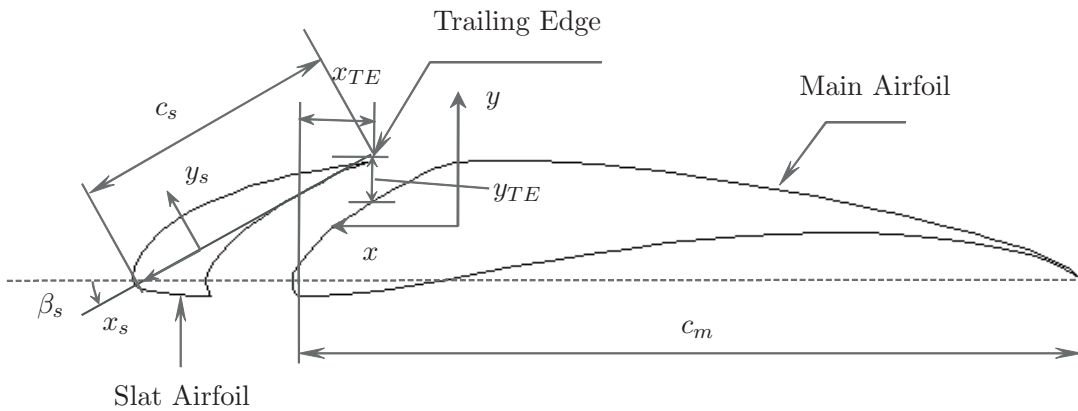
Figure 2. Double-element airfoil

double-element airfoil, the position and orientation of the slat airfoil with respect to the main airfoil are expressed by three parameters. Two parameters described the position of the trailing edge (TE) of a slat airfoil along the local $x - direction$ (x_{TE}) and the local $y - direction$ (y_{TE}). A third parameter, the slat angle (β_s), represented the orientation of the slat airfoil as the angle between the chord length of the slat airfoil with the local $x - direction$. This parameter is positive in the nose-up direction. In Table 1, TE corresponds with the trailing edge.

Table 1. Parameters of double-element airfoil

Description	Symbol	Value	Unit
Slat TE position x-direction	x_{TE}	0.012	m
Slat TE position y-direction	y_{TE}	0.004	m
Slat Aerofoil angle	β_s	-20	°

3. Wind tunnel experiment
A wind tunnel testing is performed in this work to:

- determine the optimal angle of a slat airfoil (β_s) with respect to the main airfoil.
- determine the lift and a drag coefficient of the double-element airfoil.
- validate the 2D CFD simulation results.

The dimensions of the wind tunnel used in this experiment are 305 mm width, 305 mm height and 610 mm length [18]. The range of the wind speed achievable is 4.5 m/s to 60 m/s. The wind tunnel used in this research has a limitation on the angle of attack which can be adjusted in the range of $-24°$ to $+24°$ due to the size of the wind tunnel. To avoid blockage effects the wind tunnel experiments are carried out at lower range of angle of attack $-20°$ to $+20°$. Also, it is important to mention here that the wind tunnel results are not influenced by blockage effect. Therefore, a 2D CFD simulation result obtained within this range of the angle of attack is compared with the wind tunnel test results.

The slat airfoil is bolted with a main airfoil by two side links fixed to the main airfoil, and a linear adjustment is provided by a slot on the link end so that, the position parameter x_{TE} can be adjusted. The y_{TE} position can be adjusted by rotating the links around main airfoil. The third parameter β_s is set by an angular position of a slat airfoil with respect to two side links parallel to the chord length of the main airfoil. The main and the slat airfoil blades are

manufactured by 3D printing technology, and plastic material is used. The optimum length of the double-element airfoil blade is 250 mm for this wind tunnel and is represented by h length of the double-element airfoil test blade.

The main and the slat airfoils are manufactured individually, and fixed to each other by side links as shown in Figure 3. Figure 3.a shows the top view of the double-element S1210 airfoil and Figure 3.b shows the bottom view of the double-element S1210 airfoil. A single airfoil is formed by joining a slat airfoil with the main airfoil and later used as a single airfoil test specimen in Aerolab wind tunnel. Then experiments are performed to find out the lift and the drag coefficients for a single and a double-element airfoil.
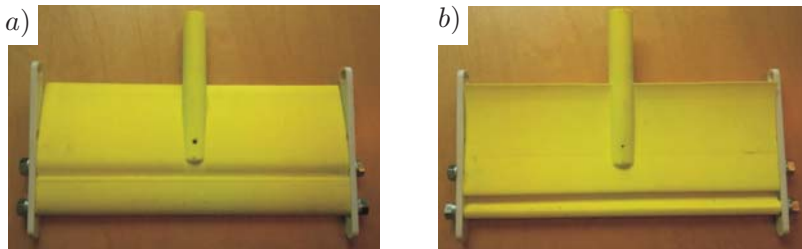
Figure 3. Double-element S1210 airfoil test specimen

The Aerolab wind tunnel has a data display and an acquisition system through which, the normal force N_f and the tangential force A_f acting on the double-element airfoil are obtained and stored in a text format. Theses forces are then converted to experimental lift force L_f and the drag force D_f by the following equation:

$$\left.\begin{aligned} L_f(\alpha) &= N_f\cos(\alpha) - A_f\sin(\alpha) \\ D_f(\alpha) &= N_f\sin(\alpha) + A_f\cos(\alpha) \end{aligned}\right\} \tag{1}$$

Finally, the experimental lift coefficient $c_{L_{expt}}$ and an experimental drag coefficients $c_{D_{expt}}$ are obtained:

$$\left.\begin{aligned} c_{L_{expt}} &= \frac{L_f}{\frac{1}{2}\,\rho V_m^2\,(c_m + c_s)\,h} \\ c_{D_{expt}} &= \frac{D_f}{\frac{1}{2}\,\rho V_m^2\,(c_m + c_s)\,h} \end{aligned}\right\} \tag{2}$$

Figure 4 shows the experimental lift coefficient of a single airfoil (SA) and a double-element airfoil (DA) for various Reynolds numbers.

At different Reynolds number, it is interesting to see that, the maximum lift coefficient for a single and double-element airfoil is increases, and also the stall angle is increased due to effect of the slat airfoil in front of the main airfoil. The effect of transition flow (laminar separation bubble)is occurred at $Re < 100,000$, therefore it is focused at $Re > 100,000$ in this paper. The tabular values represent the maximum lift coefficient for a single and double-element airfoil for different Reynolds number, and the difference in a stall angle is calculated and concluded with observations.

In Table 1, α_{max} represents the stall angle in the wind tunnel test. The difference of the stall angle between a single and double-element airfoil at $Re = 50,000$ is $11.2°$ which is very interesting, and it reduces to $8.6°$ for Re=100,000. From this it can be concluded that the S1210 double-element airfoil arrangement performs very well in the range of $Re = 50,000$ to $Re100,000$ by delaying the stall angle. Whereas, the difference of the maximum lift is gradually increasing
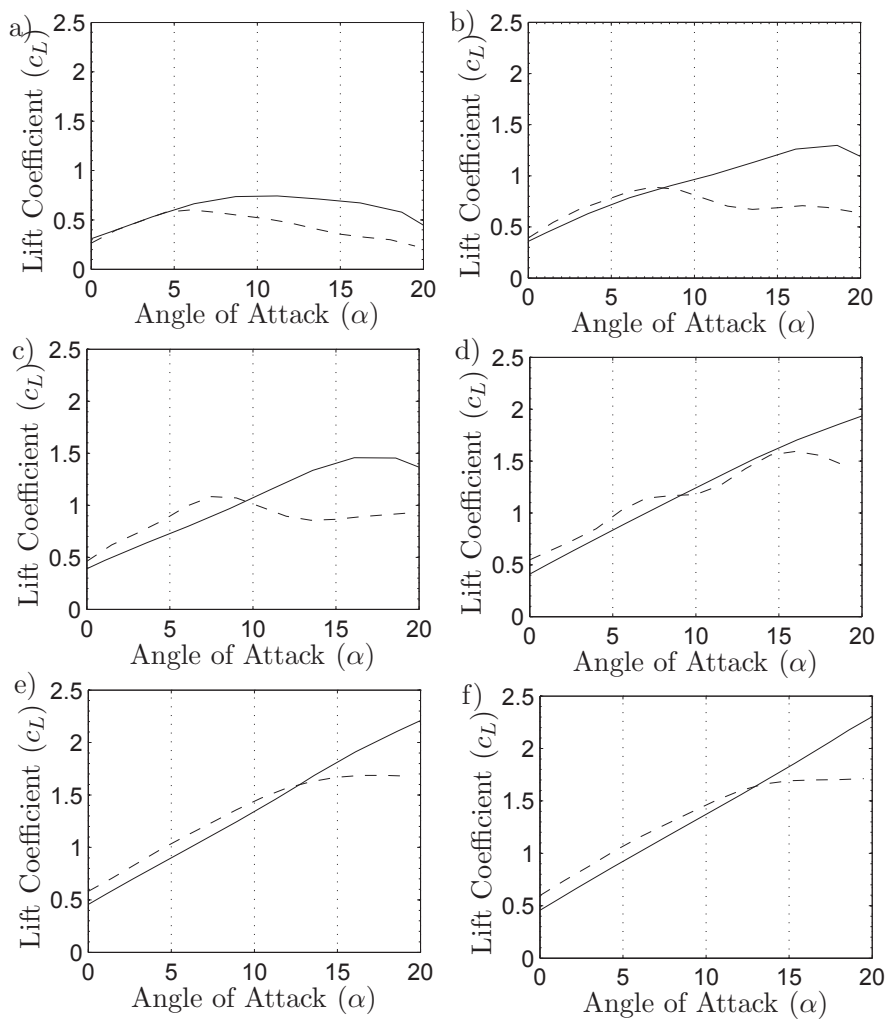
Figure 4. Wind Tunnel test results for Single and Double-element airfoils.
a) Re = 40,000 . b) Re = 55,000 . c) Re = 75,000. d) Re = 100,000. e) Re = 200,000. f) Re = 240,000
——: Double-element S1210 airfoil   - - - -: Single-element S1210 airfoil

Table 2. The maximum experimental lift coefficient of a single (SA) and a double-element (DA) S1210 airfoil.

| Re	$\alpha_{max}(SA)$	$c_{L_{max}}(SA)$	$\alpha_{max}(DA)$	$c_{L_{max}}(DA)$	$\Delta\alpha_{max}$	$\Delta c_{L_{max}}$
40,000	6°	0.6015	11.2°	0.7425	5.2°	0.1410
50,000	7.5°	0.8907	18.6°	1.257	11.2°	0.3663
75,000	7.5°	1.083	16.1°	1.457	8.6°	0.3740
100,000	16°	1.593	20°	1.935	—	—
200,000	16.4°	1.687	20°	2.200	—	—
240,000	19.5°	1.712	20°	2.310	—	—

which produces the extra power output. However, for the VAWT the delay of the stall angle improves the power efficiency more than the maximum lift coefficient. At the high wind speed conditions the effect of a slat airfoil on main airfoil has been less than in the low wind speed conditions. The S1210 airfoil has characteristics of the high lift coefficient at a low Reynolds number which supports the previous conclusion from the wind tunnel results.

The lift coefficient curve of a single airfoil at $Re \geq= 200,000$ remains the same with a very less increment in the maximum value, which indicates further increase in the Reynolds number and will not improve the maximum lift coefficient value. The double-element airfoil lift coefficient at $Re \geq= 200,000$ is increasing and a stall condition of an airfoil is yet to reach at $20°$ angle of attack. The maximum lift coefficient of a single airfoil is increased by 40% at $Re = 200,000$ and the angle of attack by $20°$ in the double-element airfoil. At an angle of attack below $12°$ the lift coefficient curves of the double-element airfoil at the $Re \geq= 200,000$ follows sagging nature in the curve, as compared to a single airfoil lift coefficient curve. It indicates that, the double-element airfoil is not having any effect of an increase in a lift coefficient under this condition. Therefore, wind tunnel results show that, the double-element airfoil is effective at $Re \geq= 100,000$ for a S1210 airfoil.

4. 2D CFD modeling and simulation

In this study, a 2D geometric mesh was created using ANSYS ICEM CFD. The domain was a circle with a radius of 4 m, corresponding to 40 times the chord length of the main airfoil. A structured Hexa mesh was used. The height of the first cell from the boundary surface was $3\mu m$, which grew at a ratio of 1.2. A smooth transition was maintained between the smaller boundary quad elements and the much larger elements away from the airfoil surfaces.

The boundary layer was captured by using the O-Grid blocking topology within ICEM CFD in a C-shaped pattern. The boundary layer around the airfoil and the wake zone with finer sized mesh elements behind the airfoil were captured with the C-shaped O-Grid. First, a grid was fixed to a distance of $1.0x10^{-6}m$ to ensure a dimensionless number $y+ \leq 1.5$, to properly resolve the boundary layer close to the wall surface and to obtain accurate reports of the lift and drag coefficient (between the domain and boundary layer). The use of a structured mesh with a circular air domain to simulate different angles of attack increased the flexibility of mesh generation and the convergence in the solution. The cell count was 150,000. Figure 7 shows the mesh used for the double-element S1210 airfoil. Air was considered to be an isothermal
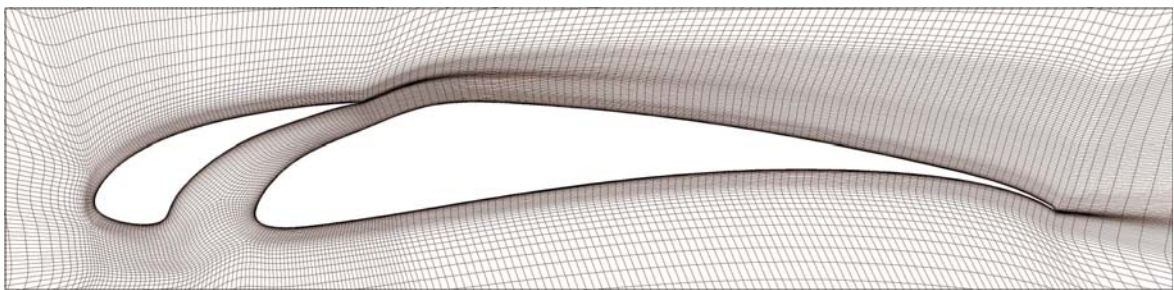
Figure 5. Grid around double-element Airfoil

and incompressible gas with constant density in the solver settings. A single set of momentum equations was solved. Mass and force balances were ensured by using the continuity equation and the momentum equation set in the solver, respectively. To simulate turbulence, the viscous Spalart All-maras (1 equation) model was used, with the Strain/Vorticity-based SA Production

mode. This mode was developed for aerospace lift and drag studies and has been used to simulate airfoils. It is a computationally efficient mode that can predict wall forces accurately and has been developed basically for aerospace lift and drag studies. On top of that, this model is chosen because it is computationally efficient and it has been used to correctly simulate airfoil.

To solve the system of governing partial differential equations, the continuity equation was discretized. The Reynolds average Navier-Stokes equation (RANS) was formulated by using a finite volume method with an algebraic segregated solver, as implemented in ANSYS Fluent. Continuity and momentum equations were linked by the Semi-Implicit Method for Pressure-Linked Equations (SIMPLE) algorithm. An algebraic multigrid (AMG) technique was used in the iterative solver to obtain improved convergence rates. All simulations were performed under steady-state conditions. Under relaxation conditions, factors of 0.2 and 0.6 were applied to the pressure and momentum parameters, respectively, trading processing speed for more accurate prediction of the physics. A run was continued until the lift and drag coefficients attained steady values that indicated a converged solution.

At the airfoil walls, the no-slip boundary condition was assumed, which is an appropriate condition for the velocity component at the wall. At the domain boundary, a velocity inlet-type boundary condition was applied, in which the free-stream velocity was set, and the angle of attack was changed between $\pm40°$. Multiple simulations were performed at different angles of attack for $Re = 200,000$.

Figure 7 shows the lift and drag coefficients of the double-element airfoil obtained from CFD simulations and compared to the wind-tunnel results. The CFD lift coefficient curve showed a
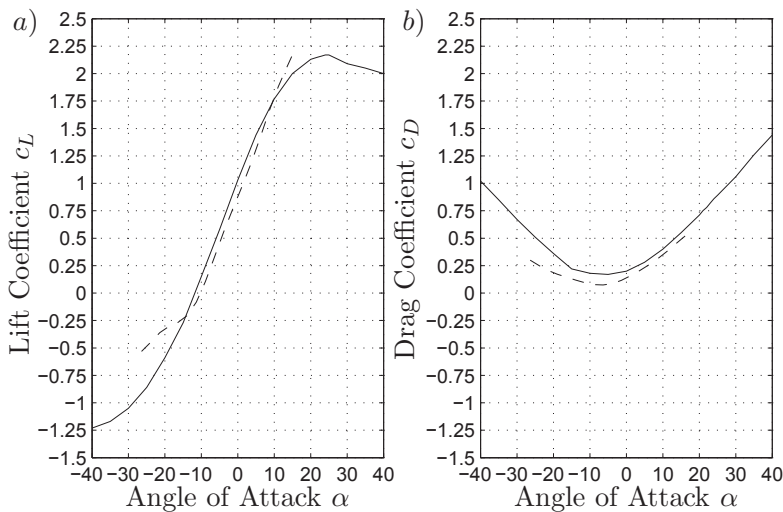
Figure 6. 2D CFD model validation for double-element S1210 airfoil at $Re = 200,000$.
a) Lift coefficient. b) Drag coefficient.
- - - - - : Wind tunnel results ——— :2D CFD results

very good fit with the wind-tunnel results (Figure 7.a). At angles of attack $\alpha \geq 10°$, the lift curve in the wind-tunnel testing began to increase. The simulated lift curve from the 2D CFD model showed the real situation of the flow physics due to non-confined flow, in which the stall angle was the real stall angle of the double-element S1210 airfoil.

The value of the stall angle for the double-element S1210 airfoil was $25°$, compared to $15°$ for the single S1210 airfoil. A large difference in stall angle between the airfoils ($\alpha_{stall} = 10°$) will contribute to increased airfoil power performance. The design proposed in this paper for

the double-element airfoil achieved a delay in the stall angle by using a slat airfoil in front of the main airfoil. The accuracy of the 2D CFD results were within 5% for an angle of attack (α) in the range of $\pm15°$. For $\alpha \geq 10°$, the 2D CFD model underestimated the lift coefficient.

5. Conclusion

A low Reynolds number, a high lift airfoil is selected to design a double-element airfoil. A simple way of dividing a single airfoil into a double-element airfoil is given, based on the literature of double-element airfoil flow physics. It is certainly a rough estimate of slat and main airfoil sizes due to very limited or almost zero available research work on two-element airfoil for $Re \leq 500,000$ particularly used in a wind energy application. A thin airfoil S1210 was selected which performs well at low Reynolds number $Re \leq 200,000$.

A wind tunnel test for a single S1210 airfoil and a double-element S1210 airfoil has been performed for various Reynolds numbers. It is observed from the wind tunnel tests that, the use of a double-element airfoil instead of a single airfoil has increased the lift coefficient and delayed the stall angle which is very advantageous in the VAWT. An increase in the maximum lift coefficient for $Re \geq 100,000$ has been very prominent which, indicates that, at the low wind speed the double-element airfoil performance has been considerable. It is also observed that, there is decrease in the lift coefficient of a double-element airfoil under the angle of attack at which the single airfoil stalls. This phenomenon is not explainable at this stage. The wind tunnel test results are further used to validate the 2D CFD model for the double-element airfoil.

The validation of a 2D CFD model has been a critical part of this research work. A mesh quality had been ensured at the critical area between the slat and the main airfoil by refined mesh. The 2D CFD simulations are in an acceptable range. However, it will be a very accurate validation, if the 3D CFD simulation is performed. A best compromise between the expense of 3D CFD simulation and quality of 2D CFD simulation data obtained in this work was made. Finally, 2D CFD data was accepted for further research work. Further, research needs to carry out in both case wind tunnel experiment and the CFD simulation.

References

[1] Darrieus G. J. M., 1931, Turbine having its rotating shaft transverse to the flow of the current, United States Patent office, Patent No. 1835018.
[2] Muller G., Jentsch M. F., Stoddart E., 2009, Vertical axis resistance type wind turbines for use in buildings, Renewable Energy, Vol. 34, pg. 1407-1412.
[3] Sharpe T., Proven G., 2010, Crossflex: Concept and early development of a true building integrated wind turbine, Energy and Buildings, Vol. 42, pg. 2365-2375.
[4] Eriksson S., Bernhoff H., Leijon M., 2008, Evaluation of different turbine concepts for wind power, Renewable and Sustainable Energy Reviews, Vol. 12, pg. 1419-1434.
[5] Chougule P.D., Nielsen S.R.K., 2014, Overview and Design of self-acting pitch control mechanism for vertical axis wind turbine using multi body simulation approach, A proceedings of Science of making true from wind 2014, under peer review.
[6] Bhutta M. M. A., Hayat N., Fahrooq A.U., Ali Z., Jamil Sh. R., Hussian Z., 2008, Evaluation of different turbine concepts for wind power, Renewable and Sustainable Energy Reviews, Vol. 12, pg. 1419-1434.
[7] Smith A. M. O. , 1975, Hight Lift Aerodynamics, Journal of Aircraft, Vol. 12 , N0. 6.
[8] Bah E. A., Sankar L., Jagoda J., 2013, Investigation on the Use of Multi-Element Airfoils for Improving Vertical Axis Wind Turbine Performance, 51st AIAA Aerospace Sciences Meeting Including The New Horizons Forum and Aerospace Exposition.
[9] Lew P., 2011, Multi-element wind turbine airfoils and wind turbines incorporating the same, United States Patent office, Patent no. US 2011/0255972 A1.

[10] M. Gaunaa, N. N. Sørensen and C. Bak, 2010, Thick multiple element airfoils for use on the inner part of wind turbine rotors, The science of making torque from wind, June 28-30, Crete, Greece.

[11] Buhl T., 2009, Research in Aeroelasticity EFP-2007-II, Ris-R 1698(EN).

[12] Giguere P., Selig M.S. 1997, Low Reynolds number airfoils for small horizontal axis wind turbines, Wind Engineering, Vol. 21 No. 6, pg. 367-380.

[13] Mohamed M.H., 2012, Performance investigation of H-rotor Darrieus turbine with new airfoil shapes, Energy, Vol. 47 No. 6, pg. 522-530.

[14] Claessens M. C., November 2006, The design and testing of airfoils for application in small vertical axis wind turbines, A Master Thesis, Delft University of Technology.

[15] Selig M.S. , Guglielmo J.J., Broeren P., Giguère P., 1995, Summary of Low-Speed Airfoil Data, Volume 1, SoarTech Publications, Virginia Beach, Virginia.

[16] Selig M.S. , McGranahan B.D., 2003, Wind Tunnel Aerodynamic Tests of Six Airfoils for Use on Small Wind Turbines Period of Performance, NREL/SR-500-34515, pg. 64.

[17] Singh R. K. , Ahmed M. R., Zullah M. A. , Lee Y-H. , 2012, Design of a low Reynolds number airfoil for small horizontal axis wind turbines, Renewable Energy vol. 42, pg. 66-75.

[18] Aerolab, Aerolab,Educational Wind Tunnel, Maryland USA, http://www.aerolab.com/downloadable-documents/ewtbrochure.pdf.

Overview and Design of self-acting pitch control mechanism for vertical axis wind turbine

using multi body simulation approach

Overview and Design of self-acting pitch control mechanism for vertical axis wind turbine using multi body simulation approach

Prasad Chougule
Søren Nielsen

Department of civil Engineering, Aalborg University, Sohngaardsholmsvej 57, 9000-Aalborg, Denmark.

E-mail: `pdc@civil.aau.dk`; Ph. No. +45 5261 7115

Abstract. Awareness about wind energy is constantly growing in the world. Especially a demand for small scale wind turbine is increasing and various products are available in market. There are mainly two types of wind turbines, horizontal axis wind turbine and vertical axis wind turbines. Horizontal axis wind turbines are suitable for high wind speed whereas vertical axis wind turbines operate relatively low wind speed area. Vertical axis wind turbines are cost effective and simple in construction as compared to the horizontal axis wind turbine. However, vertical axis wind turbines have inherent problem of self-start inability and has low power coefficient as compare to the horizontal axis wind turbine. These two problems can be eliminated by incorporating the blade pitching mechanism. So, in this paper overview of various pitch control systems is discussed and design of self-acting pitch mechanism is given. A pitch control linkage mechanism for vertical axis wind turbine is modeled by multi-body approach using MSC Software. Aerodynamic loads are predicted from a mathematical model based on double multiple stream tube method. An appropriate airfoil which works at low Reynolds number is selected for blade design. It is also focused on commercialization of the vertical axis wind turbine which incorporates the self-acting pitch control system. These aerodynamic load model will be coupled with the multi-body model in future work for optimization of the pitch control linkage mechanism. A 500 Watt vertical axis wind turbine is designed and it is planned to implement the self-acting pitch control mechanism in real model.

1. Introduction

30% of electrical energy produced worldwide is being used by households, and the demand for energy is increasing rapidly causing a strain on existing electricity solutions. The demand for electricity is rapidly growing in urban areas as people are migrating from the big cities. Electricity demand in developed countries is far more different than the developing countries, and undeveloped countries where large scale projects can be a challenge. Developed countries need massive supply of electricity for its own cities for future exponential demand whereas developing countries needs to lift up their un-electrified population with supplying electricity for livelihood along side with urban demand. The price of electricity is increasing every day as well. In short-the micro electricity generation has gained lot of importance in current energy scenario and many wind turbine designs are under development phase to capture power of wind [1].

Mainly, there are two types of wind turbines, horizontal axis wind turbine (HAWT) and vertical axis wind turbine (VAWT). In recent research work it has been documented that VAWTs are more economical and suitable for urban use due to their noise-free and aesthetic design [2]. Still there is a room to improve the efficiency of the VAWTs since they are not completely understood. The VAWT power efficiency can be increased by various means, one by selecting a proper airfoil shape, and a review of different airfoils is given in [3] in which it is found that the thin airfoil performs better than thick airfoil. Secondly, designing a proper airfoil can improve a power efficiency of VAWT, an optimized airfoil to increase the torque output is designed and patented by [4]. Also use of multi-element airfoil in VAWT blade design has shown improvement in power efficiency, [5], [6]. Thirdly, a pitch control system can improve the power efficiency considerably and also eliminate the self-start problem of VAWT,[7]. The theory of blade pitch control has been explained by [8] in which three different ways of pitch control are given. The practical implementation of these methods is tried on research purpose, but there are very few successful research wind turbines with a pitch control mechanism, one of them can be found at [9]. It is time to implement the research out come to develop an industrial product.

In this work an attempt is made to design a VAWT with self-acting pitch control mechanism. Essentially, a blade pitch angle is changed during the rotation of VAWT which reduces the angle of attack and avoid the blade from stalling. Blade pitching can be done by a linkage mechanism in which all three blade will change there angles by same amount of blade pitch angle. The advantage of self-acting collective pitch control system is, it is very simple in construction and easier to implement in the VAWT prototype. It can work for all rotational speed of the VAWT in other words it can work for various tip speed ratios (TSR). The drawback is it is not the optimum solution to increase a the power efficiency. Another mechanism, which work on aerodynamic forces, in which during rotation of VAWT, a freely moving mass will move in and out along the blade arm to adjust the blade pitch angle. It is also called stabilized mass balance in which aerodynamic force creates the blade pitch movement. The drawback of this system is it can be optimized for particular rotational speed. A VAWT of particular dimensions is designed and a multi body simulation approach is used to design a blade pitch linkage mechanism. A MSC software tool, ADAMS 2013.1 is used to model the VAWT and a blade pitch linkage mechanism. The job of deciding sizes of linkage element had become easier due to the simulations in MSC software tool. Initially single blade with its rotating arm was modeled and rotational joints were defined and then motion was imposed to the rotor arm. It was very convenient to introduce an angle measure for blade pitch which helped to finalize the linkage sizes.

The purpose of multi body approach is to determine in future the physical properties of the VAWT, such as mass of blade, mass of blade arm and optimized sizes of blade pitch control linkage mechanism. A predicted load of on VAWT will help to parameterize all these physical properties of different element of VAWT. Further, the moment at the VAWT tower can be calculated for design of support structure. A displacement of blade structure due to aerodynamic loading can also be calculated for design of blade arm.

In *selection of airfoil and design of VAWT*, an overview of airfoils used for VAWT blade design is given and an appropriate airfoil is selected and later on design specifications are given. and design of VAWT is given. In *aerodynamics of VAWT and pitch angle calculations*, a method to determine the aerodynamic forces is selected and the detail about pitch angle determination is given. In *pitch control system modeling*, an overview of different pitch control methods are discussed and further a multi body approach is used to design a self acting pitch control linkage mechanism. In *simulation and results*, power coefficient versus wind speed and tip speed ratio is calculated with and without pitch control. Also a future work is discussed. In *conclusion*, the outcome of the research work is submersed.

2. Selection of airfoil and design of VAWT

2.1. Airfoil

The airfoil is main concern in the success of VAWT performance. Until recently VAWT is been not in focus of researchers after HAWTs commercial success in late 90's to develop the highly efficient technological product. Now it has become interest for many researchers to look back the aerodynamics of VAWT so that the proper airfoil can be designed. There are few successful commercial product which are developed based on aerodynamic airfoil design for VAWT application [10]-[12]. The result of this ended with interesting discoveries, and lead to the innovative VAWT commercial products [1]. The airfoil shape contributes in the generation of a lift coefficient by pressure difference in upper and lower surface.

In this paper, a recently designed airfoil for a small horizontal axis wind turbine is used which startup at a low wind speed, the airfoil is called *airfish* AF300, [13]. The author has mentioned that, this airfoil works for Reynolds number ranging from $Re = 38,000$ to $Re = 205,000$, which means, it is intended for low wind speed condition. AF300 is designed by addition of 1% to 3% in the trailing edge of the airfoil S1223 and 1% to 5% thickness in trailing edge of the airfoil S1210 [14].

2.2. Design of VAWT

A design of rotor for VAWT is very important in which the blade pitch mechanism can be efficiently incorporated with less geometrical complexities. The size of the rotor is based on the solidity and the aspect ratio, for which rotor performance is good at the desired wind speed. The aspect ratio is the ratio of the rotor height to the rotor diameter. The aspect ratio for VAWT of peak power under 20 kW is chosen between 0.5 to 1.5 [15]. The higher the aspect ratio of the rotor, the larger the rotational speed of the rotor due to slenderness. The rotor designed in this work has a height $H = 1.5m$ and a diameter $D_r = 1.25m$ which gives a aspect ratio of 1.2.

Rotor solidity is yet another parameter of VAWT design which is defined as the ratio of the total blade planform area to the turbine swept area. It is well known that, the solidity affects the power coefficient of the rotor and is thoroughly studied by, [16],[17]. The solidity of the rotor can be expressed as,

$$\sigma = \frac{N\,c}{D_r} \tag{1}$$

Where N is total number of blades, c is the chord length of the blade and D_r is the rotor diameter. Higher solidity means the higher peak power coefficient due to to fact that it gives more torque as compare to the less solidity rotor. However, the power coefficient over tip speed ratio remains narrow. The solidity of the rotor, is depends on the range of the operating speed of the rotor. The rotor which is designed for low wind speed, will have low rotational speed, and it has to have a high solidity and vice a versa. So, it is better to choose moderate range of operating speed by compromising power coefficient and the total power output. As observed by Kirke, the solidity for the straight-bladed VAWT is good between 0.1 to 0.3 [16]. In this work a solidity $\sigma = 0.27$ which falls within the best range.

It is well known that the VAWT creates cyclic vibrations due to periodic loading which is critical for mechanical structure and electrical power system design. Periodic fluctuation occurs due the number of blades used in VAWT. A two-bladed VAWT has a higher torque fluctuation than the three-bladed VAWT, and so forth, [18]. The position of blade and the variation of aerodynamic forces on these blades causes the torque fluctuations and self starting issues [19]. A three-bladed VAWT with 120° azimuthal angle difference has less torque fluctuations due to the relatively steady aerodynamic forces. Also, three-bladed VAWT has fewer cost than the four-bladed VAWT.

A wind turbine blade is manufactured by hand lay-up process using glass fiber material, for more details on blade manufacturing one may contact corresponding author of this paper. A

die for AF300 airfoil blade structure is first manufactured and it can be used to make multiple blades. A linkage mechanism is not yet manufactured which will be done after multi-body simulations. An direct electrical alternator of 3 phase is also designed and manufactured. An alternating current and voltage will be measured by a data logger which has a DC current and voltage measuring circuitry. A wind speed, wind direction and a rotor speed can be measured with the customized data logger.

Figure 1. 500 Watt VAWT

3. Aerodynamics of VAWT and pitch angle calculation

The aerodynamics of VAWT and the flow around the rotor are mainly studied with the multiple actuator disc theory [20]. The Velocity components at various locations in the flow area are interesting and calculated by the momentum theory and the blade element theory. The double multiple stream tube method (DMSTM) proposed by [21] is used in this work. In DMSTM, the flow field outside the rotor is divided into two subfields placed; upstream and downstream of the rotor. The fluid flow is considered to be inviscid and incompressible for the calculation of the induced velocity through the each stream tube.

3.1. Pitch angle calculation

In a VAWT with blade pitch control mechanism, a blade is rotated by an angle for which the torque is maximum. Change of blade angle causes reduction in the flow angle. From Figure 2, the expression of the flow angle is given by,

$$\varphi_{ij}(\vartheta_{ij}) = \alpha_{ij}(\vartheta_{ij}) + \beta_{pi}(\vartheta_{ij}) \tag{2}$$

where $\alpha_{ij}(\vartheta_{ij})$ is the local angle of attack, and $\beta_{pi}(\vartheta_{ij})$ is the blade pitch angle for blade 1,2 and 3 in upstream and down stream of the rotor respectively. The blade pitch angle for blade 1,2 and 3 in collective pitch control mechanism is given as follows;

$$\beta_{pi}(\vartheta_{ij}) = \beta_i(\vartheta_{ij}) \sin(\vartheta_{ij}) \tag{3}$$

where $i = 1, 2, 3$ corresponds to the number of blades and in equations (2) and (3) $j = u$; $m = 0, cn = \pi$ and for $j = d$; $m = \pi, n = 2\pi$. A numerical simulation is carried out by keeping
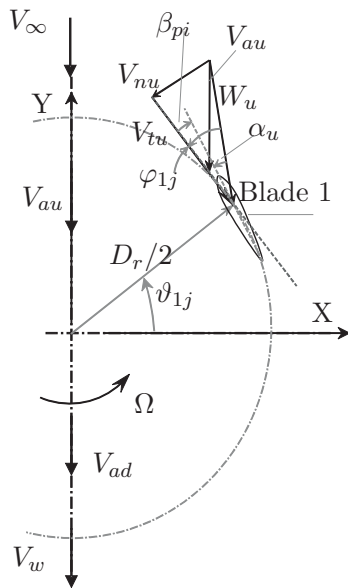
Figure 2. Velocity diagram for airfoil

pitch angle amplitude $\beta_i = \pm 5°$. The mechanism is able to accommodate blade pitch amplitude in the range of $\pm 40°$. The pitch control mechanism designed in this work has a capability of sinusoidal variation of the blade pitch angle with respect to the blade position in rotor plane. Therefore a flow angle and blade pitch angle variation with respect to the azimuthal position of the blade is plotted in the Figure 3. In Figure 3.a flow angle variation with respect to azimuthal
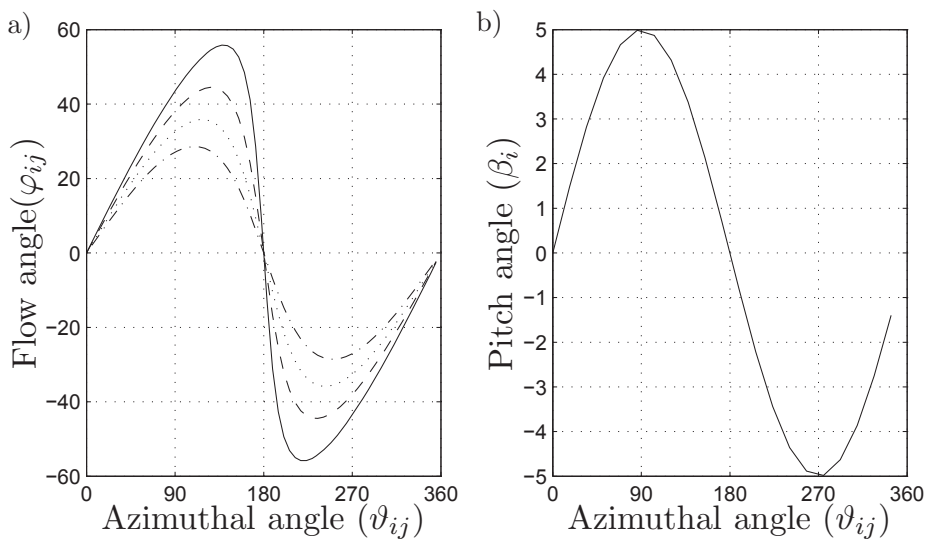
Figure 3. Azimuthal angle of blade and flow angle a) Flow angle , b) Pitch angle
——— : TSR=1.25.   - - - - : TSR=1.5.   · · · · · · : TSR=2.0.   — · — : TSR=2.5.

angle is shown for selected TSR's. For low TSR the flow angle is higher than the high TSR. The amplitude of blade pitch angle is keep constant for this analysis. However it would be

needed to change according to the flow TSR. In future it planed to design such a system which accommodate the change of blade pitch amplitude with respect to the TSR's.

4. Pitch control system Modeling
4.1. Overview of pitch control system
To extract the more power output from VAWT a blade angle with respect to its axis is changed. This can be done by active or passive force. An overview of different methods used for blade pitching are described in, [8]:

- self acting pitch control also called as passive pitch control.
- force pitch control also called as active pitch control.

A Self acting variable pitch mechanism uses aerodynamic forces to actuate self acting devices and works by creating pitching moment about blade pivot [22]. This method is totally based on the individual aerodynamic load balance on each blade. A formulation of the pitch angle is based on the aerodynamic load balance at each blade. To implement this method in practice, it is difficult to design an optimal mechanism which works in the operating range of the VAWT. The mechanism can perform very well at particular wind conditions. It is not yet commercially implemented in the VAWT, but a conceptual design can be found in [8]. In another mechanism, the passive pitch control system uses mass stabilized or mass spring stabilized blades. In which a mass act as a centrifugal force generator during rotation. One such mechanism is given by [23]. In this concept, a blade starts at a higher angle of attack to produce torque at lower speeds. When the rotational speed increases, the mass is forced outwards, and the blade is moved to a reduced angle of attack.

In the individual blade pitch control method, theses problems of large vibration and complexity of design parameters of the collective pitch control system are eliminated. Aerodynamic performance of the individual pitch control system for VAWT showed an increase in performance by 60% as compared with standard VAWT without pitch control [24]. With this method a pitch angle for each blade is calculated separately by two ways, i) based on sinusoidal input where the pitch angle is directly related to the azimuthal angle of the blade and the magnitude of fixed pitch angle or ii) a pitch angle required for each blade is calculated individually to maximize the VAWT rotor torque.

In forced pitch variation, individual blades are actuated by gears or cam actuator devices called pinson cycloturbine, [25], [26] and [27]. This method is also called collective blade pitch because the change of the pitch angle is same for all blades which varies with the azimuthal position of the blade. To implement this method in practice, it is less complicated than the individual pitch control system. One problem found in this type of mechanism is that blades cannot be configured for high efficiency at high rotational speeds, which results in loss of performance [28]. A study carried out by Hwang et al. showed that the collective pitch control has generated 30% more power output than the similar wind turbine with fixed pitch control system [24]. Also, it is found by Kirke and Lazauskas that, the collective pitch control wind turbine has a higher starting torque and efficiency along with large vibration forces [29]. In this work a forced collective pitch mechanism is designed and will be implemented in VAWT.

4.2. Pitch control linkage mechanism : multi body simulation approach
Multi body system is defined for the VAWT in this section. The purpose of multi body system analysis is to design the parameters of the pitch control system, theses parameters are mainly length of links used to connect the blades. A linkage mechanism is utilized to change the pitch angle of the blade in a cyclic method, which makes this turbine to be a cyclo VAWT. The amplitude of pitch angle is decided by mathematical calculations for which the VAWT can perform well.

As shown in Figure 4, a pitch angle is changed by a linkage mechanism in cyclic order. Three blades are connected with the three links of same length (L_l). All three links are pivoted at one end of offset link of length (L_o), and the other end of the offset link is pivoted at the center of the rotor. The amplitude of offset is decided based on the total amount of blade pitch angle required which is calculated in next section. Ω represents the rotational speed of the rotor, β_p
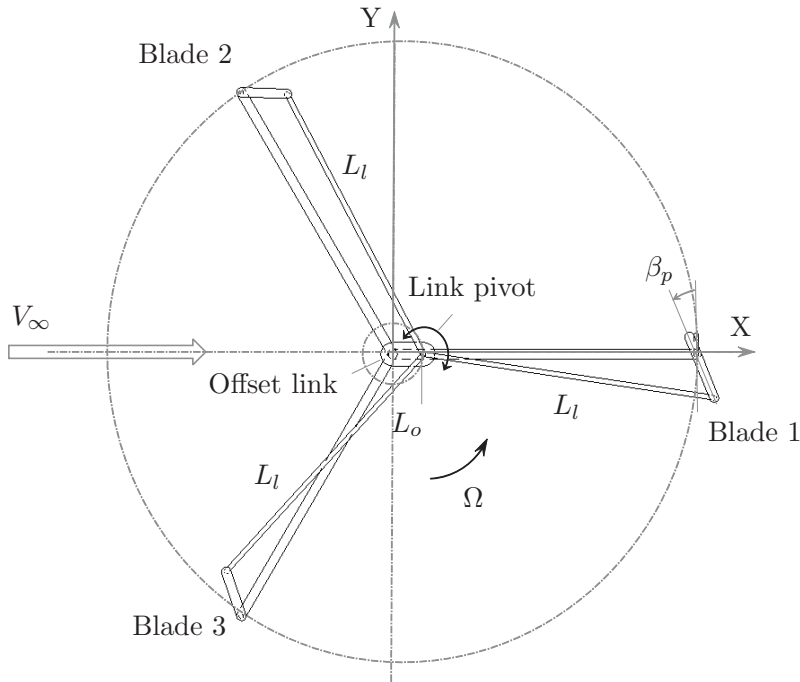

Figure 4. Schematic of pitch control mechanism

is the pitch angle of the blade. There is a need of the initial setting of the linkage mechanism with respect to the direction of wind flow. Therefore, a offset link is attached with a vane which remains in the direction of wind flow. Vane will rotate the link about its pivot at wind turbine rotor axis, causing the three link pivot to change its orientation at required position. Figure 5 shows the vane attached to the linkage mechanism. The specifications of the VAWT in this are given in Table 1.

Table 1. Specifications of VAWT

| Description	Symbol	Value	Unit
Rotor diameter	D_r	1.250	m
Rotor height	H	1.5	m
AF300 Airfoil			
Chord length	c	0.2	m
Length of Blade link	L_l	0.625	m
Length of Offset link	L_o	0.065	m
Range of pitch angle	β	$\pm40°$	
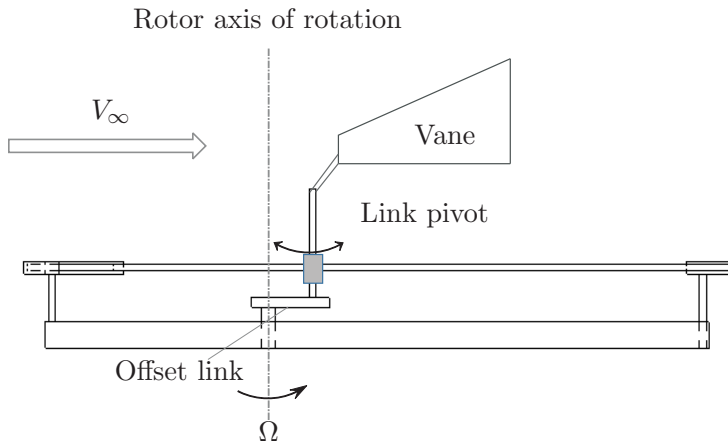
Figure 5. Vane for initial setting of mechanism

5. Simulation and Results

A VAWT performance is given by the power coefficient and the total power output. In this work a DMSTM is used to calculate the total power from the VAWT with and without pitch control mechanism. Figure 6.a shows the power coefficient of the VAWT with respect to the wind speed and the Figure 6.b shows the power coefficient of the VAWT versus the tip speed ratio. The
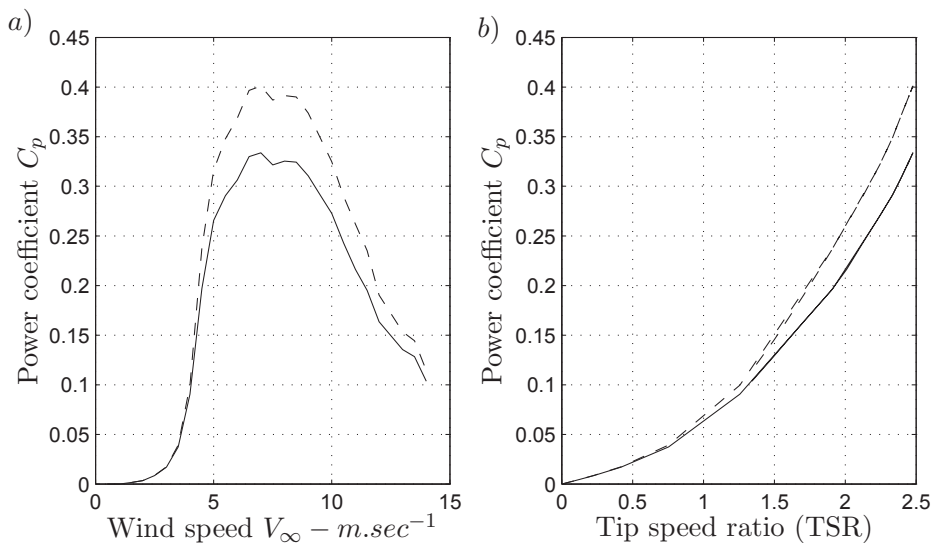
Figure 6. Power coefficient of VAWT   a C_p Vs V_∞ b C_p Vs TSR
——:   results without pitch control   - - - -:   results with pitch control

performance parameters power coefficient and power output of the VAWT are compared with the reference wind turbine (NREL) [30] and it is fund that the mathematical model deviates by 10% from the experimental results. It is accepted to proceed with the accuracy of the mathematical model used in this work. The use of 5° blade pitch angle amplitude has shown improvement of power coefficient by 12%. Also it can be seen from the Figure 7 that the maximum total power output from the VAWT is increased by 20%.
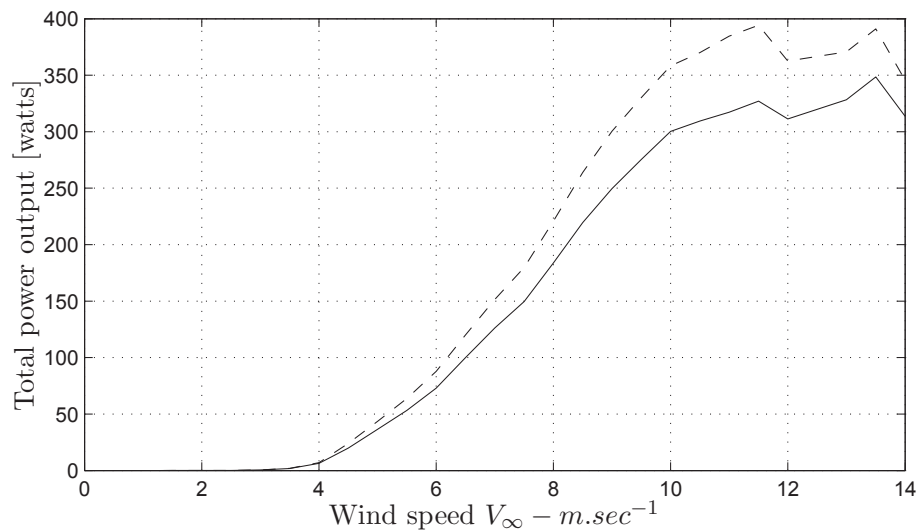
Figure 7. Total power output

——:   results without pitch control   - - - -:   results with pitch control

Conclusion

In this paper overview of various pitch control systems is discussed and design of collective pitch control linkage mechanism carried out with use of multi-body model. Aerodynamic loads are predicted from a mathematical model based on double multiple stream tube method. An appropriate airfoil which works at low Reynolds number is selected for blade design. It is also focused on commercialization of the vertical axis wind turbine which incorporates the collective blade pitch control system. It is observe from the mathematical model that with only $5°$ of blade pitch angle amplitude there has been increase in the power coefficient of the VAWT by 12%. Further a 500 Watt vertical axis wind turbine is manufactured and it is planned to implement the collective pitch control linkage mechanism. Multi-body model is going to be used for force analysis so that the linkage mechanism can be optimized. Also the purpose of using MSC Software tool was to further develop the dynamic simulation model of VAWT coupled with wind loads for detail structural analysis.

Acknowledgments

References

[1] Weblink, http://www.seao2.com/vawt/
[2] Eriksson S., Bernhoff H., Leijon M., 2008, Evaluation of different turbine concepts for wind power, Renewable and Sustainabl Energy Reviews vol. 12, pg. 1419-1434.
[3] Mohamed M.H., 2012, Performance investigation of h-rotor darrieus turbine with new airfoil shapes. Energy, vol. 47, 522530.
[4] Rahai H.R., Hefazi H., 2008, Vertical axis wind turbine with optimised blade profile, United States Patent Office, Patent no. US 2008/7393177 B2.

[5] Lew P., 2011, Multi-element wind turbine airfoils and wind turbines incorporating the same, United States Patent office, Patent no. US 2011/0255972 A1.

[6] Chougule P.D., Nielsen S.R.K., 2014, Simulation of flow over double-element airfoil and wind tunnel test for use in vertical axis wind turbine, A proceedings of Science of making true from wind 2014, under peer review

[7] Chougule P.D., Nielsen S.R.K., Basu B., 2013, Active Blade Pitch Control for Darrieus Straight Bladed Vertical Axis Wind Turbine of New Design. Basu B, editor. In Damage Assessment of Strucures X: 10th International Conference on Damage Assessment of Structures (DAMAS 2013), July 8-10, 2013, Dublin, Ireland. Zurich-Durnten, Switzerland: Trans Tech Publications Ltd. pp. 668-675. (Key Engineering Materials, Vol. 569-570).

[8] Lazauskas L., 1992, Three pitch control systems for vertical axis wind turbines compared, Wind Engineering, vol. 16, No. 5, pg. 269-283.

[9] Princeton, http://www.psatellite.com/research/windturbine/customer.php

[10] qr5 http://www.quietrevolution.com/

[11] Windspire01 http://www.windspireenergy.com/

[12] ev300 http://www.envergate.ch/

[13] Singh R.K., Ahmed M.R., Zullah M.A., Lee Y-H., 2012, Design of a low Reynolds number airfoil for small horizontal axis wind turbines, Renewable Energy vol. 42, pg.66-75.

[14] Selig M.S., Guglielmo J.J., Broeren P., Giguère P., 1995, Summary of Low-Speed Airfoil Data, Volume 1, SoarTech Publications, Virginia Beach, Virginia.

[15] Duncker T., Hall C., Miles A. Radosevic M., Rigby F., Seccafien M., Thody S., 2010, The design, build and test of smart, high efficiency darrieus turbine, The University of Adelaide, Honours Project 923.

[16] Kirke B., 1998, Evaluation of self starting vertical axis wind turbines for stand alone applications, School of Engineering,Griffith University, PhD Thesis.

[17] Howell R., Qin N., Edwards J., Durrani N., 2009, Wind tunnel and numerical study of a small vertical axis wind turbine, Renewable Energy, Hindawi Publishing Copeoration, vol. 35, No. 4, pg. 1-4.

[18] Castelli1 M.R., Betta S.De., Benini E., 2012, Effect of Blade Number on a Straight-Bladed Vertical-Axis Darreius Wind Turbine, World Academy of Science, Engineering and Technology, vol. 1, pg. 305-311.

[19] Hill N., Dominy R., G. Ingram E., Dominy J., 2008, Darrieus turbines: the physics of self-starting, Durnham University, UK, Test Report.

[20] Newman B.G., 1986, Multiple Actuator Disc Theory for Wind Turbines, Journal of Wind Energy and Industrial Aerodynamics, vol. 24, pg. 215-225.

[21] Paraschivoiu I., 1982, Double multiple streamtube model for Darrieus wind turbines, Lewis Research Center Wind Turbine Dynamics, NASA. N82-23684 pg. 14-44.

[22] Kirke B.K., Lazauskas L., 1991, Enhancing the performance of a vertical axis wind turbine using a simple variable pitch systems, Wind Engineering, vol. 15, No. 4, pg 187-195.

[23] Nahas M., 1992, A self starting Darrieus type windmill, Energy, vol. 18, No. 9, pg. 899-906.

[24] Hwang S., Hwang C.S., Min S.Y., Jeong I.O., Lee Y.H., Kim S.J., 2005, Efficiency improvement of a cyclodidal wind turbine by active control of blade motion, Flight Vehicle Research Center, vol. 1, No. 1, pg. 1-9.

[25] Nattuvetty V., Gunkel W.W., 1982, Theoretical performance of a staright bladed cycloturbine under different operating conditions, Wind Energy, vol. 6, No. 3, pg. 110-130.

[26] Dress H.M., 1987, The cycloturbine and its potential for broad application, International Symposium on Wind Engineering.

[27] Vandenberghe D., Dick E., 1987, A theoretical and experimental investigation into straight bladed vertical axis wind turbine with second order harmonic pitch control, Wind Engineering, vol.11, No. 5, pg. 237-247.

[28] Sener Y.A., 1995, Investigation of parameters of wind turbine efficiency, Akara, vol.1, No. 1 , pg. 4-7.

[29] Kirke B.K., Lazauskas L., 2008, Variable pitch Darrieus water turbines, Journal of Fluid Science and Technology, vol.3, No.3 , pg. 1-9.

[30] Windspire Energy Inc. 2010, Windspire Owners Mannual, 30 ft. Standard, Part No. 150001.

APPENDIX D
Active blade pitch control for straight bladed Darrieus vertical axis wind turbine of new design

Active Blade Pitch Control for Straight Bladed Darrieus Vertical Axis Wind Turbine of New Design

P.D. Chougule[1,a], S.R.K. Nielsen[2,b] and B.Basu[3,c]

[1,2]Department of Civil Engineering, Aalborg University, 9000, Denmark

[3]School of Engineering, Trinity College Dublin, Dublin 2, Ireland

[a]pdc@civil.aau.dk, [b]srkn@civil.aau.dk, [c]basub@tcd.ie

Abstract. As Development of small vertical axis wind turbines (VAWT) for urban use is becoming an interesting topic both within industry and academia. However, there are few new designs of vertical axis turbines which are customized for building integration. These are getting importance because they operate at low rotational speed producing very less noise during operation, although these are less efficient than Horizontal Axis Wind Turbines (HAWT). The efficiency of a VAWT has been significantly improved by H-Darrieus VAWT design based on double airfoil technology as demonstrated by the authors in a previous publication. Further, it is well know that the variation of the blade pitch angle during the rotation improves the power efficiency. A blade pitch variation is implemented by active blade pitch control, which operates as per wind speed and position of the blade with respect to the rotor. A double multiple stream tube method is used to determine the performance of the H-Darrieus VAWT. The power coefficient is compared with that of a fixed pitch and a variable pitch double airfoil blade VAWT. It is demonstrated that an improvement in power coefficient by 20% is achieved and the turbine could start at low wind speed.

Introduction

Small wind turbines are getting economically viable due to technological developments and new turbine ideas, which are producing more power output. Vertical axis wind turbines (VAWT's) are more suitable for small power generation for building due to low tip speed ratios, simple construction and independent on wind direction. However, due to low power efficiency of VAWT'shas achieved less popularity than horizontal axis wind turbines (HAWT's). The power efficiency of VAWT can be improved by individual blade pitch mechanism of which there are mainly two ways of control mechanisms: force pitch control i.e. active pitch control and self-acting pitch control i.e. passive pitch control, [1]. In forced pitch variation, individual blades are actuated by gears or cam actuator devices called pinsoncycloturbine, [2-4]. Self-acting variable pitch mechanism uses aerodynamic forces to actuate self-acting devices, which work by creating pitching moment about airfoil pivot. More details can be found in [5].

In the current theoretical work an active blade pitch mechanism has been implemented for three straight bladed Darrieus wind turbine so called $D^2A-VAWT$ proposed by the authors [6]. $D^2A-VAWT$ blade design consists of two airfoils denoted the main and slat airfoil. Individual blade pitch control law directly proportional to the pitch amplitude is implemented to change the effective angle of attack during rotation. Experimental aerodynamic characteristics of a double airfoil are used to estimate the power output. Blade pitch action for the VAWT has shown benefit in self-start ability and improvement in the power coefficient. This paper focus on theoretical analysis of pitch controller for $D^2A-VAWT$ and a comparison of the performance of a traditional VAWT and $D^2A-VAWT.$ A prototype testing of a $D^2A-VAWT$ is undergoing research work in current project and validation of the theory will be done eventually.

Wind turbine model

$D^2A - VAWT$ proposedin [6] consists of a double airfoil straight blade design as shown in Figure 1. Each blade consists of a main airfoil and a slat airfoil. The schematic of 2-Dimensional view of $D^2A - VAWT$ is represented in Figure 1.
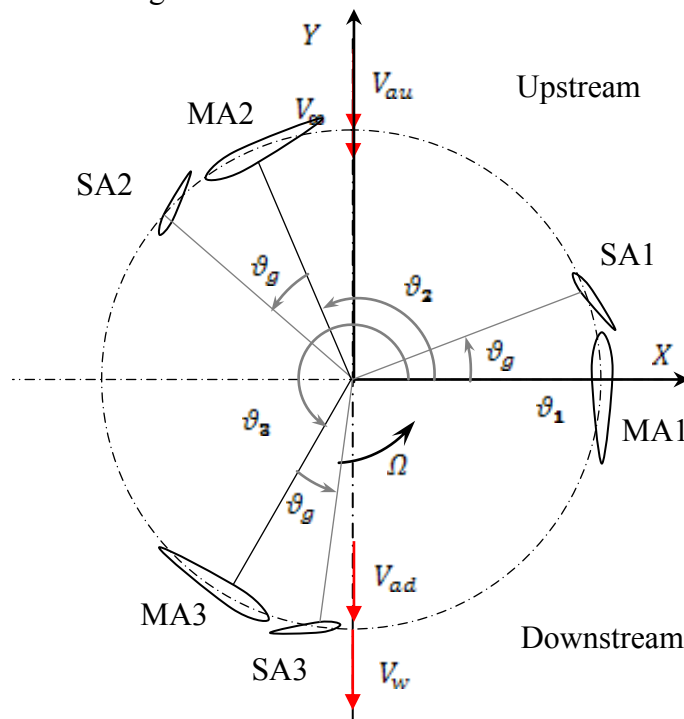

Fig.1 Schematic Diagram of Proposed $D^2A - VAWT$

In Figure 1 MAj and SAj are designating the main airfoil and the slat airfoil respectively which represents blade j. Ω is the rotor angular speed and ϑ_g is the fixed geometric angle between the main and the slat airfoil and is same for all three blades. The angles ϑ_j represents the azimuthal angle of blade j. The sign of the indicated angles has been defined in Figure 1. The geometric parameters of the $D^2A - VAWT$ are given in the Table 1. TE represents trailing edge.

Aerodynamics of $D^2A - VAWT$

Aerodynamics of VAWT and the flow around the rotor is mainly studied by multiple actuator disc theory, [7]. Velocity components at various locations in flow area are of interest which is calculated by the momentum theory and the blade element theory. There are various formulations of the method such as the single stream tube method (SSTM), multiple stream tube method (MSTM) and the double multiple stream tube method (DMSTM), where the latter approach offers more precise prediction,[8]. In DMSTM, the flow field outside the rotor is divided into two subfields placed; upstream and downstream of the rotor. The fluid flow is considered to be inviscid and incompressible for the calculation of the induced velocity through the each stream tube. Since the flow field is divided into two halves, it is necessary to derive the local angle of attack and the local relative velocity for upstream and downstream of the rotor individually. To obtain theses quantities an index j is used where j = u and j=d corresponds to upstream and downstream half of the flow region, respectively. The upstream induced velocity V_{au} is given by the following formula,

$$V_{au} = a\, V_{\infty}.$$ (1)

where, a is the upstream axial induction factor and V_∞ is the free stream velocity and $V_{au} < V_\infty$. There exists a reduction in the wind induced velocity at downstream of the rotor and denoted by V_{ad} which is given as follows,

$$V_{ad} = a_1(1 - 2a)V_\infty .\tag{2}$$

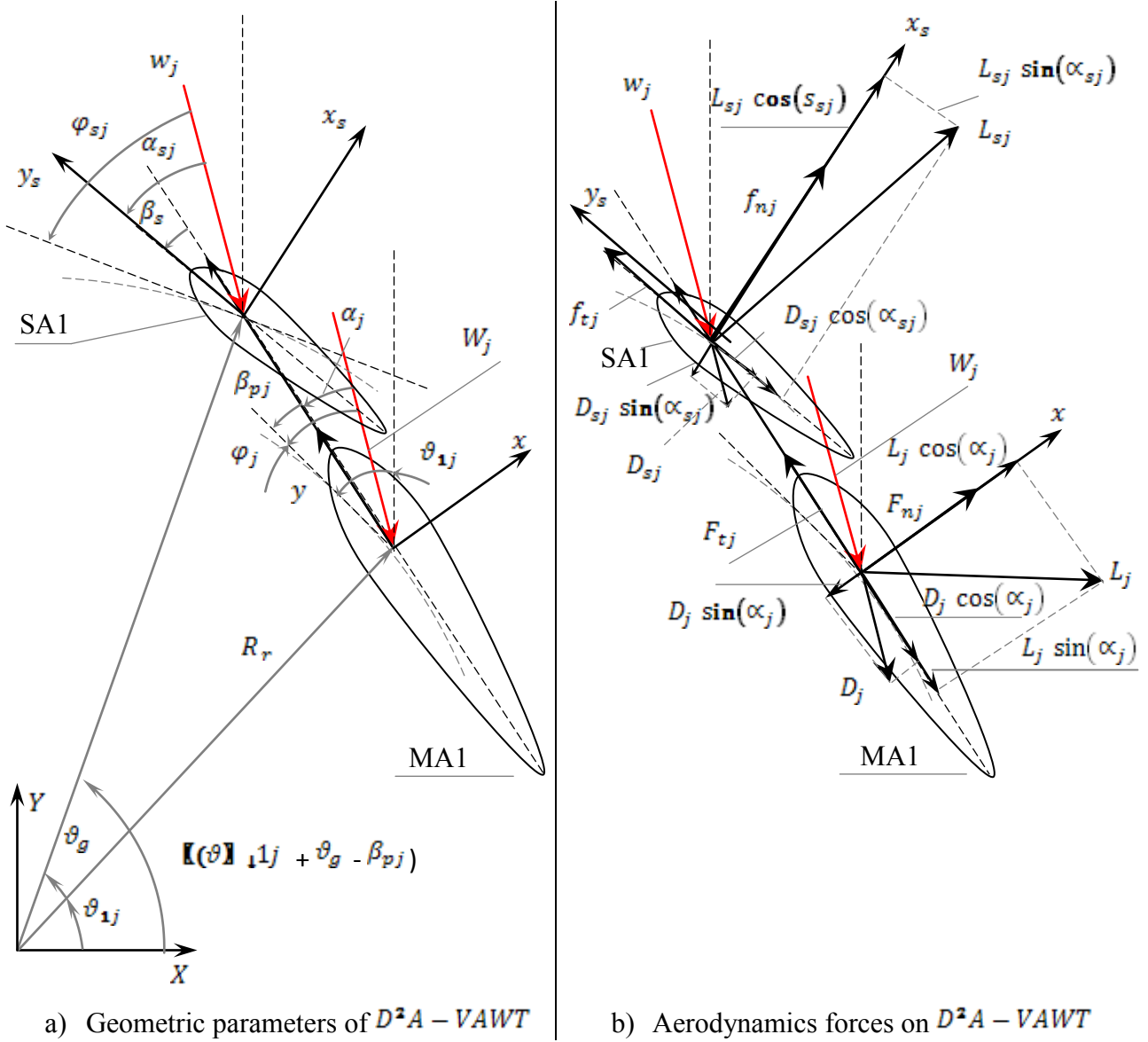a) Geometric parameters of $D^2A - VAWT$ b) Aerodynamics forces on $D^2A - VAWT$

Fig. 2: Geometric Parameters and Aerodynamic Forces on Blade 1

where a_1 is the downstream induction factor, V_{ad} corresponds to the downstream induced velocity which holds relation $V_{ad} < V_{au}$. Once the induced velocities are calculated aerodynamic forces can be obtained by airfoil free body diagrams. The geometric parameters related to the double airfoil are given in Figure 2.a.

Lift and drag forces per unit length acting on the slat airfoil are L_{sj} and D_{sj} respectively. The normal and tangential forces acting on a slat airfoil are f_{nj} and f_{tj} respectively. The basic aerodynamic formulation of the main and the slat airfoil of $D^2A - VAWT$ design are separately derived. The lift and drag coefficients of the main airfoil C_{Lj}, C_{Dj} and the slat airfoil C_{Lsj}, C_{Dsj} are taken from previous experimental study by the authors of this paper, [6].

Aerodynamics of a Main Airfoil (MA1)

The velocity at the inlet of the rotor and the outlet of the rotor is different as shown in Figure 3.a. Inlet velocity is the free stream velocity represented by V_∞ and outlet velocity is the wake velocity V_w

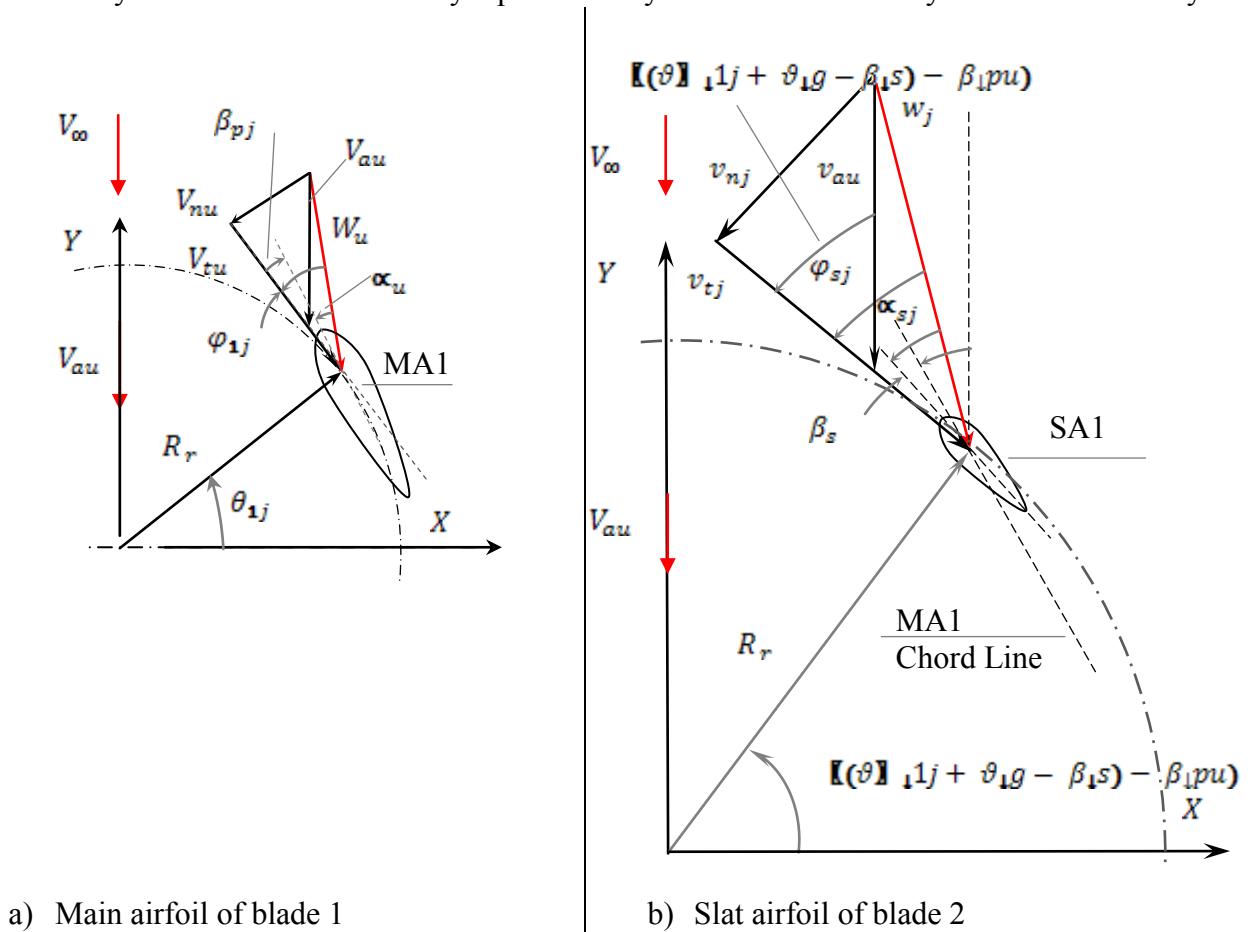a) Main airfoil of blade 1   b) Slat airfoil of blade 2

Fig.4: Velocity Component Double Airfoil

The tangential velocity component V_{tj} and the normal velocity V_{nj} component of the main airfoil in upstream half of the rotor can be expressed as,

$$V_{t_j} = R_r\,\Omega + V_{a_j}\cos(\vartheta_{1j}) \tag{3}$$

$$V_{n_j} = V_{a_j}\sin(\vartheta_{1j}) \tag{4}$$

R_r is the radius of the rotor, and ϑ_{1j} is the azimuth angle of the blade 1. Referring to Figure 4, the flow angle ϑ_{1j} can be expressed as,

$$\varphi_{1j} = \operatorname{atan}\left(\frac{V_{n_j}}{V_{t_j}}\right) \tag{5}$$

Substituting the values of V_{tj} and V_{nj} from equation (3) and (4) we get,

$$\varphi_j(\vartheta_{1j}) = \operatorname{atan}\left(\frac{\sin(\vartheta_{1j})}{\dfrac{R_r\,\Omega}{V_{a_j}} + \cos(\vartheta_{1j})}\right) \tag{6}$$

For variable pitch control of a Darrieus rotor; the flow angle is often represented by following equation,

$$\varphi_j = \alpha_j + \beta_{pj}$$ (7)

where α_j is the local angle of attack and β_{pj} is the blade pitch angle in upstream and down stream of the rotor respectively. The blade pitch angle is expressed as,

$$\beta_{pj} = -\beta_0 \sin(\vartheta_{1j})$$ (8)

β_0 is the amplitude of pitch angle variation which is equal to or less than airfoil stall angle. The negative sign indicates the sign for blade rotation. The variation of the local relative flow velocity W_j can be given as follows,

$$W_{1j}(\vartheta_{\perp 1j}) = \sqrt{(([V_1(t_{1j})]^2) + [V_1(n_{1j})]^2)}$$ (9)

The directions of the lift L_j and drag D_j forces per unit length and their tangential $F_{t_j}(\vartheta_{1j})$ and normal $F_{n_j}(\vartheta_{1j})$ force components are shown in Figure 4. The tangential force coefficient $C_{t_j}(\vartheta_{1j})$ is basically given by addition of tangential components of lift L_j and drag D_j forces. The normal force coefficient $C_{n_j}(\vartheta_{1j})$ is the difference between the normal component of the lift L_j and the drag D_j forces. The expression of tangential force coefficient $C_{t_j}(\vartheta_{1j})$ and normal force component $C_{n_j}(\vartheta_{1j})$ are given as,

$$C_{t_j}(\vartheta_{1j}) = c_{L_j} \sin \vartheta_j + c_{D_j} \cos \vartheta_j$$ (10)

$$C_{n_j}(\vartheta_{1j}) = c_{L_j} \cos \vartheta_j - c_{D_j} \sin \vartheta_j$$ (11)

The lift c_{L_j} and the drag c_{D_j} coefficients in equation (10) and (11) are obtained from experiment for particular Reynolds number. The formulation of Reynolds number of the VAWT can be given by Equation (19).

$$F_{t_j}(\vartheta_{1j}) = \frac{N_s\, c\, H}{S} \int_0^H CF_{t_j}\, dH$$ (12)

$$F_{n_j}(\vartheta_{1j}) = \frac{N_s\, c\, H}{S} \int_0^H CF_{n_j}\, dH$$ (13)

where $S = H\, 2\, R$ is the rotor frontal area, H is the total height of the rotor. By integrating along blade length a total torque on the complete blade as a function of azimuthal angle is obtained as follows,

$$T_{1_j}(\vartheta_{1j}) = \frac{N}{2\pi} \int_0^H C_{t_j}(\vartheta_{1j}) W_j^2\, dH$$ (14)

where, N is the number of blades and R_r is the radius of the rotor.
Therefore the total torque on both halves of the rotor is given by integrating over azimuthal angle as follows.

$$T_{1_j}(\vartheta_{1j}) = \frac{1}{2} \rho\, c_m\, R \int_m^n T_j(\vartheta_{1j})\, d\vartheta_1$$ (15)

In equation (15) for $j = u$: $m = 0$, $n = \pi$ and for $j = d$: $m = \pi$, $n = 2\pi$. The torque coefficient and hence the power coefficient are given as,

$$CT_j = \frac{T_j}{\frac{1}{2}\rho V_\infty S R}$$

$$(16)$$

$$C_{p_j} = \frac{R\,\omega}{V_\infty} CT_j$$

$$(17)$$

The power coefficient of the whole rotor contribution from the main airfoil is the weighted sum of the upstream power coefficient C_{pu} and the downstream power coefficient C_{pd}, which is denoted by C_p given as,

$$C_p = C_{pu} + C_{pd}$$

$$(18)$$

It is well know that VAWTs operates under low Reynolds number and the performance of the airfoil degrade as Reynolds number is lowered. So, it is important to determine the Reynolds number at the blade chord at the selection of an airfoil for use in VAWTs. Therefore, a local Reynolds number R_e of the blade 1 at different azimuthal angle ϑ_{1j} is expressed by the following equation, [9]

$$R_e(\vartheta_{1j}) = \rho \frac{c_m W_j(\vartheta_{1j})}{\mu}$$

$$(19)$$

where R_e is the rotor Reynolds number, μ is the air viscosity and c_m is the main airfoil chord length. Reynolds number varies with the relative velocity which is depends on the azimuthal angle at each blade. It is observed from the plot of Reynolds number versus azimuthal angle and relative velocity versus azimuthal angle that the variation of Reynolds number is relatively less. Hence it is assumed in this work that the Reynolds number is constant over the VAWT rotor. Therefore the aerodynamic characteristics C_{Lj} and C_{Dj} are used for calculated Reynolds number using equation (19).

Aerodynamics of a SlatAirfoil (SA1)

Aerodynamic load calculation for a slat airfoil is based on the basic formulae explained in the previous section. Figure 4.b shows that the azimuthal angle of the slat airfoil of blade 1 ϑ_{s1} is dependent on the azimuthal angle ϑ_{1j} of main airfoil of blade 1. Geometric angle of a slat airfoil ϑ_{s1j} in upstream and downstream half of the rotor for blade 1 can be expressed in following equation.

$$\vartheta_{s1_j} = \vartheta_{1j} + \vartheta_g - \beta_{pj}$$

$$(20)$$

For blade 2 and blade 3 azimuthal angles are given by changing the suffix to 2 and 3 respectively in equation (20). Therefore in what follows all equations are derived for blade 1 in which the azimuthal angle of the main airfoil is denoted by ϑ_{1j} and azimuthal angle of the slat airfoil is represented by ϑ_{s1}. It is noted that ϑ_{1j} and ϑ_{s1} varies in the range from $0\ to\ \pi$ in upstream and from $\pi\ to\ 2\pi$ in downstream half of the rotor. The fixed azimuthal angle ϑ_g is the angle between main and slat airfoil and ϑ_g is the same for all blades. The pitch angle β_{pj} in equation (20) is introduced due to effect of rotation of main airfoil. The slat airfoil position and orientation is fixed relative to main airfoil in local frame of main airfoilx-y. However, a blade pitch angle of the main airfoil is introduced which will change the position and the orientation of a slat airfoil in global fixed frame represented by X-Y coordinate system. The effect is azimuthal angle ϑ_{s1} of slat airfoil get reduced by amount of pitch angle β_{pj}.

Numerical example

The numerical analysis of $D^2A - VAWT$ is performed in this section for which, the geometric parameters are given in Table 1.

Table 1: Geometric parameters of $D^2A - VAWT$

Description	Symbol	Value	Unit
Rotor Height	H	6.1	m
Rotor Diameter	D_r	1.22	m
Main Airfoil chord length	c_m	0.085	m
Slat airfoil chord length	c_s	0.0425	m
Main airfoil thickness	t_m	0.034	m
Slat airfoil thickness	t_s	0.017	m
Slat TE position x-direction	x_{TE}	0.015	m
Slat TE position y-direction	y_{TE}	0.006	m
Slat airfoil angle	β_s	-16	$\circ$

Figure 5 shows the numerical results in which a performance is compared, with pitch controller and without pitch controllerfor blade of $D^2A - VAWT.$
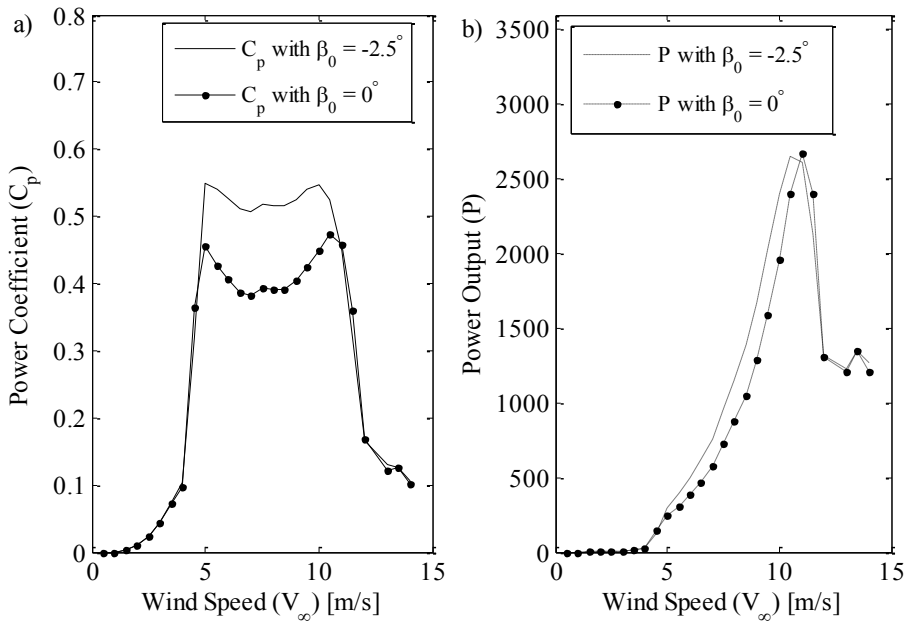

Fig. 5: Numerical results a) Power coefficient. b) Power output of $D^2A - VAWT$

The experimental aerodynamic properties of a double airfoil are used from previous research work carried out by the authors. A performance of $D^2A - VAWT$ is calculated for pitch angle $\beta_0 = 2.5°$ with geometric parameters given in Table 1. It is observed that the power coefficient of $D^2A - VAWT$ is increased by 20% due to implementation of an active blade pitch controller. The numerical results are not validated in this paper however the analytical method used is shown in [9-10] to be accurate enough for acceptance of the results. It has been shown in study [10] that the variation of results obtained by analytical DMSTM and experimental field test data for Darrieus three bladed VAWT is less than 5% over different tip speed ratios.

Summary

In this paper the performance of a new design of straight three bladed Darrieus vertical axis wind turbine is analyzed with considering the active blade pitch controller. Double multiple stream tube method is used to derivethe aerodynamic equations for $D^2A - VAWT$ and an experimental data has been used in calculation of the performance. A numerical example shows that the use of a small blade pitch angle of $2.5°$ has improved the power coefficient of $\mathbf{VAWT}$ from 45% to 55%. Due to active blade pitching action the power output curve has shown improvement by earlier generation of power which supports the self-starting ability of a VAWT.

References

[1] L. Lazauskas, Three pitch control systems for vertical axis wind turbines compared,Wind Energy, Vol.16, No.5, 1992, pp. 269-282

[2] V. Nattuvetty, W.W. Gunkel, Theoretical performance of a straight bladed cycloturbine under different operating conditions, Wind Energy, Vol.6, No.3, 1982, pp. 110-130

[3] H.M. Dress,The cycloturbine and its potential for broad application,Second International Symposium on Wind Engineering, Amsterdam, Oct 1987

[4] D. Vandenberghe, E. Dick,A theoretical and experimental investigation into straight bladed vertical axis wind turbine with second order harmonic pitch control,Wind Engineering, Vol.11 No. 5, 1987, pp. 237-247.

[5] B.K. Kirke, L. Lazauskas, Enhancing the performance of a vertical axis wind turbine using simple variable pitch systems,Wind Engineering, Vol.15 No.4, 1991, pp. 187-195.

[6] P.D.Chougule, S.R.K.Nielsen, Wind tunnel testing of multi-element airfoil and new design of vertical axis wind turbine. Proceedings of the ASME 2013 International Power Conference, Power 2013, July-August 2013. Power2013-9825.

[7] B. G. Newman, Multiple Actuator Disc Theory for Wind Turbines, Journal of Wind Energy and Industrial Aerodynamics, 24 215-225 (1986)

[8] I. Paraschivoiu, Double multiple streamtube model for Darrieus wind turbines, Lewis Research Center Wind Turbine Dynamics, NASA. 19-25 (N82-23684 14-44)

[9] I. Paraschivoiu,Wind Turbine Design: with Emphasis on Darrieus Concepts, Polytechnic International Press, ISBN: 978-2-553-00931-0 (2002).

[10] R.E. Sheldahl, P.C.Klimas, and L.V.Feltz, Aerodynamic performance of 5-meter-diameter Darrieusturbine with extruded Aluminum NACA-0015 Blades, Sandia National Laboratories, Albuquerque, N.M. Rept. SAND 80-0179, March (1980).

APPENDIX E
Aerodynamic characteristics of DU06-W200 and double-element S1210 airfoils

Table E.1 DU06-W200 Aerodynamic characteristics at $Re = 160,000$

α	c_L	c_D	α	c_L	c_D	α	c_L	c_D			
-87	-0.1731	1.8069	-25	-0.6377	0.3861	11	0.9923	0.0203	57	0.9981	0.8735
-85	-0.225	1.7641	-23	-0.5913	0.3647	12	1.0327	0.0202	58	0.9692	0.9157
-84	-0.2827	1.7105	-21	-0.5391	0.2051	13	1.05	0.0201	60	0.9346	0.9473
-83	-0.3346	1.6571	-20	-0.4812	0.1412	14	1.0615	0.0199	61	0.9058	0.9895
-81	-0.375	1.6251	-18	-0.4116	0.1197	16	1.0673	0.0303	63	0.8712	1.0105
-79	-0.4788	1.5288	-16	-0.3478	0.0876	17	0.5135	0.0302	64	0.8423	1.0316
-78	-0.5077	1.4754	-13	-0.2783	0.0768	17	0.525	0.0406	66	0.7846	1.0843
-76	-0.5423	1.4218	-11	-0.2145	0.0661	18	0.5423	0.0509	69	0.7385	1.1265
-74	-0.5885	1.3897	-9	-0.1565	0.0553	20	0.5885	0.0614	71	0.7038	1.2003
-73	-0.6231	1.3043	-8	-0.1043	0.0445	21	0.6115	0.0719	72	0.6635	1.2319
-68	-0.6493	1.2615	-6	-0.0754	0.0231	22	0.6577	0.0824	73	0.6231	1.2846
-67	-0.6667	1.2082	-5	-0.029	0.0229	24	0.6865	0.1139	74	0.5885	1.3268
-65	-0.7072	1.1654	-4	0.0058	0.0227	25	0.7212	0.1244	76	0.5423	1.3795
-64	-0.7478	1.1121	0	0	0.0117	25	0.7558	0.1454	78	0.5077	1.4111
-63	-0.7768	1.0694	1	0.0923	0.0116	26	0.7904	0.3674	79	0.4788	1.4638
-61	-0.8406	1.0267	2	0.1385	0.0114	27	0.8192	0.399	80	0.4385	1.5165
-59	-0.9449	1.0053	2	0.1904	0.0113	29	0.8654	0.42	81	0.375	1.5586
-58	-0.9855	0.9733	3	0.2308	0.0111	32	0.9808	0.4622	83	0.3346	1.6007
-56	-1.0261	0.92	3	0.3058	0.011	34	1.0154	0.4833	84	0.2827	1.6533
-53	-1.0493	0.8986	3	0.3462	0.0108	35	1.0385	0.5254	85	0.225	1.7269
-50	-1.0725	0.8772	4	0.4442	0.0107	36	1.0615	0.5571	87	0.1731	1.7899
-47	-1.0493	0.8345	4	0.3865	0.0106	37	1.0789	0.5782	89	0.1327	1.8003
-45	-1.0435	0.7918	5	0.4904	0.0106	39	1.1019	0.652			
-40	-1.0029	0.7171	5	0.5423	0.0104	42	1.1019	0.6731			
-37	-0.9623	0.6744	6	0.6231	0.0209	44	1.1135	0.7047			
-35	-0.8986	0.6424	7	0.6865	0.0102	47	1.1135	0.7469			
-33	-0.8406	0.5997	7	0.7673	0.0101	49	1.1019	0.7891			
-32	-0.7942	0.525	7	0.8538	0.0101	52	1.0789	0.8102			
-29	-0.742	0.4823	9	0.9115	0.01	53	1.0558	0.823			
-26	-0.6841	0.4502	10	0.9519	0.0204	55	1.0327	0.8418			

Table E.2 Double-element S1210 airfoil Aerodynamic characteristics at $Re = 200,000$

α	c_L	c_D	α	c_L	c_D	α	c_L	c_D	α	c_L	c_D
-180	0	0.3251	-130	1.02	1.53	10	1.77	0.4	130	0.06	1.39
-179	0.11	0.3252	-125	0.955	1.66	15	2	0.55	135	0.075	1.235
-178	0.22	0.3254	-120	0.875	1.785	20	2.13	0.71	140	0.13	1.06
-177	0.33	0.3257	-115	0.76	1.89	21	2.14	0.75	145	0.255	0.885
-176	0.44	0.3262	-110	0.63	1.98	22	2.15	0.78	150	0.3376	0.72
-175	0.524	0.3271	-105	0.5	2.05	23	2.16	0.82	153	0.405	0.644
-174	0.6228	0.3282	-100	0.365	2.095	24	2.17	0.86	154	0.4076	0.6205
-173	0.71	0.3295	-95	0.23	2.115	25	2.17	0.89	155	0.4103	0.597
-172	0.7879	0.3309	-90	0.09	2.115	30	2.09	1.06	156	0.3942	0.575
-171	0.8526	0.3326	-85	-0.05	2.095	35	2.09	1.24	157	0.3781	0.553
-170	0.8983	0.3344	-80	-0.185	2.065	40	2.04	1.4	158	0.3437	0.532
-169	0.9249	0.3363	-75	-0.32	2.015	45	1.96	1.54	159	0.3093	0.511
-168	0.9279	0.3385	-70	-0.45	1.95	50	1.87	1.665	160	0.2695	0.46
-167	0.9104	0.3409	-65	-0.575	1.87	55	1.78	1.78	161	0.2297	0.409
-166	0.8803	0.409	-60	-0.67	1.78	60	1.685	1.87	162	0.1996	0.3409
-165	0.8405	0.46	-55	-0.76	1.665	65	1.56	1.95	163	0.1821	0.3385
-164	0.8007	0.511	-50	-0.85	1.54	70	1.43	2.015	164	0.1851	0.3363
-163	0.7663	0.532	-45	-0.93	1.4	75	1.295	2.065	165	0.2117	0.3344
-162	0.7319	0.553	-40	-1.23	1.02	80	1.16	2.095	166	0.2574	0.3326
-161	0.7158	0.575	-35	-1.17	0.85	85	1.02	2.115	167	0.3221	0.3309
-160	0.6997	0.597	-30	-1.05	0.67	90	0.88	2.115	168	0.4	0.3295
-159	0.7024	0.6205	-25	-0.86	0.51	95	0.745	2.095	169	0.4872	0.3282
-158	0.705	0.644	-20	-0.59	0.36	100	0.61	2.05	170	0.586	0.3271
-155	0.7724	0.72	-15	-0.27	0.22	105	0.48	1.98	171	0.67	0.3262
-150	0.855	0.885	-10	0.15	0.18	110	0.35	1.89	172	0.78	0.3257
-145	0.98	1.06	-5	0.58	0.17	115	0.235	1.785	173	0.89	0.3254
-140	1.035	1.235	0	1.03	0.2	120	0.155	1.66	174	1	0.3252
-135	1.05	1.39	5	1.44	0.28	125	0.09	1.53			